Title
Elucidation of Initiation and Maintenance Mechanisms of X Chromosome Inactivation

Author
Minkovsky, Alissa

Publication Date
2013

Peer reviewed|Thesis/dissertation

UNIVERSITY OF CALIFORNIA

Los Angeles

Elucidation of Initiation and Maintenance Mechanisms of X Chromosome Inactivation

A dissertation submitted in partial satisfaction of the requirements for the degree

Doctor of Philosophy in Biological Chemistry

by

Alissa Minkovsky

2013

ABSTRACT OF THE DISSERTATION

Elucidation of Initiation and Maintenance Mechanisms of X Chromosome Inactivation

by

Alissa Minkovsky
Doctorate of Philosophy in Biological Chemistry
University of California, Los Angeles, 2013
Professor Kathrin Plath, Chair

X chromosome inactivation is a program of gene silencing on one of two female mammalian X chromosomes to equalize X-linked gene expression to XY male counterparts. This developmentally-regulated chromatin change is initiated on either the maternal or paternal X chromosome early in embryonic development and, once established, is maintained on the chosen chromosome for the lifetime of the female. The onset of X chromosome inactivation is regulated by the long noncoding transcript *Xist* and an open question is the field is how embryonic developmental cues trigger expression of *Xist* and onset of X chromosome inactivation. The correlation of pluripotency with repression of *Xist* in the mouse system has led to a model where pluripotency transcription factors repress X chromosome inactivation by binding to a region within the first intron of *Xist* gene. Thus differentiation would release the repression of *Xist*. We rigorously tested this intron1 hypothesis in a transgenic mouse

model and refute that intron1 binding is responsible for the developmental regulation of X chromosome inactivation.

A second set of studies focused on the maintenance phase of X chromosome inactivation with the goal of discovering novel chromatin factors that contribute to the remarkable stability of gene silencing on the entire X chromosome. We took an unbiased screening approach, designing a high throughput assay with primary mouse cells bearing reporters on the inactive X, and screened genome-wide siRNA and chemical libraries. We report that knockdown of chromatin-associated protein Atf7ip or its previously characterized interactors reactivates silenced genes of the inactive X chromosome. From chemical screening, we found that the compound Resveratrol can lead to reactivation of silenced genes as part of a novel drug combination. We show evidence that Resveratrol inhibits the dNTP biosynthetic enzyme ribonucleotide reductase in this context. This finding has spurred a collaboration investigating Resveratrol as part of a rationale drug combination for cancer therapy. In summary, these studies demonstrate that X chromosome inactivation is powerful and flexible model for the interrogation of mammalian chromatin regulation mechanisms with relevance for disease therapy.

The dissertation of Alissa Minkovsky is approved.

Michael F Carey

Geraldine A Weinmaster

Douglas L Black

Kathrin Plath, Committee Chair

University of California, Los Angeles

2013

I dedicate this work to my parents.

TABLE OF CONTENTS

FIGURES AND TABLES

ACKNOWLEDGEMENTS

I would like to express gratitude to my mentor, Dr. Kathrin Plath, for her tireless enthusiasm, attentive guidance, and respectful partnership. I feel immensely lucky to have been her student and hope I take away just a fraction of her data-driven approach to the world.

Thank you to my supportive committee members who created an ideal learning environment tempering their criticism with encouragement.

A huge thanks to my colleagues in the lab- mentors, mentees, and partners to whom I owe much of my training. Thanks to Dr. Bernadett Papp, Dr. Costas Chronis, Dr. Sanjeet Patel, Matthew Denholtz, and Ritchie Ho for always making themselves available for scientific discussion. Thanks to Dr. Vincent Pasque, Dr. Amy Pandya-Jones, Nadia Sellami, Giancarlo Bonora, and Anna Sahakyan especially for their collaboration and for their critical reading of this thesis. Anna also performed several experiments in Chapter 6 and working with her has greatly enriched my last 3 months in the lab. Thanks to Robin McKee's competent management of the lab for making experiments easier and faster to finish.

I would like to specifically acknowledge the scientists that inspired my career path from first teaching me molecular biology as a 17 year-old- Drs. Christopher Denny, Michael Carey, and Stephen Smale.

My wider community in the Department of Biological Chemistry and the UCLA MD/PhD program boasts world-class science in a congenial and collaborative atmosphere. The studies I describe here have been greatly improved through many conversations and research presentations- thanks for the many opportunities to share this work throughout. Thanks to administrators, namely Susie Esquivel and Brenda Padron, for all of their help.

I would like to thank the leadership of the MD/PhD program, Drs. Stephen Smale and Kelsey Martin, for their guidance, their responsiveness, and the very hard work they do to support a next generation of scientists. I am part of a really remarkable program, and with my best friends too. Thank you Lisa Kohn, Katy Cross, Megan So, and Kelley O'Donnell.

My family has spent so much of the past four years listening to me talk about graduate school! I am so grateful to my fiercest supporters, my parents and my sister.

Chapter 1 is a version of a publication authored by Alissa Minkovsky, Sanjeet Patel, and Kathrin Plath (Minkovsky, A., Patel, S., and Plath, K. (2012). Concise review: Pluripotency and the transcriptional inactivation of the female Mammalian X chromosome. Stem Cells *30*, 48–54.)

Chapter 2 is a version of a publication authored by Alissa Minkovsky, Tahsin Stefan Barakat, Nadia Sellami, Mark Henry Chin, Nilhan Gunhanlar, Joost Gribnau, and Kathrin Plath (Minkovsky, A., Barakat, T.S., Sellami, N., Chin, M.H., Gunhanlar, N., Gribnau, J., and Plath, K. (2013). The Pluripotency Factor-Bound Intron 1 of Xist Is Dispensable for X Chromosome Inactivation and Reactivation In Vitro and In Vivo. Cell Rep *3,3* 905-918.)

Chapters 3-8 are a version of a manuscript in preparation for publication authored by Alissa Minkovsky, Anna Sahakhyan, Elyse Rankin-Gee, Sanjeet Patel, Winnie Hwong, Robert Damoiseaux, Elizabeth Dimitriova, Caius Radu, Giancarlo Bonora, and Kathrin Plath.

This work was supported by funds from the Iris Cantor- UCLA Women's Health Executive Advisor Board and by NRSA AG039179.

VITA

2004-2005	Los Angeles Pierce College, Woodland Hills, CA
2005-2007	B.S., in Microbiology, Immunology, and Molecular Genetics Magna Cum Laude, College Honors University of California, Los Angeles
2005-2007	Howard Hughes Undergraduate Research Fellowship, Laboratory of Dr. Christopher Denny University of California, Los Angeles
2005-2007	Beckman Undergraduate Research Scholarship University of California, Los Angeles
2010	Predoctoral Fellowship, Training Program in Genetic Mechanisms University of California, Los Angeles
2010	Iris Cantor-UCLA Women's Health Pilot Research Fund, University of California, Los Angeles
2011	Teaching Assistant, Human Genetics University of California, Los Angeles
2011-2014	National Ruth L. Kirschstein Predoctoral Fellowship, NIH

PRESENTATIONS

Minkovsky A and Plath K. Characterization of *Xist* Intron 1 as a putative developmental repressor of Xist. Poster presented at EMBO 50 years of X inactivation, Oxford, England, July 2011.

Minkovsky A and Plath K. Screening for factors in X chromosome epigenetic silencing. Poster presented at Molecular Genetics of Aging, Cold Spring Harbor, New York, October 2012.

PUBLICATIONS

Minkovsky, A., Patel, S., and Plath, K. (2012). Concise review: Pluripotency and the transcriptional inactivation of the female Mammalian X chromosome. Stem Cells *30*, 48–54.

Minkovsky, A., Barakat, T.S., Sellami, N., Chin, M.H., Gunhanlar, N., Gribnau, J., and Plath, K. (2013). The Pluripotency Factor-Bound Intron 1 of Xist Is Dispensable for X Chromosome Inactivation and Reactivation In Vitro and In Vivo. Cell Rep *3,3* 905-918.

CHAPTER 1

A REVIEW OF DEVELOPMENTAL REGULATION OF XCI

X chromosome inactivation (XCI) is a striking example of developmentally regulated, wide-range heterochromatin formation that is initiated during early embryonic development. XCI is a mechanism of dosage compensation unique to placental mammals whereby one X chromosome in every diploid cell of the female organism is transcriptionally silenced to equalize X-linked gene levels to XY males. In the embryo, XCI is random with respect to whether the maternal or paternal X chromosome is inactivated and is established in epiblast cells upon implantation of the blastocyst. Conveniently, *ex vivo* differentiation of mouse embryonic stem cells (mESCs) recapitulates random XCI and permits mechanistic dissection of this stepwise process that leads to stable epigenetic silencing. Here, we focus on recent studies in mouse models characterizing the molecular players of this female-specific process with an emphasis on those relevant to the pluripotent state. Further, we will summarize advances characterizing XCI states in human pluripotent cells, where surprising differences from the mouse process may have far-reaching implications for human pluripotent cell biology.

The noncoding RNA *Xist* controls the initiation of random XCI

The importance of XCI is demonstrated by the fact that ablation of the master regulator of this process, *Xist* (X-inactive specific transcript), leads to female-specific lethality early in embryonic development in mice[1,2]. The X-linked *Xist* gene encodes an approximately 17 kb spliced and polyadenylated transcript that is essential for heterochromatin formation on the X chromosome from which it is transcribed[1-4]. In the embryo, XCI is random based on the parent-of-origin for the inactive X (X_i), such that female organisms are mosaic for which X chromosome is expressed. *In vivo,* random XCI is initiated in epiblast cells of the inner cell mass (ICM) of the blastocyst soon after

implantation and, *in vitro*, upon induction of differentiation in mESCs, which are derived from epiblast cells of the pre-implantation blastocyst. Upon initiation of XCI, *Xist* is transcriptionally upregulated on the future X_i[5,6]. It has been suggested that the transcription factor Yin-Yang 1 (YY1) tethers *Xist* RNA to its site of transcription by binding directly to both *Xist* RNA and DNA[7]. The RNA then spreads and creates an '*Xist* RNA cloud' demarcating the nuclear domain of the inactivating X yet the regulation of the release of Xist RNA from the Yy1 tether at the site of transcription is still unknown.

As *Xist* RNA molecules coat the X, they trigger transcriptional silencing with immediate exclusion of RNA polymerase II[8]. This is followed by loss of active chromatin marks and establishment of silencing chromatin marks, which occur in an ordered sequence of events and include, for example, trimethylation of histone H3 lysine 27 ($H3K27me^3$) by the Polycomb complex PRC2, DNA methylation of promoter regions, and recruitment of the repressive histone variant macroH2A[9]. The result is the X_i is maintained late replicating in S phase through the lifetime of the organism. *Xist* transcription and coating of the X_i continues in somatic cells, with *Xist* RNA dissociating from the X_i in mitosis and re-coating the X in early G1 of the cell cycle[10]. Though *Xist* depletion during initiation of XCI leads to reversal of X chromosome silencing and heterochromatin formation, its deletion in somatic cells has only minor effects on X_i reactivation as the RNA acts synergistically with other repressive chromatin modifications that accumulate on the X_i during differentiation[11,12].

Transcription and spreading of *Xist* RNA along the X is a prerequisite for silencing, which is not X-restricted as silencing can spread across X:autosome translocations and transgenic *Xist* can induce silencing of neighboring autosomal DNA[12]. The spread of *Xist* RNA-mediated silencing into autosomal regions is variable and has been proposed to correlate with the density of retrotransposons belonging to the family of long interspersed elements (L1)[13]. A recent report suggested that the silencing of X-

linked L1s occurs prior to X-linked gene silencing and may promote the nucleation of heterochromatin. Conversely, specifically a subset of young L1 elements becomes transcribed upon *Xist* RNA coating and may help the local propagation of XCI[14]. In support of a functional role for L1 elements in XCI, the human X chromosome has a two-fold enrichment in L1 elements relative to autosomes[15]. Still it remains to be seen whether the behavior of these repetitive elements is a functionally important means of *Xist*-dependent facultative heterochromatin formation. In the following sections of the review we will discuss how *Xist* is regulated in pluripotent cells of the mouse.

Acquisition of pluripotency in mouse is coupled to X_i reactivation

In the mouse, XCI occurs in two forms that differ in parent-of-origin effect and in the developmental timing of initiation. Imprinted XCI, where the paternal X chromosome (X_p) is inactivated, is established in the mouse pre-implantation embryo at the four-cell stage and occurs in all cells of the pre-implantation embryo (Fig1) [16-21]. As the mid-blastocyst stage is reached (prior to implantation), imprinted XCI is reversed only in the subset of cells in the ICM that give rise to the epiblast, so that the cells that form the future embryo carry two active X chromosomes (X_aX_a) without *Xist* RNA coating[16,18,21,22] (Fig1.1). Reactivation of the X_p is a prerequisite for subsequent random XCI in the epiblast upon implantation of the blastocyst[16,18]. In contrast, the imprinted form of XCI is maintained in the extraembryonic tissues.

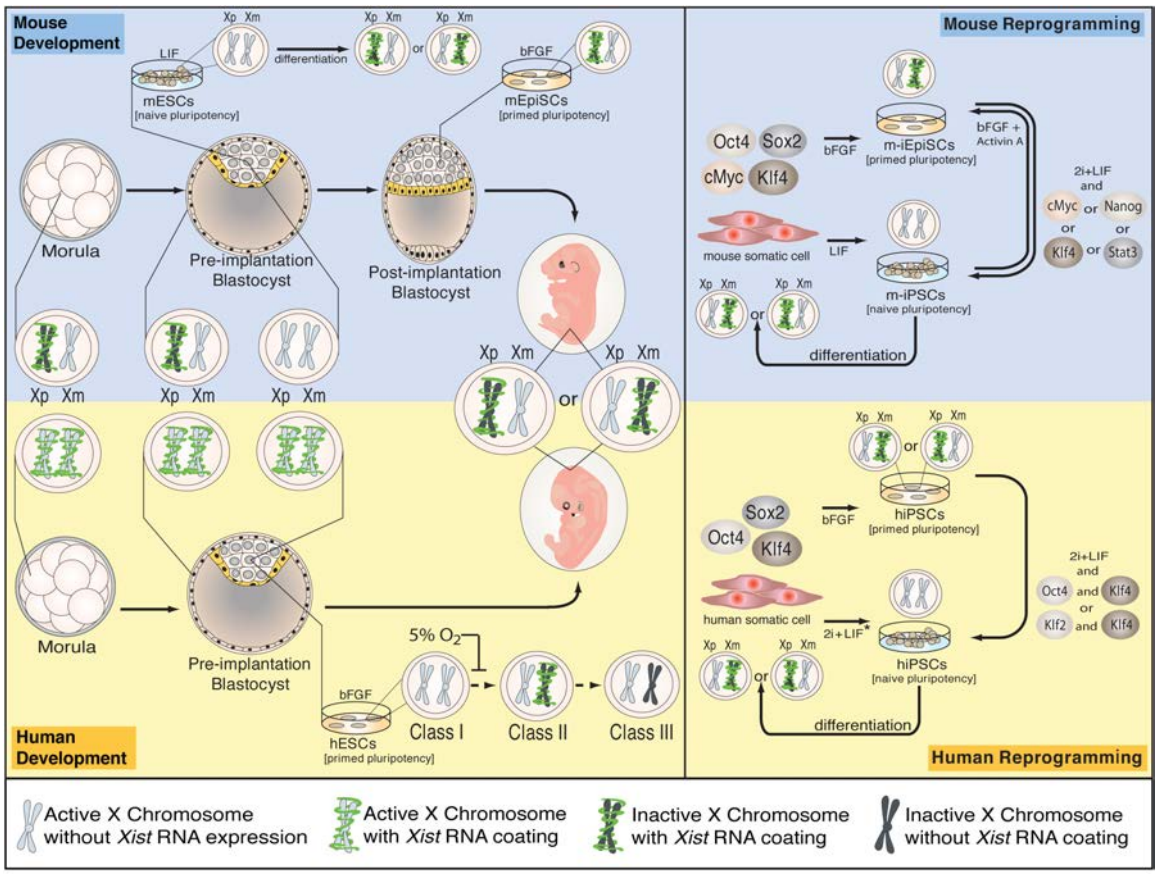

Figure 1.1 Mouse and human XCI in development and reprogramming. * The naïve human state can also be generated by overexpression of Oct4, Sox2, Nanog and Lin28 and appears to require continuous ectopic expression of reprogramming factors for stability.

Random and imprinted XCI differ in the molecular requirements for initiation and reactivation. *In vivo* evidence shows that, though *Xist* RNA coats the X_p, it is not required when imprinted XCI first occurs at the four-cell stage (as it is for random XCI). Rather, *Xist* RNA coating is needed to complete and stabilize the silencing of the imprinted X_i[17,19,20]. With respect to X_i reactivation, a recent study demonstrates that the reactivation of the imprinted X_p occurs in two steps, with induction of biallelic expression of X-linked genes preceding the disappearance of *Xist* RNA coating, in agreement with the notion that *Xist* RNA coating and silencing of the X_p are uncoupled at this point in development[21]. The mechanisms that lead to gene activation on the X_p and *Xist* silencing are still unclear but linked to the specification of the epiblast lineage, as pre-implantation embryos lacking the pluripotency transcription factor Nanog are unable to specify the

epiblast lineage and do not induce the loss of *Xist* RNA coating and Polycomb protein enrichment on the X_i[22]. Nanog appears to be directly involved in the regulation of *Xist* because pre-implantation embryos with a genetically engineered overexpression of Nanog lose *Xist* RNA more rapidly, though without affecting the timing of X_p reactivation[21]. However, Nanog may not be sufficient for this effect on *Xist* as Nanog is already present in the X_i-bearing cells of the late morula and becomes restricted as the pluripotent X_aX_a epiblast lineage forms, indicating that other epiblast-linked mechanisms must synergize with Nanog to control *Xist* repression[21,22].

It is now appreciated that X chromosome reactivation (XCR) also occurs during the experimentally induced acquisition of pluripotency through either transcription factor-induced reprogramming to induced pluripotent stem cells (iPSCs), somatic cell nuclear transfer, or ESC/somatic cell fusion[23-25]. XCR during reprogramming of mouse somatic cells to iPSCs leads to loss of heterochromatic marks of the X_i and *Xist* repression, such that random XCI is observed upon differentiation of mouse (m) iPSCs, as in mESCs[23] (Fig1.1). It has been demonstrated that XCR is a late event in miPSC reprogramming, occurring at around the time of pluripotency gene activation[26], but insight into the mechanism and the events leading to X_i reactivation is still lacking. Nevertheless, the establishment of pluripotency both *in vitro* via reprogramming and *in vivo* during the establishment of the epiblast lineage in pre-implantation embryos, is coupled to XCR and *Xist* repression. Therefore, the X_aX_a state is a key attribute of the pluripotent state of mESCs and miPSCs.

Importantly, studies with a doxycycline-inducible *Xist* transgene have shown that *Xist*-dependent gene silencing is possible in undifferentiated male and female mESCs, but no longer after induction of differentiation or in somatic cells[12]. This observation illustrates that *Xist* function is context-dependent but not with respect to sex, as factors required for the silencing process are present in male and female undifferentiated

mESCs. Since the active state of the X chromosomes must therefore be ensured by strong transcriptional repression of *Xist* in mESCs, one can view initiation of XCI upon differentiation of mESCs from the perspective of loss of *Xist* repression.

Xist is regulated by its antisense transcript *Tsix*

A major antagonizing factor to *Xist* in mESCs is another long noncoding RNA, *Tsix*, transcribed antisense to *Xist* specifically in mESCs and downregulated first on the X_i and then on the X_a during differentiation[27] (Fig1.2). Loss of *Tsix* function on one of the two female X's leads to slight upregulation of *Xist* transcript levels in undifferentiated mESCs and skewing of XCI towards the *Tsix*-deleted X upon differentiation[28,29]. These observations suggest that *Tsix* mainly regulates the monoallelic induction of *Xist* in the choice aspect of XCI. In support of this idea, live-cell imaging of differentiating female ESCs carrying X chromosomes tagged with a tetO array bound by a tetR-mCherry fusion confirmed a previously shown transient pairing of homologous *Xist*/*Tsix* regions of the two X chromosomes and demonstrated that this interaction is associated with exclusive deafening of the *Tsix* allele on the future X_i, which is proposed to allow upregulation of *Xist*[30-32]. *Tsix* antagonism of *Xist* requires transcription through the *Xist* locus and the mechanism is suggested to involve change in the chromatin structure around the *Xist* 5' regulatory region[33,34] Together these findings indicate that *Tsix* is not the only repressor of *Xist* in pluripotency and other factors must be involved in keeping *Xist* downregulated (Fig1.2).

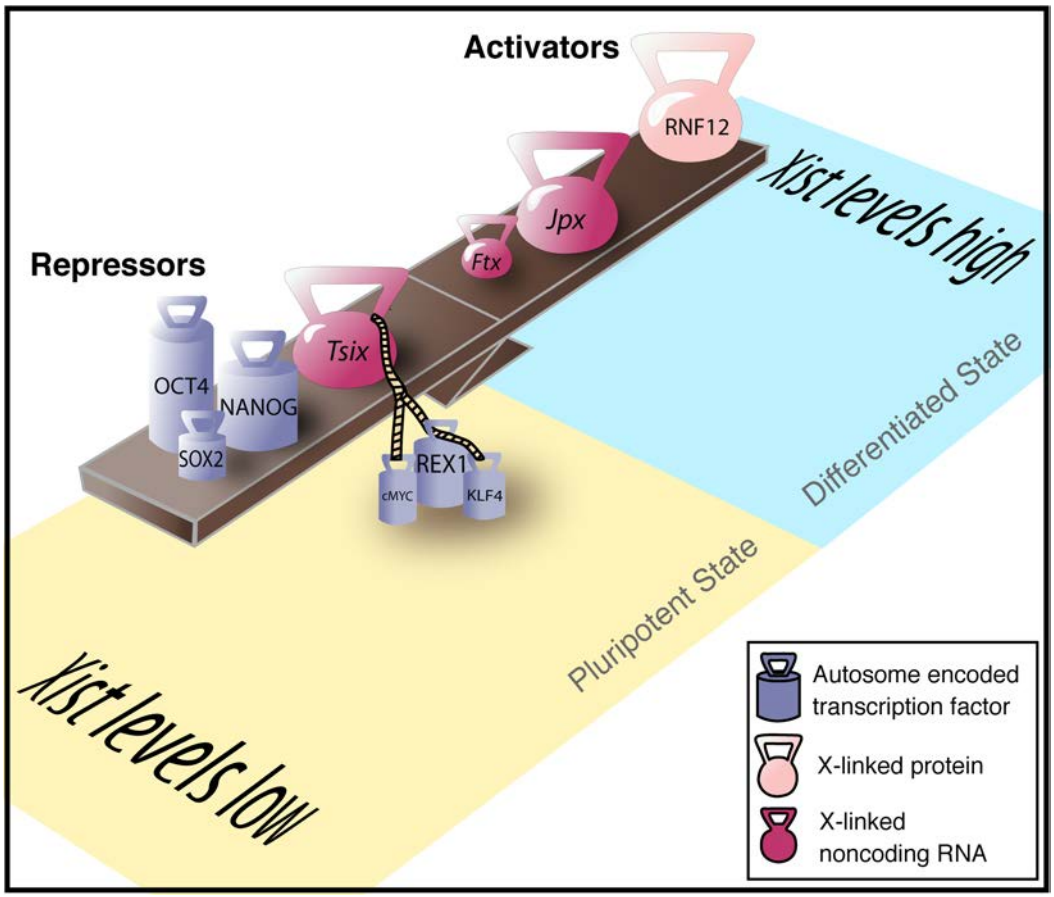

Figure 1.2. *Xist* activators and repressors regulate initiation of XCI in mESCs. *Xist* levels are low in undifferentiated mESCs before onset of XCI, because of pluripotency transcription factors repressing *Xist* directly or indirectly via *Tsix*. X-linked *Xist* activators increase *Xist* levels during differentiation, as they themselves are upregulated. Levels of autosomal factors such as pluripotency transcription factors decrease upon differentiation. Sizes and positions of weights are reflective of magnitude of *Xist*-up or downregulation phenotypes from experimental data (see text for discussion).

Pluripotency transcription factors directly repress XCI in ESCs

Oct4, Sox2, and Nanog form a transcription factor triad that is key to maintaining ESC identity by activating genes of the self-renewal program and repressing lineage commitment genes. An attractive hypothesis for how pluripotency is directly linked to *Xist* repression has come from a study that demonstrates binding of Oct4, Sox2 and Nanog to the first intron (intron1) of *Xist* in male and female mESCs and loss of this interaction upon differentiation[35]. Intriguingly, depletion of Nanog or Oct4 leads to inappropriate *Xist* upregulation in male mESCs or biallelic *Xist* upregulation in differentiating female mESCs[35,36]. It is still an open question whether specific binding at intron1 is at the heart of this XCI phenotype as these pluripotency transcription factors bind and regulate

thousands of loci in the genome to maintain pluripotency. Mechanistically, the repressive function binding to intron1 has on *Xist* expression remains unclear, though one possibility is modification of the three-dimensional chromatin configuration within the *Xist* locus[37].

Already one study reports no effect of heterozygous deletion of intron1 and a very subtle skewing of XCI to the intron1-deleted X chromosome late in differentiation[38]. Conceivably, synergism of pluripotency factor binding to intron1 of *Xist* as well as other regulatory regions could suppress XCI in mESCs. In line with this model, *Tsix* transcription, particularly transcriptional elongation, is dependent upon binding of the pluripotency transcription factors Rex1, Klf4, and cMyc, within a mini-satellite region of the regulatory region of the gene, and to a lesser extent by binding of Oct4 and Sox2, with the latter being somewhat debated [36,39]. Thus, the pluripotency network may directly repress *Xist* and activate *Tsix,* which in turn contributes to the suppression of *Xist* and XCI (Fig1.2), an idea that could be tested with double knockout studies of intron1 and *Tsix*. Nevertheless, it may be challenging to pinpoint a role of pluripotency regulators in XCI especially as additional *Xist* activators and repressors are discovered (see below) and transactivation or repression of these other factors by pluripotency regulators may indirectly exert XCI effects.

XCI in differentiating female mouse ESCs is governed by a balance of *Xist* activators and repressors

The mechanisms governing *Xist* upregulation during XCI must also ensure that only one X is silenced in female cells during differentiation. In addition to the X:X pairing model described above, another model proposes that in random XCI every individual X has an independent probability to initiate silencing, and this probability is proportional to the X:autosome ratio, keeping one X active per diploid chromosome set[40]. Accordingly,

repressors of XCI would be autosomally encoded and activators would be X-linked. In XX cells, the double dose of the activator would stimulate *Xist* upregulation and XCI on one X, and the reciprocal *cis* silencing of the X-linked activator gene would in turn protect the other X from inactivation[40].

Rnf12, the first such characterized X-linked activator of XCI, resides ~500 kilobases from *Xist*, and encodes an E3 ubiquitin ligase bearing a RING domain. In line with a role in the initiation of XCI, Rnf12 protein levels increase in differentiation and overexpression of Rnf12 stimulates ectopic XCI[41]. The heterozygous mutation of *Rnf12* in female mESCs reduces the number of female cells undergoing XCI, however, it remains unclear if there is an essential requirement for Rnf12 in random XCI as the two published homozygous knockout strategies show contrasting results of delayed differentiation and dramatic loss of XCI[38,41,42]. These differences may be attributed to differentiation protocols as the late appearance of *Xist* RNA cloud-positive cells suggests a selective outgrowth of cells undergoing XCI independently of Rnf12. Gene expression profiling suggests Rnf12 acts on *Xist*, as *Xist* was the only transcript significantly downregulated in Rnf12 knockout cells[38]. Proteomic studies will likely be necessary to see if Rnf12 plays an indirect role in XCI through ubiquitylation targets.

Two additional noncoding RNAs have recently also been identified as X-linked *Xist* activators. *Jpx*, located upstream of *Xist,* escapes XCI and increases ~10-fold during mESC differentiation. Its heterozygous deletion leads to loss of XCI and subsequent cell death upon embryoid body differentiation of female X_aX_a mESCs[43]. These phenotypes can be rescued by an autosomal *Jpx* transgene, indicating that this novel gene can function in *trans*, which contrasts *Xist* and *Tsix*[43]. Strikingly, the double knockout of *Jpx* and *Tsix* completely restores XCI kinetics and viability and will be exciting to see how this observation and the mechanistic action of *Jpx* is explained[43]. Like *Jpx*, the noncoding transcript encoded by the neighboring *Ftx* gene is also

transcriptionally upregulated with female mESC differentiation. Targeted deletion of *Ftx* suggests that its role is in controlling the chromatin structure of the *Xist* promoter[44]. It is tempting to speculate that continuous expression of these noncoding transcripts may be necessary for *Xist* itself to escape XCI. *Rnf12* and *Jpx* are both bound by Oct4, Sox2, and Nanog in mESCs, suggesting that pluripotency factors could also act on XCI through these X-linked activators[45].

In summary, the activation of *Xist*, repression of *Tsix*, and XCI during mESC differentiation depends on the downregulation of pluripotency factors and the expression of X-linked activators such as Rnf12, *Jpx* and *Ftx,* linking XCI status to the global pluripotency gene-expression network and ensuring sex-specificity of the developmental process.

XCI in human development

Studies on XCI in human pluripotent cells have been more limited in scope because of technical challenges in manipulating human pre-implantation embryos and the ethical challenges of acquiring them. However, studies of XCI in the human system remain essential because the XCI process appears to be different from that in mouse. For instance, human pre-implantation embryos demonstrate *XIST* expression from both X chromosomes and human full-term placentas have random, rather than imprinted XCI found in mouse[46,47] (Fig1.1).

RNA fluorescence in situ hybridization (FISH) shows *XIST* activation as a transition from a pinpoint signal to a '*XIST* RNA cloud' that can be appreciated in human female pre-implantation embryos as early as the eight-cell stage[48]. In one study, the majority of these *XIST* RNA-coated chromosomes show features of transcriptional silencing and enrichment of *XIST*-dependent repressive histone marks in the morula[48]. Contradictory results come from a more recent study which finds that the trophectoderm and the inner

cell mass of both female and male human pre-implantation blastocysts carry active X chromosomes coated by *XIST* RNA[49]. The discrepancy between the two studies may be due to different culture conditions as well as hybridization efficiencies in the FISH procedure. Regardless, it appears there is no imprinted XCI in human embryogenesis, that human XCI has different developmental timing, and that *XIST* RNA coating of the X and XCI are uncoupled in early human embryos (Fig1.1).

Studies of additional factors involved in human XCI are limited to *TSIX,* which may not play a functional role in human cells. *TSIX* is transcribed in fetal cells, term placenta, and human ESCs but is truncated and lacks the CpG island essential for expression in mouse cells[50,51]. Since in human pre-Implantation development *XIST* expression appears to be uncoupled from XCI, *TSIX*-mediated regulation may be unnecessary. However, *TSIX* has not been studied in human pre-implantation blastocysts nor during initiation of XCI, therefore a potential role may have been missed[52]. Other modulators of XCI in mouse, namely *JPX, FTX,* and RNF12, have been mapped in the human genome but their functions have not yet been tested, mostly due to the lack of an *in vitro* system that allows their mechanistic dissection (see below).

Different XCI states are found in human ESCs

XCI state in human (h) ESCs is complicated by a gradual drift so that one hESC line can exhibit different states of XCI[53-56]. hESCs are grouped into three classes to describe the XCI states that are typically observed (Fig1.1)[53]. Class I hESCs are X_aX_a and upregulate *XIST* and undergo XCI upon differentiation, similar to mESCs. This class seems to be the most difficult to stabilize *in vitro* because they readily transition to class II, which have initiated XCI already in the undifferentiated state and carry a *XIST*-coated X_i. Class II hESCs often further transition to class III where the silent state of the X_i is largely maintained but *XIST* is lost from the X_i along with the *XIST*-dependent histone

mark H3K27me^3 which leads to partial reactivation of some X_i-linked genes[54,56]. *XIST* likely becomes silenced by methylation of its promoter region, and class III hESCs do not re-express *XIST* upon differentiation[57,53]. Given that both class I and III hESCs do not express *XIST* and lack an X_i enrichment of H3K27me^3, extrapolating the XCI state solely on the basis of lack of *XIST* RNA FISH or H3K27me^3 signal or even global gene expression data, has obfuscated the collective understanding of XCI in hESCs. Rather, characterization of XCI in hESC requires validation against the gold-standard assays of RNA FISH for mono- or biallelic expression of X-linked genes in addition to *XIST*.

hESCs derived and maintained in hypoxia, which is thought to better represent physiologic oxygen tension in development, preferentially remain in class I as demonstrated by RNA FISH for *XIST* and X-linked genes[56]. A switch to atmospheric oxygen tensions leads to irreversible transition to class II and subsequently to class III, strengthening the observation that female hESCs are unstable with respect to their XCI state (Fig1.1)[56]. It will be important to determine whether this fluctuating XCI status is indicative of global epigenetic instability in hESCs.

X chromosome state in human iPSCs

Like in the mouse, human (h) iPSCs are similar to their hESC equivalent based on functional assays of pluripotency, genome-wide expression and chromatin analysis, and XCI state. At early passage, hiPSCs are class II (X_aX_i with *XIST* RNA coating) which readily transition to class III as *XIST* RNA is lost from the X_i (Fig1.1)[58]. The same X chromosome is inactivated in all cells of a given hIPSC line reflecting the origin from a single somatic cell[58,59]. These results suggest the absence of X_i reactivation during human cell reprogramming and enable the generation of hiPSC lines expressing either only the X_m or X_p[58]. Such approaches have allowed for generation of genetically-matched hiPSC lines expressing either the mutant or wild-type X-linked gene MECP2

from fibroblasts of female patients with Rett syndrome[59,60]. However, complete skewing of XCI to one X chromosome occurs upon extended passaging of fibroblasts, preventing the generation of hiPSC lines with different X chromosomes inactivated[59]. Two contradictory studies that report X_i reactivation in a subset of hiPSC lines have not performed the single cell FISH analysis of X-linked gene expression, and the skewed XCI in neurons generated from hiPSCs in one of the studies would be consistent with the lack of X_i reactivation[61,62]. Nevertheless, these results do not exclude that different culture and reprogramming conditions could lead to XCR during hiPSC induction.

Naïve versus primed pluripotency

The different XCI states in mouse and human ESCs and iPSCs suggest that either there have been significant changes to XCI in mammalian evolution or, alternatively, that these XCI states are reflective of two different developmental states 'suspended' *ex vivo* through current ESC culturing techniques. Although pluripotent cells by definition can give rise to cells of all three germ layers, distinct states of pluripotency have recently been described *in vitro,* represented by mESCs and mouse epiblast stem cells (mEpiSCs). mESCs, derived from epiblast cells of pre-implantation blastocysts, are cultured in the presence of the cytokine LIF whereas mEpiSCs are obtained from post-implantation epiblast and cultured in the growth factor bFGF, in the absence of LIF. Since mEpiSCs express genes associated with early events in differentiation they are considered to be in the "primed" pluripotent state, whereas the typical mESC is in the "naïve" pluripotent state[63]. mEpiSCs resemble class II hESC/iPSCs in many aspects including their flat colony morphology, bFGF culture requirement, and the presence of an X_i coated by *Xist* RNA and enriched for $H3K27me^3$ and the Polycomb protein Ezh2[64-66]. X_iX_a mEpiSCs can also be generated from pre-implantation blastocysts cultured with bFGF (just like hESCs), differentiated from mESCs with bFGF and Activin A, and

obtained via reprogramming of fibroblasts with Oct4, Sox2, Klf4 and cMyc in bFGF-containing media as opposed to LIF[66-68] (Fig1.1B). Together, the parallels between hESCs and mEpiSCs suggest that the culture of human pluripotent cells has been optimized for the primed state and not for the naïve state.

More research is necessary to molecularly define whether mEpiSCs exhibit different types of XCI states as do hESCs/iPSCs. Interestingly, it appears that compared with mouse fibroblasts, the form of XCI in mEpiSCs is a developmental intermediate and more labile with regard to reactivation based on studies transplanting nuclei into xenopus germinal vesicles[65]. In this reprogramming system, the X_i of female mEpiSCs is receptive to nuclear reprogramming whereas the mouse fibroblast macroH2A-enriched X_i is resistant[65].

Molecular manipulation can transition mEpiSCs to the naïve pluripotent state and these approaches have been extended to the human system to generate X_aX_a hESCs and hiPSCs. The reprogramming of mEpiSCs to an mESC-like state is achieved through a combination of ectopic expression of any one of the transcription factors Klf4, cMyc, Stat3 or Nanog and addition of LIF and 2i (a combination of two small molecules inhibiting GSK3β in the Wnt signaling pathway and mitogen-activated protein kinase signaling, which is thought to promote naïve pluripotency) (Fig1.1)[22,66,69-71]. A subsequent study applied this approach to hESCs and found similar requirements for acquisition of naïve pluripotency in primed hESCs when Klf4 and Klf2 or Klf4 and Oct4 are overexpressed[72]. Prolonged maintenance of the naïve human pluripotent state appears to depend on constitutive overexpression of the reprogramming factors, indicating that the naïve human state is metastable[72,59]. As expected from the mouse system, naïve human pluripotent stem cells are X_aX_a without *XIST* expression, and diverge from primed pluripotent cells in both culture requirements and molecular profile as determined by gene expression microarrays[72]. As in mouse, *XIST* is re-expressed and random XCI

initiated upon differentiation of naïve human cells[59,72]. The derivation of X_aX_a human pluripotent cells, either in the primed state under hypoxic conditions or in the naïve state, should in the future allow the modeling of initiation of XCI *ex vivo*.

Yet, the relevance of modeling human XCI *ex vivo* for the XCI process occurring during human embryonic development is still unclear. During derivation and culture of human pluripotent cells, the XCI state diverges from that described for pre-implantation embryos, as the X_aX_a pattern with biallellic *XIST* coating of pre-implantation embryos has not been detected in cell cultures *ex vivo*. Therefore more studies are warranted but, with the approaches of these recent studies, we can already begin to define the molecular interplay of pluripotency and XCI, akin to the mouse system, and extend these findings to optimize reprogramming to pluripotency.

CHAPTER 1 REFERENCES

1. Penny GD, Kay GF, Sheardown SA et. al. Requirement for Xist in X chromosome inactivation. **NATURE**. 1996;379(6561):131–137.

2. Marahrens Y, Panning B, Dausman J et. al. Xist-deficient mice are defective in dosage compensation but not spermatogenesis. **GENES AND DEVELOPMENT** 1997;11(2):156-166.

3. Brockdorff N, Ashworth A, Kay GF et. al. Conservation of position and exclusive expression of mouse Xist from the inactive X chromosome. **NATURE**. 1991;351(6324):329-331.

4. Brown CJ, Ballabio A, Rupert JL et al. A gene from the region of the human X inactivation center is expressed exclusively from the inactive X chromosome. **NATURE**. 1991;349(6304):38–44.

5. Sun BK, Deaton AM, Lee JT. A transient heterochromatic state in Xist preempts X inactivation choice without RNA stabilization. **MOLECULAR CELL**. 2006;21(5):617–628.

6. Panning B, Jaenisch R. DNA hypomethylation can activate Xist expression and silence X-linked genes. **GENES AND DEVELOPMENT.** 1996;10(16):1991-2002.

7. Jeon Y, Lee JT. YY1 tethers Xist RNA to the inactive X nucleation center. **CELL** 2011;146(1):119-133.

8. Chaumeil J, Le Baccon P, Wutz A et.al. A novel role for Xist RNA in the formation of a repressive nuclear compartment into which genes are recruited when silenced. **GENES AND DEVELOPMENT.** 2006;20(16):2223–2237.

9. Chow J, Heard E. X inactivation and the complexities of silencing a sex chromosome. **CURRENT OPTION IN CELL BIOLOGY**. 2009;21(3):359-366.

10. Clemson CM, McNeil JA, Willard HF et. al. XIST RNA paints the inactive X chromosome at interphase: evidence for a novel RNA involved in nuclear/chromosome structure. **THE JOURNAL OF CELL BIOLOGY.** 1996;132(3):259–275.

11. Csankovszki G, Nagy A, Jaenisch R. Synergism of Xist RNA, DNA methylation, and histone hypoacetylation in maintaining X chromosome inactivation. **THE JOURNAL OF CELL BIOLOGY.** 2001;153(4):773–784.

12. Wutz A. A shift from reversible to irreversible X inactivation is triggered during ES cell differentiation. **MOLECULAR CELL**. 2000; Apr;5(4):695-705.

13. Lyon MF. X-chromosome inactiavtion: a repeat hypothesis. **CYTOGENETICS AND CELL GENETICS**. 1998;80(1-4):133-137.

14. Chow JC, Ciaudo C, Fazzari MJ et al. LINE-1 Activity in Facultative Heterochromatin Formation during X Chromosome Inactivation. **CELL**. 2010;141(6):956–969.

15. Bailey JA, Carrel L, Chakravarti A, Eichler EE. Molecular evidence for a relationship between LINE-1 elements and X chromosome inactivation: the Lyon repeat hypothesis.

PROCEEDINGS OF THE NATIONAL ACADEMY OF SCIENCES. 200;97(12):6634-6639.

16. Okamoto I, Otte A, Allis C et.al. Epigenetic dynamics of imprinted X inactivation during early mouse development. **SCIENCE**. 2004;303(5658):644-649.

17. Kalantry S, Purushothaman S, Bowen RB et. al. Evidence of Xist RNA-independent initiation of mouse imprinted X-chromosome inactivation. **NATURE**. 2009;460(7255):647–651.

18. Mak W, Nesterova TB, de Napoles M et al. Reactivation of the paternal X chromosome in early mouse embryos. **SCIENCE**. 2004;303(5658):666–669.

19. Namekawa SH, Payer B, Huynh KD et. al. Two-Step Imprinted X Inactivation: Repeat versus Genic Silencing in the Mouse. **MOLECULAR AND CELLULAR BIOLOGY**. 2010;30(13):3187–3205.

20. Patrat C, Okamoto I, Diabangouaya P et al. Dynamic changes in paternal X-chromosome activity during imprinted X-chromosome inactivation in mice. **PROCEEDINGS OF THE NATIONAL ACADEMY OF SCIENCES**. 2009;106(13):5198–5203

21. Williams LH, Kalantry S, Starmer J et al. Transcription precedes loss of Xist coating and depletion of H3K27me3 during X-chromosome reprogramming in the mouse inner cell mass. **DEVELOPMENT.** 2011; 138(10):2049-2057.

22. Silva J, Nichols J, Theunissen TW et al. Nanog Is the Gateway to the Pluripotent Ground State. **CELL**. 2009;138(4):722–737.

23. Maherali N, Sridharan R, Xie W, et al. Directly reprogrammed fibroblasts show global epigenetic remodeling and widespread tissue contribution. **CELL STEM CELL.** 2007;1(1):55–70.

24. Eggan K, Akutsu H, Hochedlinger K et. al. X-Chromosome inactivation in cloned mouse embryos. **SCIENCE**. 2000 Nov 24;290(5496):1578-1581.

25. Tada M, Takahama Y, Abe K et. al. Nuclear reprogramming of somatic cells by in vitro hybridization with ES cells. **CURRENT BIOLOGY**. 2001 ;11(19):1553-1558.

26. Stadtfeld M, Maherali N, Breault DT, Hochedlinger K. Direct molecular cornerstones during fibroblast to iPS cell reprogramming in mouse. **CELL STEM CELL.** 2008;2(3):230-240.

27. Lee JT, Davidow LS, Warshawsky D. Tsix, a gene antisense to Xist at the X-inactivation centre. **NATURE GENETICS**. 1999;21(4):400-404.

28. Lee JT, Lu N. Targeted mutagenesis of Tsix leads to nonrandom X inactivation. **CELL**. 1999;99(1):47–57.

29. Sado T, Wang Z, Sasaki H et. al. Regulation of imprinted X-chromosome inactivation in mice by Tsix. **DEVELOPMENT**. 2001;128(8):1275–1286.

30. Masui O, Bonnet I, Le Baccon P et al. Live-Cell Chromosome Dynamics and Outcome of X Chromosome Pairing Events during ES Cell Differentiation. **CELL**. 2011;145(3):447–458.

31. Xu N, Tsai C, Lee J. Transient homologous chromosome pairing marks the onset of X inactivation. **SCIENCE**. 2006 ;311(5764):1149-1152.

32. Bacher C, Guggiari M, Brors B et. al. Transient colocalization of X-inactivation centres accompanies the initiation of X inactivation. **NATURE CELL BIOLOGY.** 2006;8(3):293-299.

33. Sado T, Hoki Y, Sasaki H. Tsix silences Xist through modification of chromatin structure. **DEVELOPMENTAL CELL**. 2005;9(1):159-165.

34. Navarro P, Pichard S, Ciaudo C et. al. Tsix transcription across the Xist gene alters chromatin conformation without affecting Xist transcription: implications for X-chromosome inactivation. **GENES AND DEVELOPMENT**. 2005;19(12):1474-1484.

35. Navarro P, Chambers I, Karwacki-Neisius V et. al. Molecular coupling of Xist regulation and pluripotency. **SCIENCE** 2008;321(5896):1693-1695.

36. Donohoe ME, Silva SS, Pinter SF et al. The pluripotency factor Oct4 interacts with Ctcf and also controls X-chromosome pairing and counting. **NATURE**. 2009;460(7251):128–132.

37. Tsai C, Rowntree R, Cohen D et al. Higher order chromatin structure at the X-inactivation center via looping DNA. **DEVELOPMENTAL BIOLOGY**. 2008;319(2):416–425.

38. Barakat TS, Gunhanlar N, Pardo CG et al. RNF12 activates Xist and is essential for X chromosome inactivation. **PLOS GENETICS**. 2011;7(1):e1002001.

39. Navarro P, Oldfield A, Legoupi J et al. Molecular coupling of Tsix regulation and pluripotency. **NATURE**. 2010;468(7322):457–460.

40. Monkhorst K, Jonkers I, Rentmeester E et. al. X inactivation counting and choice is a stochastic process: evidence for involvement of an X-linked activator. **CELL**. 2008;132(3):410-421.

41. Jonkers I, Barakat T, Achame E et al. RNF12 is an X-Encoded dose-dependent activator of X chromosome inactivation. **CELL**. 2009;139(5):999–1011.

42. Shin J, Bossenz M, Chung Y et al. Maternal Rnf12/RLIM is required for imprinted X-chromosome inactivation in mice. **NATURE**. 2010;467(7318):977–981.

43. Tian D, Sun S. The Long Noncoding RNA, Jpx, Is a Molecular Switch for X Chromosome Inactivation. **CELL**. 2010 ;143(3):390-403.

44. Chureau C, Chantalat S, Romito A et al. Ftx is a non-coding RNA which affects Xist expression and chromatin structure within the X-inactivation center region. **HUMAN MOLECULAR GENETICS**. 2011;20(4):705–718.

45. Chen X, Xu H, Yuan P et al. Integration of external signaling pathways with the core transcriptional network in embryonic stem cells. **CELL**. 2008;133(6):1106–1117.

46. Daniels R, Zuccotti M, Kinis T et al. XIST Expression in Human Oocytes and Preimplantation Embryos. **THE AMERICAN JOURNAL OF HUMAN GENETICS**. 1997;61(1):33–39.

47. de Mello J, de Araújo É, Stabellini R et al. Random X Inactivation and Extensive Mosaicism in Human Placenta Revealed by Analysis of Allele-Specific Gene Expression along the X Chromosome. **PLOS ONE** 2010;5(6):e10947.

48. van den Berg IM, Laven JSE, Stevens M et al. X Chromosome Inactivation Is Initiated in Human Preimplantation Embryos. **AMERICAN JOURNAL OF HUMAN GENETICS.** 2009;84(6):771–779.

49. Okamoto I, Patrat C, Thépot D et al. Eutherian mammals use diverse strategies to initiate X-chromosome inactivation during development. **NATURE**. 2011;472(7343):370–374.

50. Migeon BR, Chowdhury AK, Dunston JA et al. Identification of TSIX, encoding an RNA antisense to human XIST, reveals differences from its murine counterpart: implications for X inactivation. **AMERICAN JOURNAL OF HUMAN GENETICS**. 2001;69(5):951–960.

51. Migeon BR, Lee CH, Chowdhury AK et al. Species differences in TSIX/Tsix reveal the roles of these genes in X-chromosome inactivation. **AMERICAN JOURNAL OF HUMAN GENETICS**. 2002;71(2):286–293.

52. Migeon BR. Is Tsix repression of Xist specific to mouse? **NATURE GENETICS**. 2003;33(3):337; author reply 337–338.

53. Silva S, Rowntree R, Mekhoubad S et al. X-chromosome inactivation and epigenetic fluidity in human embryonic stem cells. **PROCEEDINGS OF THE NATIONAL ACADEMY OF SCIENCES**. 2008;105(12):4820-4825.

54. Shen Y, Matsuno Y, Fouse SD et al. X-inactivation in female human embryonic stem cells is in a nonrandom pattern and prone to epigenetic alterations. **PROCEEDINGS OF THE NATIONAL ACADEMY OF SCIENCES** 2008;105(12):4709–4714.

55. Dvash T, Lavon N, Fan G. Variations of X Chromosome Inactivation Occur in Early Passages of Female Human Embryonic Stem Cells. **PLOS ONE**. 2010 ;5(6):e11330.

56. Lengner CJ, Gimelbrant AA, Erwin JA et al. Derivation of Pre-X Inactivation Human Embryonic Stem Cells under Physiological Oxygen Concentrations. **CELL**. 2010;141(5):872–883.

57. Dvash T, Fan G. Epigenetic regulation of X-inactivation in human embryonic stem cells. **EPIGENETICS**. 2009;4(1):19–22.

58. Tchieu J, Kuoy E, Chin MH et al. Female Human iPSCs Retain an Inactive X Chromosome. **CELL STEM CELL**. 2010;7(3):329–342.

59. Pomp O, Dreesen O, Leong D et. al. Unexpected X Chromosome Skewing during Culture and Reprogramming of Human Somatic Cells Can Be Alleviated by Exogenous Telomerase. **CELL STEM CELL.** 2011**;***9*:156–165.

60. Cheung AYL, Horvath LM, Grafodatskaya D et al. Isolation of MECP2-null Rett Syndrome patient hiPS cells and isogenic controls through X-chromosome inactivation. **HUMAN MOLECULAR GENETICS.** 2011;20(11):2103–2115.

61. Marchetto MCN, Carromeu C, Acab A et al. A Model for Neural Development and Treatment of Rett Syndrome Using Human Induced Pluripotent Stem Cells. **CELL**. 2010;143(4):527–539.

62. Kim K-Y, Hysolli E, and Park IH. Neuronal maturation defect in induced pluripotent stem cells from patients with Rett syndrome. **PROCEEDINGS OF THE NATIONAL ACADEMY OF SCIENCES.** 2011;108(33):1-6.

63. Nichols J, Smith A. Naive and Primed Pluripotent States. **CELL STEM CELL**. 2009;4(6):487–492

64. Tesar P, Chenoweth J, Brook F et al. New cell lines from mouse epiblast share defining features with human embryonic stem cells. **NATURE**. 2007;448(7150):196–199.

65. Pasque V, Gillich A, Garrett N et al. Histone variant macroH2A confers resistance to nuclear reprogramming. **THE EMBO JOURNAL**. 2011;30(12): 2373-2387.

66. Guo G, Yang J, Nichols J et al. Klf4 reverts developmentally programmed restriction of ground state pluripotency. **DEVELOPMENT**. 2009;136(7):1063–1069.

67. Najm FJ, Chenoweth JG, Anderson PD et al. Isolation of epiblast stem cells from preimplantation mouse embryos. **CELL STEM CELL**. 2011;8(3):318-25.

68. Han DW, Greber B, Wu G et al. Direct reprogramming of fibroblasts into epiblast stem cells. **NATURE CELL BIOLOGY**. 2010 ;13(1):66-71

69. Bao S, Tang F, Li X et al. Epigenetic reversion of post-implantation epiblast to pluripotent embryonic stem cells. **NATURE**. 2009;461(7268):1292–1295.

70. Hanna J, Markoulaki S, Mitalipova M et al. Metastable Pluripotent States in NOD-Mouse-Derived ESCs. **CELL STEM CELL**. 2009;4(6):513–524.

71. Yang J, Oosten ALV, Theunissen TW et al. Stat3 Activation Is Limiting for Reprogramming to Ground State Pluripotency. **CELL STEM CELL**. 2010;7(3):319–328.

72. Hanna J, Cheng AW, Saha K et al. Human embryonic stem cells with biological and epigenetic characteristics similar to those of mouse ESCs. **PROCEEDINGS OF THE NATIONAL ACADEMY OF SCIENCES.** 2010;107(20):9222–9227.

CHAPTER 2

THE ROLE OF *XIST* INTRON1

The pluripotency factor-bound intron 1 of *Xist* is dispensable for X chromosome inactivation and reactivation *in vitro* and *in vivo*

Summary

X chromosome inactivation (XCI) is a dynamically-regulated developmental process with inactivation and reactivation accompanying the loss and gain of pluripotency, respectively. A functional relationship between pluripotency and lack of XCI has been suggested, whereby pluripotency transcription factors repress the master regulator of XCI, the noncoding transcript *Xist*, by binding to its first intron (intron1). To test this model, we have generated intron1-mutant embryonic stem cells (ESCs) and two independent mouse models. We found that *Xist's* repression in ESCs, its transcriptional upregulation upon differentiation, and its silencing upon reprogramming to pluripotency are not dependent on intron1. Although we observed subtle effects of intron1-deletion on the randomness of XCI and in the absence of the antisense transcript *Tsix* in differentiating ESCs, these have little relevance *in vivo* as mutant mice do not deviate from Mendelian ratios of allele transmission. Together, our findings demonstrate that intron1 is dispensable for the developmental dynamism of *Xist* expression.

Introduction

To balance the expression of X-linked genes between males and females, female mammals silence one of the two X chromosomes in a developmentally regulated process called X chromosome inactivation (XCI). XCI occurs in two waves in the course of mouse embryogenesis. The earliest form of XCI is imprinted as it is selective for the paternally-inherited X chromosome (Xp) and starts at the 2-4 cell stage in pre-implantation embryo (Huynh and Lee, 2003; Kalantry et al., 2009; Namekawa et al., 2010; Patrat et al., 2009). At the pre-implantation blastocyst stage, imprinted XCI is retained in the trophectoderm and primitive endoderm lineages, but reversed in arising pluripotent epiblast cells yielding a state with two active X chromosomes (XaXa) (Mak et al., 2004; Okamoto et al., 2004; Silva et al., 2009; Williams et al., 2011). Upon

implantation, these epiblast cells establish a random form of XCI that stochastically initiates on the maternal or paternal X chromosome and is retained through the lifetime of mitotic divisions (Kay et al., 1993; Rastan and Robertson, 1985). Similarly, mouse embryonic stem cells (ESCs), which are derived from epiblast cells of the pre-implantation blastocyst, undergo random XCI when induced to differentiate *ex vivo*. The only exception to somatic maintenance of random XCI is inactive X (Xi) reactivation in the germline, which is assumed to be essential for female fertility and occurs in primordial germ cells as they traverse the hindgut to seed the genital ridges (Chuva de Sousa Lopes et al., 2008; de Napoles et al., 2007; Sugimoto and Abe, 2007). Xi reactivation is also a feature of experimentally induced acquisition of pluripotency via transcription factor-mediated reprogramming to induced pluripotent stem cells (iPSCs), fusion of somatic cells with ESCs, or somatic cell nuclear transfer (Eggan et al., 2000; Maherali et al., 2007; Tada et al., 2001).

The cycles of X chromosome inactivation and reactivation are associated with changes in *Xist* RNA coating, where cells with a Xi display coating by the non-coding *Xist* RNA on the inactive X chromosome, and those with two active X chromosomes lack *Xist* RNA expression (Brockdorff et al., 1991; Brown et al., 1991). *Xist*'s function has been most studied in the random form of XCI in the mouse system, where it is shown to be the critical trigger of XCI. The upregulation of *Xist* RNA and coating of the X at the onset of random XCI immediately lead to transcriptional silencing of X-linked genes and result in the exclusion of RNA polymerase II and the recruitment of repressive chromatin-modifying protein complexes such as the Polycomb complex PRC2 which establishes an accumulation of H3K27me3 (Chaumeil et al., 2006; Chow and Heard, 2009; Plath et al., 2003; Silva et al., 2003). A stereotypic order of changes in chromatin structure culminates in heritable silencing of either the maternally or paternally transmitted X chromosome in each cell of the female adult mammal. *Xist* is essential for

XCI to occur *in cis* as its deletion leads to silencing of the other X chromosome carrying an intact *Xist* allele, regardless of parent-of-origin (Marahrens et al., 1997; Penny et al., 1996). Moreover, the importance of *Xist* regulation for the developmental and sex-specific context of XCI is demonstrated by its sufficiency: overexpression of a X-linked *Xist* cDNA transgene in male mESCs (XY:tetOP-*Xist*) initiates XCI and cell death due to silencing of the single X chromosome (Wutz and Jaenisch, 2000).

Xist is transcribed from a larger locus on the X chromosome that has been defined as the minimal critical region for XCI and besides housing *Xist*, contains other protein-coding and noncoding activators and repressors of *Xist,* some of which act in *cis* and others in *trans* (Rastan and Robertson, 1985; reviewed in Minkovsky et al., 2012). The best characterized repressor of *Xist* is its antisense transcript, *Tsix*, that is highly transcribed in epiblast cells of the pre-implantation blastocyst and in undifferentiated mouse ESCs/iPSCs, where *Xist* is repressed (Lee et al., 1999; Sado et al., 2001; Maherali et al., 2007). Deletion of *Tsix* leads to only slight *Xist* upregulation without causing precocious XCI or *Xist* RNA coating in self-renewing, undifferentiated ESCs. However, upon differentiation, XCI is skewed to the *Tsix*-deleted X in female cells heterozygous for the mutant *Tsix* allele (Lee et al., 1999; Lee, 2000; Luikenhuis et al., 2001; Sado et al., 2001). The effect of *Tsix* deletion on *Xist* indicates that it participates in parallel pathways with other regulators of *Xist* repression or activation.

Interestingly, the pluripotency factors Oct4, Sox2, and Nanog, have been implicated in the control of *Xist* expression in pluripotent cells. Navarro and colleagues found that in ESCs, Oct4, Sox2, and Nanog bind the first intron of the *Xist* gene (intron1) (Navarro et al., 2008), a finding that has been recapitulated in many genomic datasets and extends to additional pluripotency regulators such as Tcf3 and Prdm14, and early developmental regulators such as Cdx2 (Fig S1A, Loh et al., 2006; Marson et al., 2008; Ma et al., 2011; Erwin et al., 2012). Such genomic regions of extensive pluripotency

transcription factor co-occupancy in the ESC genome occur more commonly than would be expected by chance (Chen et al., 2008). It is thought that these co-bound genomic regions represent functionally important sites and often represent enhancer elements (Chen et al., 2008). Further support for a gene regulatory role of intron1 is that, in ESCs, the intron1 region has a propensity to be in the three-dimensional proximity to the promoter of *Xist* and adopts a DNAse hypersensitive state (Tsai et al., 2008). Additionally, pluripotency factors appear directly linked to *Xist* regulation. Upon Nanog deletion or inducible repression of *Oct4*, *Xist* is upregulated and binding of the pluripotency factors to intron1 is lost (Navarro et al., 2008). In males ESCs, which normally do not upregulate *Xist*, experimentally forced Oct4 repression can even induce *Xist* RNA coating in up to 10% of the cells (Navarro et al., 2008). Another study could not replicate *Xist* RNA coating upon *Oct4* knockdown in male ESCs, but observed biallelic XCI in differentiating female ESCs upon *Oct4* knockdown (Donohoe et al., 2009). A role for Nanog in *Xist* suppression is also supported by its expression pattern with regard to domains of Xi reactivation in the pre-implantation blastocyst, where the restriction of Nanog expression demarcates the fraction of cells undergoing reactivation of the imprinted Xi (Silva et al., 2009). Furthermore, pre-implantation embryos lacking Nanog are unable to specify epiblast cells and to lose *Xist* RNA, whereas forced expression of Nanog induces a more rapid loss of *Xist* RNA coating in developing pre-implantation embryos (Silva et al., 2009; Williams et al., 2011).

Together these findings led to the model that pluripotency factor binding to intron1 is critical for repression of *Xist* in undifferentiated XaXa ESCs. However, in the experiments leading to this conclusion, cell identity and therefore likely the expression of many genes were modulated by experimental changes in pluripotency factor expression, which could confound the interpretation that Oct4, Nanog and other pluripotency factors act directly on intron1 of *Xist* to regulate XCI. It has also been suggested that the

pluripotency transcription factors control the levels of positive and negative regulators of *Xist*, as they are binding to *Tsix* and the trans-acting activator of XCI, *Rnf12* (Donohoe et al., 2009; Gontan et al., 2012; Navarro et al., 2010, 2011) Accordingly, an experiment directly addressing the functional importance of binding to intron1 showed only subtle dysregulation of XCI: in female ESCs carrying a heterozygous deletion of intron1 of *Xist,* XCI remained suppressed in the undifferentiated state. However, upon differentiation, *Xist* appeared more highly expressed from the chromosome carrying the mutation supporting a role for intron1 in suppressing *Xist* during differentiation (Barakat et al., 2011). Furthermore, deletion of intron1 in the context of a transgene carrying the extended *Xist* locus moderately increased expression of *Xist* in undifferentiated ESCs, which was amplified by simultaneous deletion of the antisense transcript *Tsix* (Nesterova et al., 2011). Notably, these results were variable between clones potentially reflecting the effect of transgene copy number and variations (Nesterova et al., 2011). Binding to *Xist* intron1 has also been proposed to govern the switch from imprinted to random XCI in pre-implantation development (Erwin et al., 2012). *In vitro*, gel shift assays suggest that the binding events between *Xist's* intron1 and the pluripotency regulator Oct4 and the trophectoderm regulator Cdx2 are direct but mutually exclusive (Erwin et al., 2012).

Collectively, these findings motivated us to examine the role of *Xist* intron1 further to test the model wherein pluripotency factor binding silences *Xist* to prevent XCI in pluripotent cells, and to determine the role of the intronic region in X chromosome reactivation events, both *in vivo* and *in vitro*.

Results

Generation of conditional *Xist* intron1 ESC lines

To further define the role of *Xist* intron1, we used gene targeting to generate a conditional allele in male and female mouse ESCs. We tested the requirement of intron1 in both sexes since male ESCs are able to undergo XCI upon forced expression of *Xist,*

providing a sensitive background for monitoring *Xist* regulation independently of other X chromosomes present in a cell (Wutz and Jaenisch, 2000). By contrast, heterozygous female ESCs permit investigation of kinetics of XCI upon induction of differentiation and insight into potential effects on skewing of XCI between the targeted and wildtype chromosome.

To delineate the region of intron1 involved in *Xist* repression, we inspected where pluripotency transcription factors bind within the intron1 region as detected by published ChIP-seq data sets (Marson et al., 2008). We also determined the localization of pluripotency factor DNA binding motifs, and considered sequence conservation across mammals (Fig S2.1). We found that co-occupancy of pluripotency factors occurs in a 600bp region within the full 2.8kb sequence of intron1. Most of the intron1 sequence is not conserved in placental mammals, however, two highly conserved composite Oct4-Sox2 DNA binding motifs, which are found to stabilize a ternary Oct4-Sox2-DNA complex in the expression of many ESC-specific genes, underlie the ChIP-Seq binding peaks of Oct4 and Sox2 (Fig S2.1, Reményi et al., 2003; Marson et al., 2008; Mason et al., 2010, UCSC phastCons). Based on these data, we decided to delete 800 bp of intron1, and subsequently refer to this mutation as 'intron1' (Minkovsky/Plath allele, Fig S2.1).

We flanked the 800 bp intron1 region with loxP sites, simultaneously inserting a hygromycin resistance cassette (yielding a targeted allele with 3loxP sites), and subsequently generated experimental (1lox) and control (2lox) alleles by transient expression of Cre recombinase in hemizygously targeted male and heterozygous female ESCs (Fig 2.1, Fig S2.2). To be able to monitor the effects of the deletion of intron1 on *Xist in cis* in female cells, we employed genetically polymorphic F1 2-1 female ESCs (129/Cas) carrying a MS2 RNA tag in exon 7 of *Xist* on the 129 allele (Jonkers et al., 2008). Southern blotting and PCR analysis confirmed that intron1 was targeted *in cis* to

the MS2 RNA tag in females ESCs (Fig S2.2). Male and female targeted ESC lines showed normal chromosome complement upon karyotyping (Fig S2.2 and data not shown).

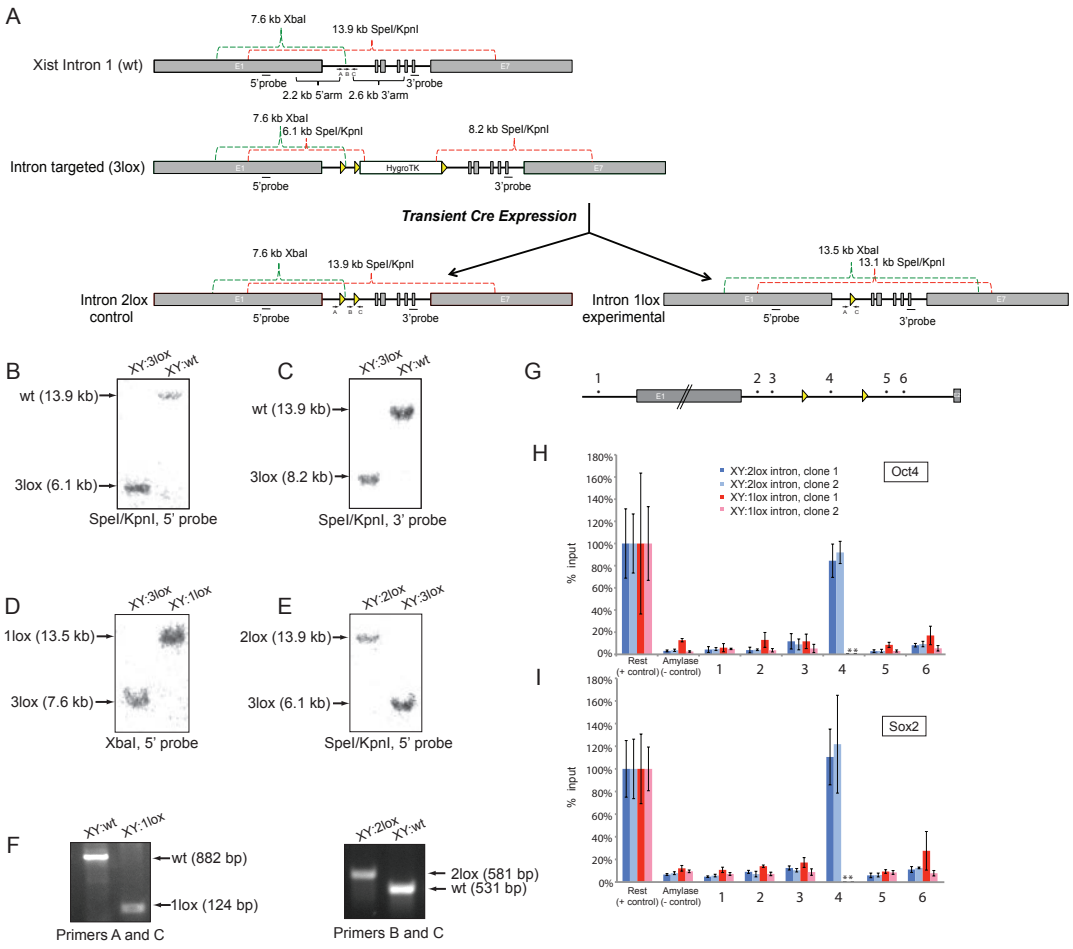

Figure 2.1. Generation of male mouse ESCs carrying a conditional *Xist* intron1 allele. **(A)** Gene targeting and Southern blotting strategy schematic for male ESCs. Transient expression of Cre recombinase in properly targeted 3lox clones yielded both 2lox (control) and 1lox (experimental) ESC lines. **(B-E)** Representative images of correctly targeted clones from Southern blot analysis. **(F)** PCR genotyping with primers A and C shows the presence of the 1lox allele, and with primers B and C that of the 2lox allele. **(G)** Analysis of Oct4 and Sox2 binding in male ESCs with and without intron 1 by ChIP-PCR. Location of ChIP-qPCR primer sets used in the subsequent figures. **(H)** Quantitative ChIP_qPCR analysis of Oct4 binding to regions indicated in (G) and a known positive and negative control for Oct4 binding (Berg et al., 2008) in 2lox and 1lox intron1 male ESCs (two clones each).. Values represent the amount precipitated after normalization to input chromatin and are given relative to binding within the positive control region. Error bars indicate standard deviation from triplicate qPCR measurements. * indicates high Ct values for the input samples in the genetically deleted regions, probably arising from support feeder cells.

To confirm that deletion of 800 nucleotides from intron1 sufficiently removes pluripotency factor binding, we performed chromatin immunoprecipitation against Oct4 and Sox2 coupled to quantitative PCR for the targeted region of intron 1, neighboring intronic regions, the *Xist* promoter, and previously validated control regions (Navarro et al., 2008). Importantly, we did not observe an increase in Oct4 or Sox2 binding in these regions upon deletion of intron1 (Fig 2.1G-I). Thus, compensatory binding at cryptic binding sites upon intron1 deletion appears unlikely.

Ectopic *Xist* RNA coating is not observed in intron1 deleted undifferentiated and differentiating male and female ESCs

To understand the role of intron1 in the regulation of XCI, we first performed fluorescence in situ hybridization (FISH) to analyze the expression and localization of *Xist* and *Tsix* RNA at the single cell level using strand-specific RNA probes. Undifferentiated male and female ESC lines displayed no significant *Xist* RNA cloud or pinpoint signal in the presence or absence of intron1 (Fig 2.2A/B). The absence of *Xist* RNA coating in the undifferentiated ESC state was confirmed by the lack of a Xi-like enrichment of H3K27me3, which is known to occur on the Xi when *Xist* RNA coats (Plath et al., 2003; Silva et al., 2003) in Nanog-positive cells (Fig S2.3A/B). In agreement with this finding, the signal for *Tsix* was present in the majority of cells in each case and indistinguishable among all tested genotypes (Fig 2.2A).

Upon induction of differentiation by embryoid body (EB) formation, the lack of intron1 did not induce *Xist* RNA in male ESCs to a level detectable by FISH (data not shown), and yielded no Xi-like enrichment of H3K27me3 (Fig S2.3C/D), indicating that intron1 is not an essential regulator of *Xist* suppression in differentiating male ESCs when all other regulators of XCI are intact. Heterozygous 1lox/wt female ESCs formed *Xist* RNA clouds and H3K27me3 Xi foci at comparable rates to 2lox/wt control ESCs (Fig

2.2C/D, Fig S2.3C/D). *Xist* RNA levels were also similar between undifferentiated and differentiating male and female ESCs, with or without intron1, in RT-PCR experiments (Fig 2.2E). Proper differentiation was confirmed by decrease in *Nanog* transcript levels (Fig 2.2F). Furthermore, the use of *Xist* intron1-spanning PCR primer pairs ruled out dramatic secondary effects of intron1 deletion on *Xist* splicing (data not shown).

Next, we assessed whether XCI is skewed upon intron1 deletion in differentiating female ESCs. The polymorphic 129/cas F1 2-1 female ESC line is known to have a baseline skewing of XCI towards the 129 allele such that approximately 70% of the cells will silence the 129 allele, due to strain-specific haplotypes (Cattanach and Isaacson, 1967). Due to the integration of the MS2 RNA tag on the intron targeted 129 X chromosome, combined RNA-FISH for MS2 and *Xist* sequences can distinguish between *Xist* being expressed from the targeted chromosome (positive for both *Xist* and MS2 signals) and the untargeted X (only marked by the *Xist* probe) (Fig 2.2C, Jonkers et al., 2008). We found that, at the single cell level, female 1lox intron/wt ESCs consistently had ~15% more cells expressing the MS2-tagged *Xist* than their 2lox/wt counterparts, in three of four *ex vivo* differentiation methods (Fig 2.2G, Fig S4). This mild skewing effect in differentiating female ESCs is consistent with published results (Barakat et al., 2011).

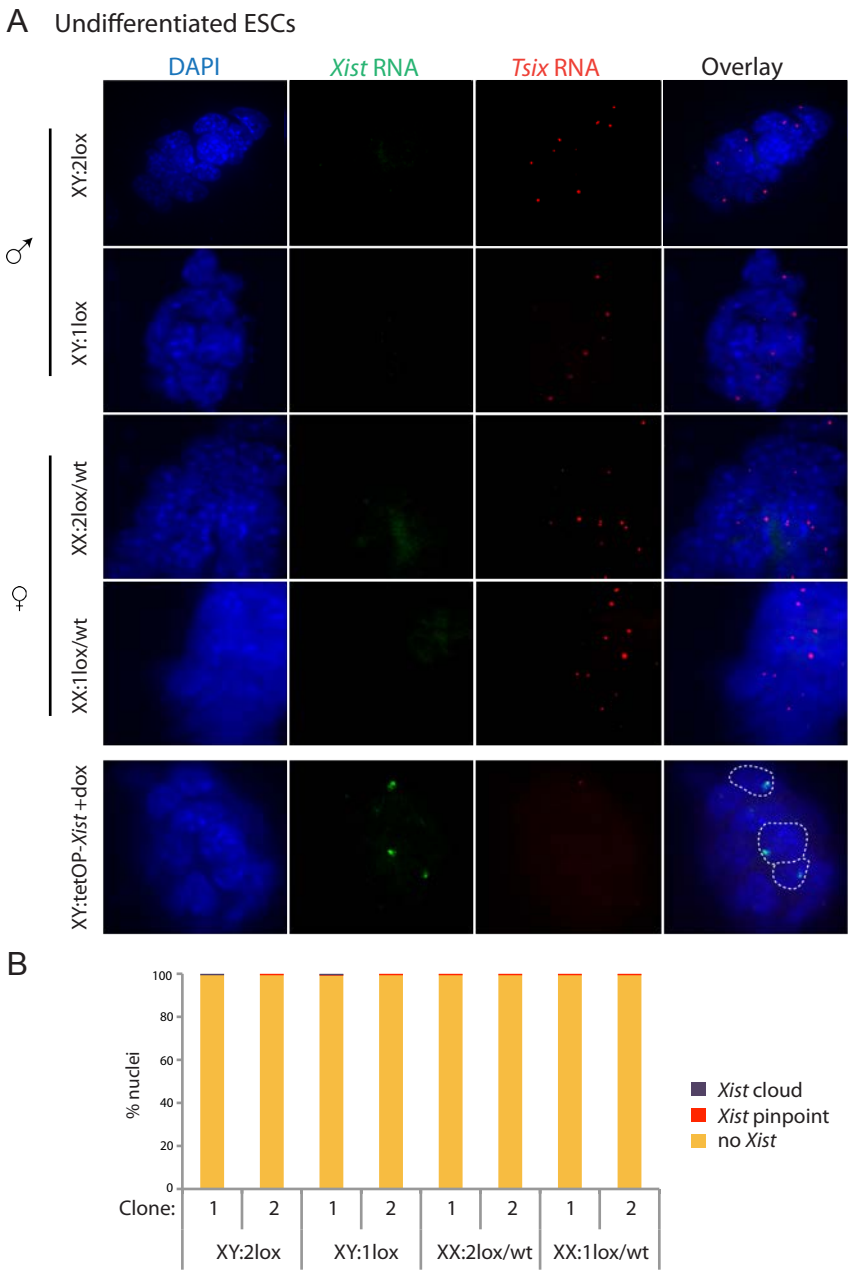

Figure 2.2. Analysis of *Xist* expression in undifferentiated and differentiating female and male ESC lines in the presence and absence of intron1. (A) Strand-specific FISH for *Xist* RNA (green) and *Tsix* RNA (red) in undifferentiated male and female ESCs of the indicated genotypes, using RNA probes. Dapi staining (blue) indicates nuclei. Representative images are shown. A male ESC line carrying a dox-inducible *Xist* allele in the endogenous locus was used as positive control for the *Xist* staining pattern, at 24 hours of dox addition. **(B)** Graph summarizes the proportion of dapi-stained nuclei with indicated patterns of *Xist* RNA based on an experiment as described in (A). Pairs of independent ESC clones of the given genotype were stained and counted. In each case 500 nuclei were assessed. *Continued on the next page.*

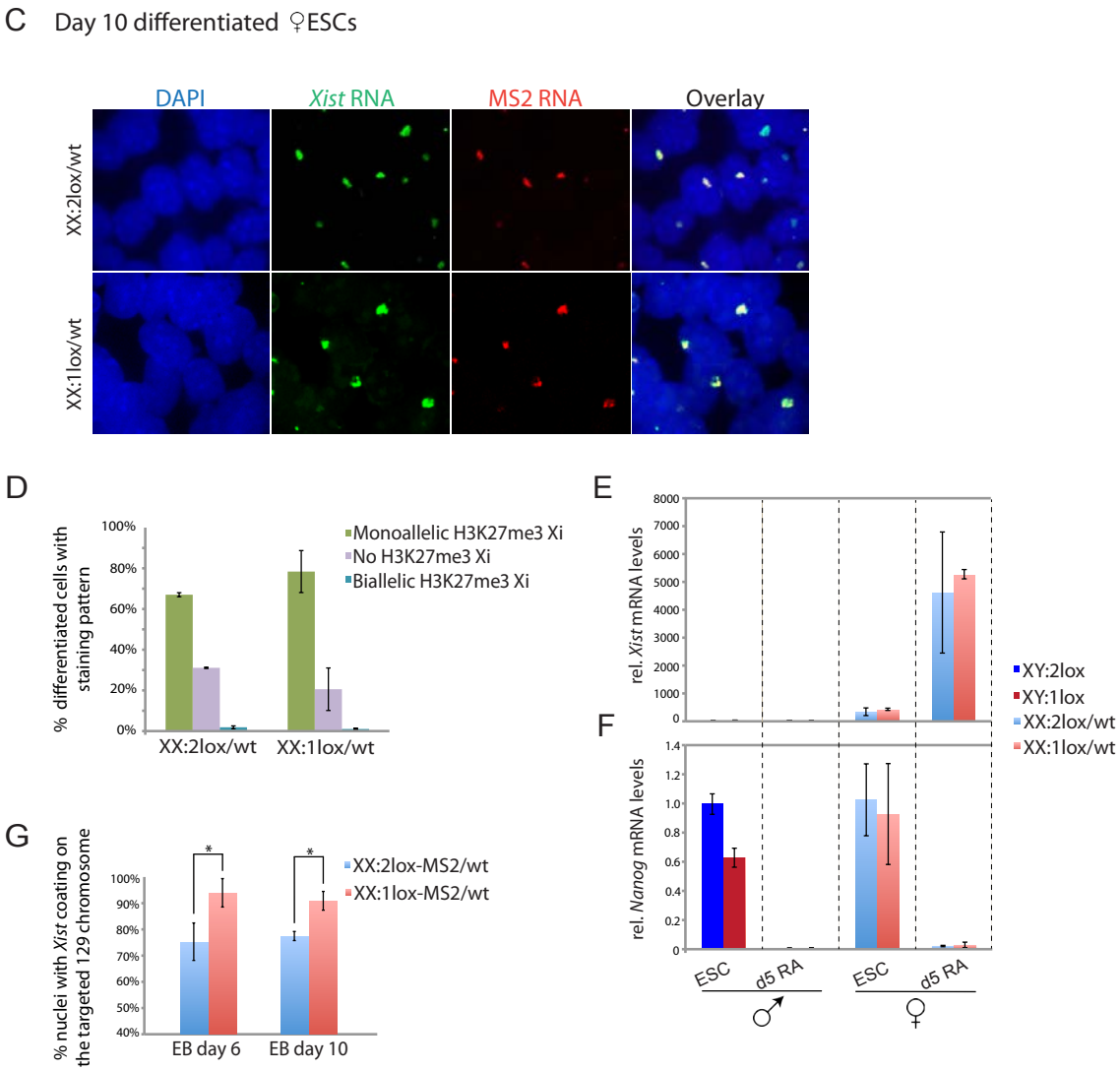

Figure 2.2 cont'd (C) FISH with DNA probes targeting *Xist* RNA (green) and the *MS2* tag (red), respectively, in female ESCs of indicated genotypes at day 10 of EB-differentiation. **(D)** Graph summarizing the proportion of Nanog-negative cells in day 10 EB-differentiated female ESCs with no, one, or two H3K27me3 Xi-like accumulations. Notably, the number of cells within each H3K27me3 pattern is not statistically different (by Student's t-test) between presence and absence of intron1. Values are means of counts of independent clones as shown in FigS4D, in each case at least 500 nuclei were assessed. **(E)** RT-PCR for *Xist* RNA levels normalized to *Gapdh* expression from one representative clone of indicated ESC genotypes in the undifferentiated state (ESC) and at day 5 of retinoic-acid differentiation (d5 RA). Error bars indicate standard deviation from triplicate RT-PCR measurements in one experiment. **(F)** As in (E), except that *Nanog* transcript levels were analyzed. **(G)** Quantification of allele-specific *Xist* RNA cloud patterns from the experiment shown in (C) at day 6 and day 10 of EB-differentiation, given as mean of values from counts of two independent ESC clones of the indicated genotype. *Xist* expression from the 129 chromosome (targeted chromosome) is detected by both the *Xist* and MS2 probes, while *Xist* expression from the CAST chromosome is only detected by the *Xist* probe. The graph depicts the percentage of cells where the intron1-targeted 129 chromosome is coated by *Xist* RNA, as identified by co-localization of the Xist and MS2 signals. *denotes $p<0.05$ by Student's t-test with 500 *Xist* clouds analyzed for each sample.

Genetic interaction of *Xist* intron1 with *Tsix*

Next, we investigated the possibility that the intron1-dependent skewing of XCI in differentiating female ESCs represents a mild effect on the intron1-deleted X chromosome at the transition to the differentiated state. We reasoned that such an effect may be more strongly revealed in the absence of other regulators of *Xist* and sought to assay such an effect on a 'sensitized' background for *Xist* transcription. *Tsix* represents the prime candidate for a redundant *Xist* repressor that could compensate to repress *Xist* in the absence of intron1. One study supports the view that a functional role for the intron can be uncovered in the absence of *Tsix*, as male ESCs with randomly integrated genomic *Xist* transgenes lacking intron1 and a functional *Tsix* allele dysregulated the expression of the transgenic *Xist* (Nesterova et al., 2011). We therefore performed the above analyses in male ESCs lacking intron1 in the endogenous *Xist* allele on the background of a previously characterized *Tsix* loss of function mutation at the endogenous locus (Fig 2.3, Lee et al., 1999; Luikenhuis et al., 2001; Sado et al., 2001). We targeted the disruption of *Tsix* to both 2lox and 1lox intron male ESCs using a construct from the Sado lab that inserts a splice acceptor-IRES*βGeo* cassette in exon 2 of *Tsix* resulting in an early transcriptional stop (Fig 2.3A). Correct targeting and loss of the *Tsix* transcript were confirmed by Southern blotting and absence of the FISH signal for *Tsix* after targeting (Fig 2.3B/C).

As expected, in the presence of intron1 (2lox intron1), *Tsix* deletion in male ESCs induced a mild transcriptional upregulation of *Xist* RNA compared to XY:2lox/*Tsix*-wt ESCs in RT-PCR experiments, reaching a level found in female ESCs (Fig 2.3D). Upon differentiation XY:2lox intron/*Tsix*-Stop ESCs further upregulated *Xist* transcript levels ~5 fold (Fig 2.3D). However, this induction was rarely correlated with an *Xist* RNA cloud signal detectable by RNA FISH in or an Xi-like H3K27me3 accumulation (Fig 2.3E-H)

before and after induction of differentiation, in agreement with previous reports (Luikenhuis et al., 2001; Sado et al., 2002). Combined deletion of intron1 and *Tsix* did not alter the *Xist* status in undifferentiated ESCs, but upon induction of differentiation resulted in a *Xist* RNA cloud-like signal in FISH experiments in 3-6% of cells compared to 0.2-0.8% in differentiating XY:2lox intron/*Tsix*-Stop cells (Fig 2.3E/G). We did not, however, see any significant intron1-dependent effect on *Xist* RNA levels by RT-PCR comparing XY:2lox intron/*Tsix*-Stop and XY:1lox intron/*Tsix*-Stop cells (Fig 2.3D) or an increase in the number of H3K27me3 Xi-like accumulations (Fig 2.3F/H). Thus, even though *Xist* RNA was induced in a slightly larger proportion of differentiating cells in the absence of both *Tsix* and intron1 than in the absence of either *Tsix* or intron1, this upregulation does not appear to be sufficient to mediate H3K27me3 enrichment on the targeted X chromosome, suggesting that the RNA does not efficiently coat the chromosome in these cells or that the recruitment of Polycomb proteins is affected. We conclude that these experiments reveal a subtle role of intron1 in the control in *Xist* expression, which may be related to the weak skewing phenotype of XCI described above for differentiating intron1-mutant heterozygous female ESCs (Fig 2.3, Fig S2.4).

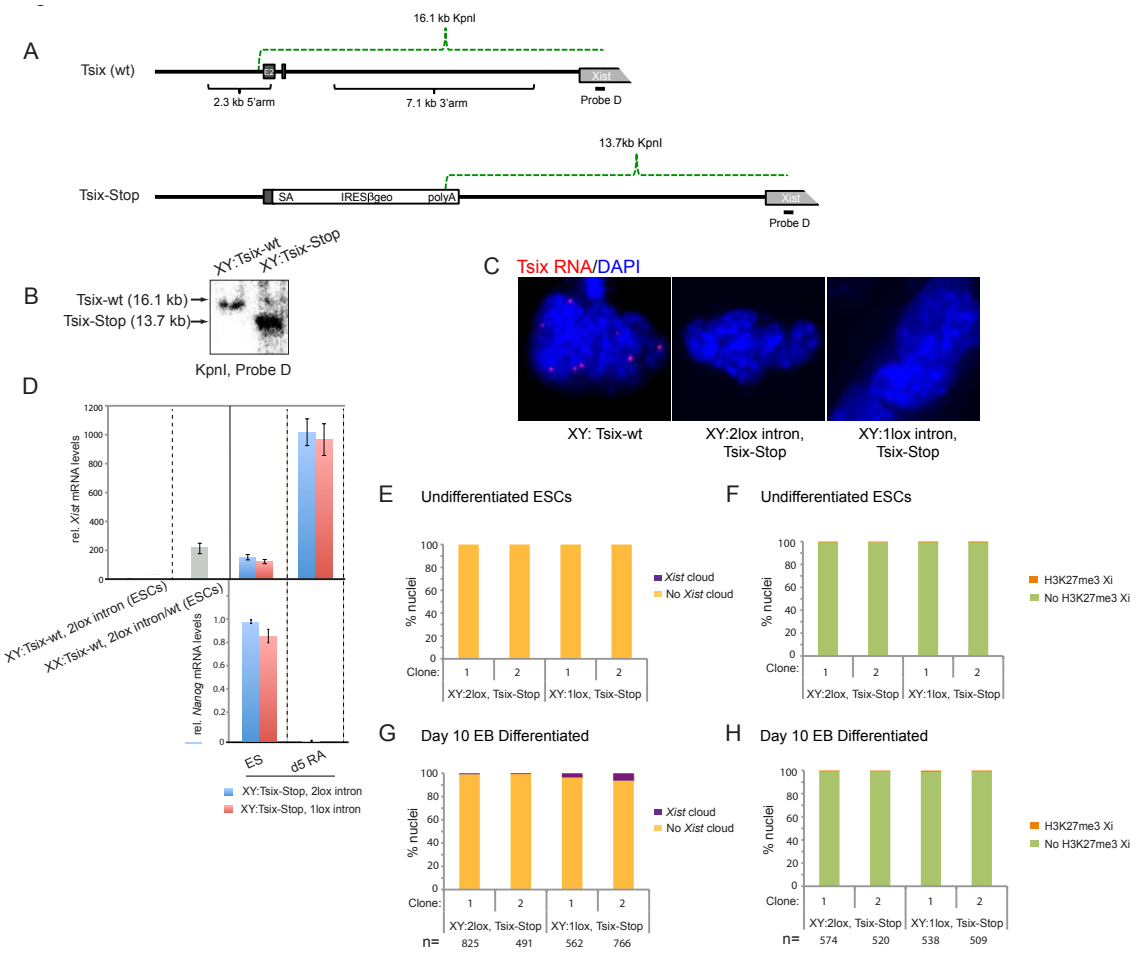

Figure 2.3. *Xist* RNA pattern in male ESCs lacking *Tsix* and intron1. (A) Gene targeting and Southern blotting strategy schematic for the generation of the *Tsix*-Stop allele in male ESCs according to Sado et al., 2001 using the pAA2Δ1.7 targeting vector. **(B)** Male 2lox and 1lox intron1 ESC clones were targeted with the *Tsix*-Stop allele. A correctly targeted 2lox intron1/*Tsix*-Stop male ESC clone is shown in this Southern blot analysis. **(C)** Strand-specific FISH for *Tsix* RNA (red) in undifferentiated male ESCs of the indicated genotypes, using an RNA probe, indicates the absence of the *Tsix* FISH signal in *Tsix*-Stop targeted clones. **(D)** Graph summarizing the transcript levels for *Nanog* and *Xist* normalized to *Gapdh* transcript levels as determined by RT-PCR from a representative clone of each genotype in the undifferentiated state (ES) and at day 5 of retinoic acid-differentiation (d5 RA). Control *Xist* RNA levels from wildtype undifferentiated male and female ESCs are shown on the left. Error bars indicate standard deviation from triplicate RT-PCR measurements in one experiment. **(E)** Graph summarizing the percentage of undifferentiated ESCs of the given genotype with and without a *Xist* RNA cloud-like pattern. Two independent male ESC clones for each genotype were analyzed by *Xist* RNA FISH with a RNA probe and 500 nuclei were assessed. **(F)** As in (E), except that the percentage of undifferentiated ESCs with and without a H3K27me3 Xi-like signal is given. **(G)** *Xist* RNA cloud quantification as in (E), except that *Nanog*-negative cells were quantified upon day 10 of EB differentiation. **(H)** As in (F) for H3K27me3 patterns at day 10 of EB differentiation in indicated ESC lines.

In a second assay, we tested the consequence of intron1 deletion upon modulation of global *Oct4* transcript levels. We first confirmed the previously reported relationship between the decrease of *Oct4* levels and *Xist* RNA induction (Navarro et al., 2008; Donohoe et al., 2009). Specifically, upon *Oct4* depletion in the male ZHBTc4 ESC

line, in which *Oct4* expression can be silenced acutely by the addition of doxycycline, *Xist* RNA levels were induced almost 100-fold 96 hours post induction of *Oct4* repression (Fig S2.5A), and *Xist* RNA could be detected by FISH in a small number of cells (Fig S2.5B/C). Notably, we observed that *Oct4* transcript levels drop with faster kinetics than *Xist* RNA levels increase, suggesting that the effect of *Oct4* on intron1 is indirect and may require efficient differentiation, which occurs at 96 hours post *Oct4* repression as indicated by the loss of the pluripotency factor Nanog (Fig S2.5D). In agreement with this conclusion, siRNA-mediated knockdown of *Oct4* in ESCs did not increase *Xist* RNA levels more than two-fold after 72 hours confirming a previous report (Fig S2.5E, Donohoe et al., 2009). Furthermore, the absence of intron1 did not significantly alter *Xist* RNA levels in female ESCs or male ESCs lacking *Tsix* in *Oct4* knockdown conditions (Fig S2.5E). These data indicate that the slight increase in *Xist* levels immediately upon *Oct4* depletion are independent of intron1.

Intron1 acts as an enhancer in a reporter assay in differentiating ESCs

The model of pluripotency-factor binding to intron1 to repress *Xist* motivated us to directly assess whether intron1 behaved as a silencer in ESCs in a reporter assay. We transfected constructs with intron1 or control sequences upstream of a minimal promoter driving luciferase and did not see intron1-dependent decreases in reporter activity (data not shown). The small effect of intron1 deletion on *Xist* RNA levels detected in differentiating ESCs in the absence of *Tsix* motivated us to revisit these experiments and instead investigate whether *Xist* intron1 represents a developmentally-regulated enhancer that becomes active upon induction of differentiation. We therefore tested transactivation activity of intron1 in undifferentiated and differentiating ESCs using stably integrated luciferase reporter constructs (Fig 2.4). Male ESCs were electroporated with hygromycin resistance-bearing constructs containing either the part of intron1 that

we deleted in our experimental cell lines, or two control sequences representing the upstream and downstream flanking regions of the intron1 region (Fig 2.4A). The experimental intron1 region (B in Fig 2.4B) was cloned in triple copy to amplify any putative enhancer activity of this region. Pooled clones were subjected to monolayer differentiation by LIF withdrawal with and without retinoic acid treatment. Only cells bearing the intron1 construct covering the pluripotency factor binding site showed a robust increase in luciferase activity upon differentiation (Fig 2.4B). In agreement with the notion that intron1 does not act as an active enhancer in undifferentiated ESCs, we did not find a histone acetylation mark characteristic of active enhancers, namely H3K27ac, examining our own and published Chip-Seq data sets from ESCs, despite binding of intron1 by a battery of pluripotency factors and p300 in undifferentiated ESCs (mouse ENCODE, Creyghton et al., 2010, data not shown).

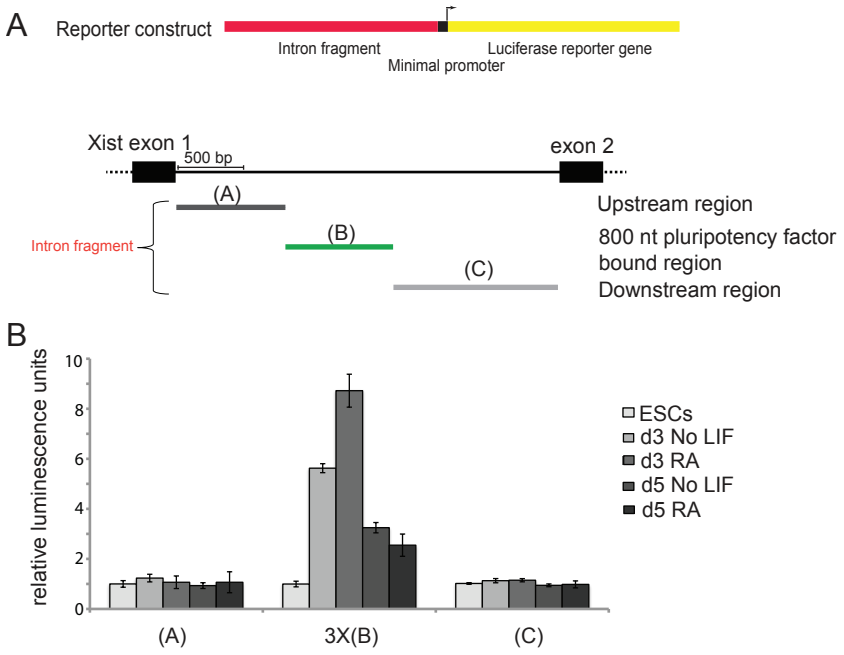

Figure 2.4. Enhancer assay of *Xist* intron1. (A) Schematic representation of genomic fragments of the entire genomic intron1 regions cloned upstream of a luciferase reporter gene driven by a minimal promoter. The intronic region was broken up in three parts, with B representing the part bound by pluripotency factors and flanked by loxP sites as described in Figure 2.1 (Minkovsky/Plath allele), and A and C representing regions not bound by the pluripotency factors in ChIP-Seq experiments (Fig S1). Note that B was concatenated 3X in the reporter construct. **(B)** Three independent stable cell lines were generated by electroporation of male ESCs with the three constructs described in (A). Cells carrying the reporter constructs were selected with hygromycin, and an equal number of cells was plated and maintained in the undifferentiated state or differentiated for d3 and d5 by LIF withdrawal and/or retinoic acid (RA) addition. After treatment 1/10th of the cells in the well were analyzed by luciferase assay. For each reporter construct, values represent mean luminescence units normalized to values from the respective cell line in the undifferentiated state, n=3, ±1SD.

We also considered recently published spatial organization data which demonstrated that the *Xist* gene lies in a topologically associating domain (TAD) with genes encoding the non-coding RNAs *Ftx* and *Jpx/Enox*, and the protein-coding genes *Rnf12/Rlim*, *Zcchc13*, and *Slc16a2* (Nora et al., 2012). It has been proposed that promoters and enhancers predominantly interact (loop) within TADs (Dixon et al., 2012; Nora et al., 2012). Notably, significant intra-TAD contacts originating from within intron1 of *Xist,* indicative of putative enhancer/promoter looping, were only found in differentiated and not in undifferentiated ESCs (Nora et al., 2012) (Fig S2.6A), consistent with our finding of reporter activity upon differentiation. However, similar to our result that *Xist* levels in female and males ESCs did not significantly change in the absence of

intron1, we also did not see intron1-dependent transcriptional differences in the three genes that come in contact with intron1 within the *Xist*-containing TAD, before and during differentiation (Fig S2.6B). Thus, even though intron1 is pluripotency factor-bound in ESCs, it may only gain significant enhancer activity upon differentiation though still not to an extent where deletion affects transcription of *Xist* or of neighboring protein-coding genes.

Together these *ex vivo* studies in undifferentiated and differentiating male and female ESCs point to a minor role for intron1 in the regulation of *Xist* expression, uncovered only when another *Xist* repressor is deleted, and some aspect of X chromosome choice (potentially also through slight modulation of *Xist* RNA levels). These data do not support intron1 as a main aspect of the mechanism of transcriptional repression of *Xist,* at least in this tissue culture model.

Mice are normal in the absence of intron1

Next, we assayed the significance of intron1 *in vivo*. Our male ESCs deleted for intron1 (1lox) were injected into C57BL/6 blastocysts. Chimeras were obtained at high efficiency and bred with C57BL/6 females to obtain germline transmission of the mutant allele. Importantly, the 1lox intron1 allele showed normal propagation through the maternal or paternal germline and mice completely lacking intron1 (crossing 1lox/1lox females with 1lox males) could be efficiently bred without any female-specific defect (Fig 2.5A). Since X chromosome reactivation occurs in the female germline and is likely essential for female fertility, we assessed litter size of the F2 generation of female homozygous knockout mice, finding their litter sizes unaffected (data not shown).

To strengthen these observations of normal transmission of the intron1 mutation and rule out that genetic background obscured a potential intron1 phenotype *in vivo*, we generated a second mouse model carrying an independent intron1 mutation. We

generated mice using previously published females 129/cas F1 female ESCs in which a larger (1.815 kb) region was deleted on the 129 X chromosome (Barakat/Gribnau allele) (Fig S2.1A, Barakat et al., 2011). We previously observed a slight upregulation of *Xist* RNA levels on the deleted chromosome in differentiating female ESCs, in agreement with our results indicating skewing of X-inactivation towards the deleted chromosome. Importantly, this second mouse model also displayed normal mendelian transmission of the intron1 lox allele (Fig 2.5B).

To assay whether random XCI has occurred in female mice carrying a paternally inherited X chromosome lacking intron1 and a maternally inherited wildtype X chromosome, and whether the lack of the intron leads to any skewing of XCI *in vivo*, we analyzed the allele-specific expression of *Xist* and two X-linked genes, *Mecp2* and *G6pdx*, in polymorphic heterozygous females ($1lox^{C57BL/6}/wt^{CAST/Ei}$) and a wildtype control ($wt^{C57BL/6}/wt^{CAST/Ei}$), respectively, where the C57BL6 X chromosome was transmitted from the father and the CAST/Ei wildtype X from the mother, by semi-quantitative RT-PCR on RNA isolated from various tissues (Fig 2.5C-E). In these experiments, we used the Barakat/Gribnau mouse model described in Figure 5B (Fig S2.1A). Normally, the paternal X chromosome initially undergoes imprinted XCI, which is reversed in the epiblast cells of the pre-implantation blastocyst to allow subsequent random XCI. The intron1 region has been implicated to be important for Xi-reactivation in the ICM, and thus, if the absence of intron1 prevents reactivation of imprinted XCI, we may observe non-random XCI in the adult mouse (Navarro et al., 2008).

However, we did not find differences in allele-specific expression pattern in the presence and absence of intron1 in heterozygous female mice (Fig 2.5C-E). As expected, the C57BL/6 Xist allele is more often expressed than the CAST/Ei X, consistent with a modifier effect, likely resulting in more cells with an inactivated C57BL/6 X (Cattanach and Isaacson, 1967). Because of the stochastic and clonal nature

of XCI patterns in the adult mouse, variations in skewing towards *Xist* RNA from the C57BL/6 allele ranged from 50-90% (Fig 2.5C,E). Notably, we did not see a preference of *Xist* upregulation on the intron1-deleted X chromosome in tissues of the adult mouse *in vivo*, albeit we observed slightly skewed *Xist* RNA levels in heterozygous differentiating female ESCs carrying the same mutant intron1 allele (Barakat et al., 2011). In agreement with this notion, the X-linked genes *Mecp2* and *G6pd*x, both subject to silencing on the Xi, showed reciprocal and intron1-independent levels of expression from the C57BL/6 chromosome compared to *Xist*, as would be expected from the fact that the *Xist*-expressing chromosome is more likely to be silent (Fig 2.5D/E). These data suggest that the paternal transmission of the intron1 mutation does not interfere with reactivation of imprinted XCI and subsequent random XCI. A reverse cross in which the maternal allele lacked intron1 also resulted in random XCI (data not shown). In summary, the intron1 genomic region is dispensable in the mouse and does not critically control *Xist* expression and skewing of XCI *in vivo*.

A Minkovsky/Plath Allele

Paternal Genotype	Maternal Genotype	Average Litter Size	Offspring ♂		Offspring ♀		*p*-Value
			XY:+	XY:1lox	XX:+/+	XX:1lox/+	
XY:+	**XX:1lox/+**	7.2	10	10	6	10	>0.25[a]
			XY:+	XY:1lox	XX:1lox/+	XX:1lox/1lox	
XY:1lox	**XX:1lox/+**	6.7	10	12	14	11	>0.25[a]
			XY:1lox		XX:1lox/1lox		
XY:1lox	**XX:1lox/1lox**	8.0	23		17		>0.25[b]

B Barakat/Gribnau Allele

Paternal Genotype	Maternal Genotype	Average Litter Size	Offspring ♂		Offspring ♀		*p*-Value
			XY:+	XY:1lox	XX:1lox/1lox	XX:1lox/+	
XY:+	**XX:1lox/+**	6.7	2	6	3	9	>0.10[a]
			XY:+		XX:1lox/+		
XY:1lox	**XX:+/+**	6.5	11		15		>0.25[b]
			XY:+	XY:1lox	XX:1lox/+	XX:1lox/1lox	
XY:1lox	**XX:1lox/+**	6.1	13	15	8	13	>0.25[a]
			XY:1lox		XX:1lox/1lox		
XY:1lox	**XX:1lox/1lox**	5.3	32		37		>0.25[b]

[a-b] Chi-square test for expected 1:1:1:1 (a) or 1:1 (b) ratio

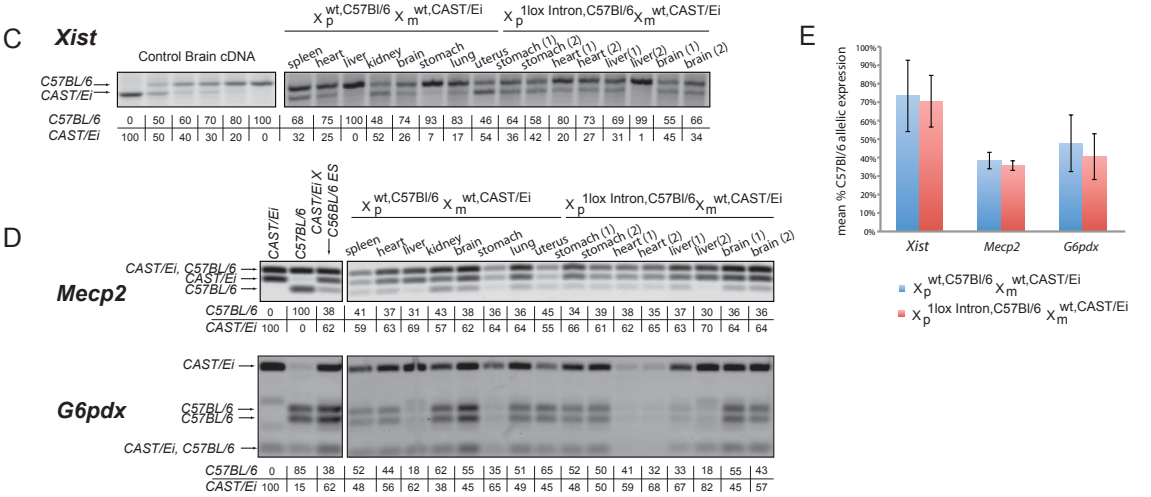

Figure 2.5. Transmission of the intron1 mutation *in vivo*. (A) Table summarizing the number and genotypes of offsprings from indicated mouse crosses using the intron1 allele generated in the Plath lab (see Figure 2.1). **(B)** As in (A), except that mice carrying a second, independent intron1 deletion generated by the Gribnau lab were crossed (see Figure S1 for comparison of alleles, Barakat et al., 2011). **(C)** Allele-specific RT-PCR analysis of *Xist* RNA detecting a length polymorphism that distinguishes *Xist* RNA originating from the C57BL/6 and CAST X chromosome in organs of one female wildtype mouse and two littermate heterozygous 1lox/wt mice obtained by crossing a C57BL/6 male (with and without the intron1 1lox allele) with a wildtype CAST/Ei female. Panel includes controls on the left mixing pure C57BL/6 and CAST/Ei brain cDNA template in given ratios. Numbers below the tissue samples represent the relative band intensity for the C57BL/6 and CAST/Ei *Xist* allele determined by comparison with the control samples. **(D)** Examination of tissues as in (C) for allelic expression of X-linked genes *MeCP2* (top) and G6pdx (bottom) by RFLP RT-PCR. Panel includes controls (left) from pure C57BL/6 or CAST/Ei mice as well as RNA isolated from a polymorphic C57BL/6 and CAST/Ei ES cell line. **(E)** Graph averaging the allele-specific expression data in (C) and (D) across all tissue and mice per genotype ±1 SD.

Intron1 is not required for loss of *Xist* RNA upon reprogramming to iPSCs

While there was no dramatic effect on XCI state *in vivo*, we sought to understand the requirement for intron1 in *Xist* silencing associated with reprogramming to iPSCs. We have shown previously that female iPSCs derived from mouse embryonic fibroblasts (MEFs) carry two active X chromosomes, where *Xist* is efficiently repressed and *Tsix* upregulated, as seen in mouse ESCs (Maherali et al., 2007). Another study suggested that Xi-reactivation occurs late in reprogramming at around the time pluripotency genes become expressed, again suggesting that pluripotency transcription factors could contribute to Xi-reactivation and the silencing of *Xist*, potentially via binding to intron1 (Stadtfeld et al., 2008). To test the role of intron1 in the *Xist* silencing process during reprogramming, we bred male mice carrying the 2lox intron1 allele (obtained upon blastocyst injection of our male 2lox ESCs described in Figure 2.1, Minkovsky/Plath allele) with female mice heterozygous for an *Xist* knockout allele (Marahrens et al., 1997), yielding female XX:2lox intron/*ΔXist* MEFs. Due to the presence of the *Xist* knockout allele, the X chromosome bearing the intron1 allele is exclusively inactivated *in vivo* by normal developmental mechanisms (Marahrens et al., 1998). MEFs isolated from d14.5 embryos had uniform *Xist* coating (Fig 2.6C) and were transduced with retroviruses encoding the reprogramming factors Oct4, Sox2, and Klf4, and subsequently infected with adenovirus encoding Cre recombinase at day 4 of reprogramming to efficiently delete the intron1 region or with titer-matched empty adenovirus in control samples (Fig 2.6A). This experimental setup allowed us to test the role of intron1 on reprogramming efficiency for the same infected fibroblast population. Genotyping confirmed that Ad-Cre addition resulted in efficient deletion of the intron1 region (Fig 2.6B). To test whether intron1 deletion affects the efficiency of reprogramming, we determined the number of Nanog-expressing colonies at day 13 after reprogramming factor introduction as Nanog expression has been shown to mark

faithfully reprogrammed cells in retroviral reprogramming experiments (Maherali et al., 2007). We found a comparable number of Nanog-positive colonies in the presence and absence of intron1 (Fig 2.6D). Normally, at this point of reprogramming, *Xist* RNA coating is just lost in Nanog- positive cells (Tchieu/Plath et al, manuscript in preparation). In agreement with this notion, an examination of all Nanog-positive cells for the presence or absence of a *Xist* RNA cloud demonstrated that nearly all Nanog-positive cells carrying the 2lox intron1 allele (Ad-Null reprogramming cultures) lack a *Xist* RNA cloud at d13 of reprogramming (Fig 2.6C/E). Importantly, even in the absence of intron1 (Ad-Cre samples), Nanog-positive cells displayed loss of the *Xist* RNA cloud (Fig 2.6C/E) and of the Xi-like H3K27me3 focus (data not shown). Furthermore, from the Ad-Cre treated reprogramming cultures, 14 iPSC clones were isolated and clonally propagated and all confirmed to have lost both intron1 and the *Xist* RNA cloud, demonstrating the efficient deletion of the intronic sequence early in reprogramming (Fig 2.6F). To ensure that the ability of an intron1-deleted inactive X chromosome to downregulate *Xist* was not due to intron 1-dependent events occurring within the first four days of reprogramming, i.e. prior to Cre-mediated deletion, we also reprogrammed MEFs carrying a germline transmitted 1lox intron allele. These XX:1lox intron/*ΔXist* MEFs displayed normal *Xist* RNA coating before reprogramming (detectable in 95% of the cells) and lost *Xist* RNA in Nanog-positive colonies (Fig 2.6H). When comparing to sibling XX:2lox intron/*ΔXist* MEFs, MEFs lacking intron1 form Nanog-positive colonies with similar efficiencies (Fig 2.6I). Together, these studies rule out that *Xist* intron1 is necessary for the downregulation of *Xist* in reprogramming to pluripotency.

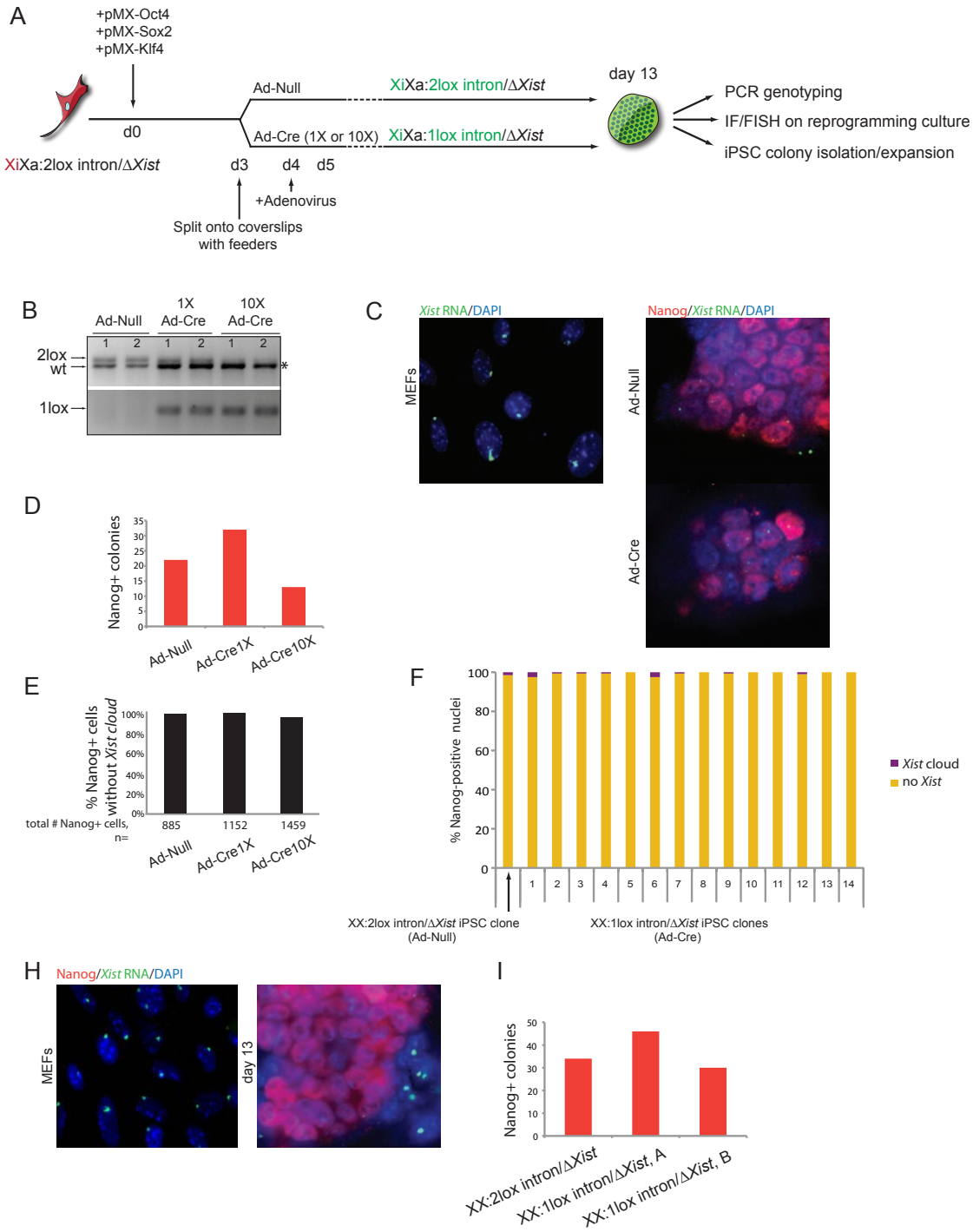

Figure 2.6. The absence of intron1 on the Xi does not interfere with loss of *Xist* RNA coating upon reprogramming of MEFs to iPSCs. (A) Schematic representation of the reprogramming experiment with female MEFs bearing the conditional intron1 allele on the Xi and a *Xist* knockout allele on the Xa. Reprogramming was induced by infection with pMX retroviruses encoding the reprogramming factors and the reprogramming culture was split at day three post-infection. Deletion of the conditional intron1 allele was induced by delivery of 1X or 10X adenoviral particles carrying Cre-recombinase performed at day 4. Control 1X Ad-Null treatment was done in parallel. At day 13 of reprogramming, efficient deletion of intron1 was assessed by genotyping, reprogramming efficiency assessed by Nanog-positive colony count, and loss of *Xist* RNA coating in Nanog-positive cells was examined by IF/FISH. In addition, individual colonies were

picked, expanded, and analyzed further. **(B)** PCR genotyping for the presence of the 2lox and 1lox intron1 alleles in reprogramming cultures at day 13, using primers pairs A and C (top panel) or B and C (bottom panel) (as in Figure 2.1F), indicates efficient deletion of intron1 upon Ad-Cre treatment. 1 and 2 represent independent reprogramming samples. The asterisk marks the wt allele, which is attributed to the presence of feeder cells in reprogramming cultures. **(C)** FISH of starting MEFs before introduction of pMX retrovirus displaying *Xist* coating (left) and Immunostaining/FISH images (right) of representative Nanog-positive colonies in reprogramming cultures treated with Ad-Null and Ad-Cre, respectively, at day 13 of reprogramming, showing Nanog expression (red), FISH for *Xist* RNA using a DNA probe (green), and dapi (Blue). Note that Nanog-positive cells at this stage of reprogramming only display a biallelic pinpoint signal with the double-stranded DNA probe, which can be attributed to *Tsix* expression. **(D)** Graph summarizing reprogramming efficiency by counting Nanog+ colonies at day 13. **(E)** Graph showing the percentage of Nanog-positive cells without a *Xist* RNA cloud at day 13 of reprogramming. All Nanog+ cells (number is given) on the reprogramming culture coverslip were counted and analyzed for the *Xist* signal. **(F)** The graph summarizes the percentage of Nanog-positive nuclei with and without *Xist* RNA clouds in individually expanded iPSC clones from Ad-Null or Ad-Cre reprogramming cultures (200 nuclei counted for each sample). Genotyping of all iPSC clones confirmed that intron1 was deleted in all iPSCs expanded from Ad-Cre reprogramming cultures. **(H)** MEFs were obtained from XX:1lox intron/*ΔXist* embryos and reprogrammed with Oct4, Sox2, and Klf4. Immunostaining/FISH images show the presence of normal Xist RNA coating in the starting MEFs and the absence of *Xist* RNA coating in resulting Nanog-positive colonies at day 13 of reprogramming. **(I)** Graph showing counts of Nanog-positive colonies at day 13 of reprogramming for two different XX:1lox intron/*ΔXist* MEF preparations (A and B, from different matings) and one XX:2lox intron/*ΔXist* line.

Discussion

In summary, our data argue that *Xist* intron1 does not represent an essential tether coupling repression of both *Xist* and XCI to the pluripotent state. ESCs lacking intron1 do not dysregulate *Xist* expression in the undifferentiated state nor upon *in vitro* differentiation, reprogramming to the iPSC state leads to *Xist* repression on an Xi lacking intron1, and mice lacking intron1 do not display any of the gross reproductive abnormalities that would be expected if XCI was perturbed.

The deletion of intron1 represents a clean experimental system to probe the functional role of a genomic element that displays very strong pluripotency transcription factor binding, unhampered by the secondary effects on initiation of XCI associated with global modulation of protein factors implicated in the maintenance of the pluripotent state. While correlative binding studies were supported in part by *Xist* dysregulation in ESC lines with inducible deletions of the pluripotency factors Nanog and Oct4, our study cautions against extrapolating these findings to the behavior of wildtype ESCs and mice. A compromised pluripotency factor network could unmask the mild intron1 contribution to the *Xist* repressive pathway. In the case of the ZHBTc4 cell line, this altered network

may show Rnf12 upregulation followed by downregulation of the pluripotency factor Rex1, sufficient to trigger XCI in male cells independent of intron1 (Barakat et al., 2011a; Gontan et al., 2012). We also noted that ZHBTc4 ESCs lack pinpoint *Tsix* signal and draw a corollary between their *Xist* upregulation and our male ESCs deleted for *Tsix (*that, when differentating, have a significantly greater number of *Xist* clouds upon deletion of intron1).

In light of the two mild phenotypes (skewing effect of deleting intron1 in female ESCs heterozygous for the allele and the increase in *Xist* clouds in *Tsix* and intron1-deleted differentiating male ESCs), we hypothesize that intron1 loss leads to mild destabilization of *Xist* transcriptional repression at the transition to the differentiated state, in the narrow development window of XCI initiation. Unable to capture a transcriptional difference in *Xist* levels at the onset of *in vitro* differentiation, we believe that more sensitive methods of transcript quantitation or investigation of chromatin state may address this hypothesis.

We noted a discrepancy between the *ex vivo* XCI skewing phenotype and the normally occurring *in vivo* XCI choice in the absence of the intron. This lack of intron1 deletion effect in adult mice and in ESC differentiation induced by bFGF/Activin (Supp Fig 2.5) which is sensitive to clonogenic skewing of XCI because of serial passage and outgrowth of few cells (unlike monolayer differentiation, Chenoweth and Tesar, 2010), suggests that *Xist* regulation is more robust *in vivo* than *in vitro* in the absence of the intron1. For instance, slightly different cis-acting elements could be used *in vivo* and *in vitro* for regulating *Xist* expression. Thus, the cell culture-observed favoring of the intron-deleted *Xist* could not be organismally relevant or the stochastic developmental nature of XCI could overshadow the effect.

It seems that the regulation of *Xist*, at the helm of a chromosome-wide program of gene expression, is genetically ensured by a complex multifactor mechanism. The dispensability of intron1 for repression of *Xist* may be mouse-specific as mice appear to be unique in the functionality of *Tsix* and also in the sufficiency of *Xist* activators such as Rnf12 to elicit *Xist* upregulation: addition of one copy of Rnf12 is sufficient to drive *Xist* expression in undifferentiated female ESCs (Jonkers et al., 2009). Other eutherians such as bovines and humans, with truncated and likely non-functional *TSIX*, may rely more on intron1-dependent mechanisms for *Xist* repression (Chureau et al., 2002). Therefore, evolution of the overlapping *Tsix* gene and the network of XCI activators in mice may have become the dominant mechanism in *Xist* repression.

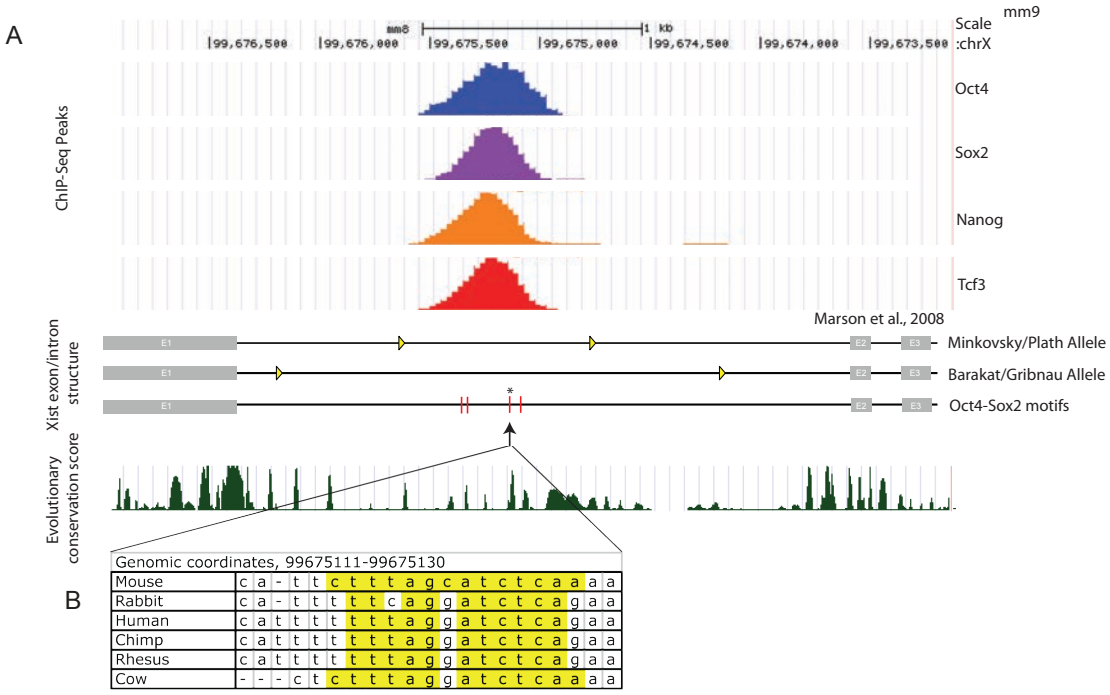

Figure S2.1. Characterization of the targeted region of Xist intron1. The targeted region of Xist intron1 contains published ChIP-seq pluripotency factor binding peaks and captures conserved Oct4-Sox2 binding motifs. (A) Genome browser (http://genome.ucsc.edu/) view of the Xist locus (exons and introns are indicted; genome build mm9) with Chip-Seq peaks (Marson et al., 2008) for Oct4, Sox2, Nanog, and Tcf3, and PhastCons mammalian conservation track. Yellow triangles denote loxP sites for the Minkovsky/Plath allele as in the Figure 1 targeting scheme, and for the Barakat/Gribnau intron1 allele (Barakat et al., 2011). Red tick marks denote positions of Oct4-Sox2 DNA sequence motifs identified by Contrast Motif Finder (Mason et al., 2010). (B) One of two highly scoring Oct4-Sox2 motifs (*) is shown by genomic sequence alignment from six eutherian mammals with invariant motif positions highlighted.

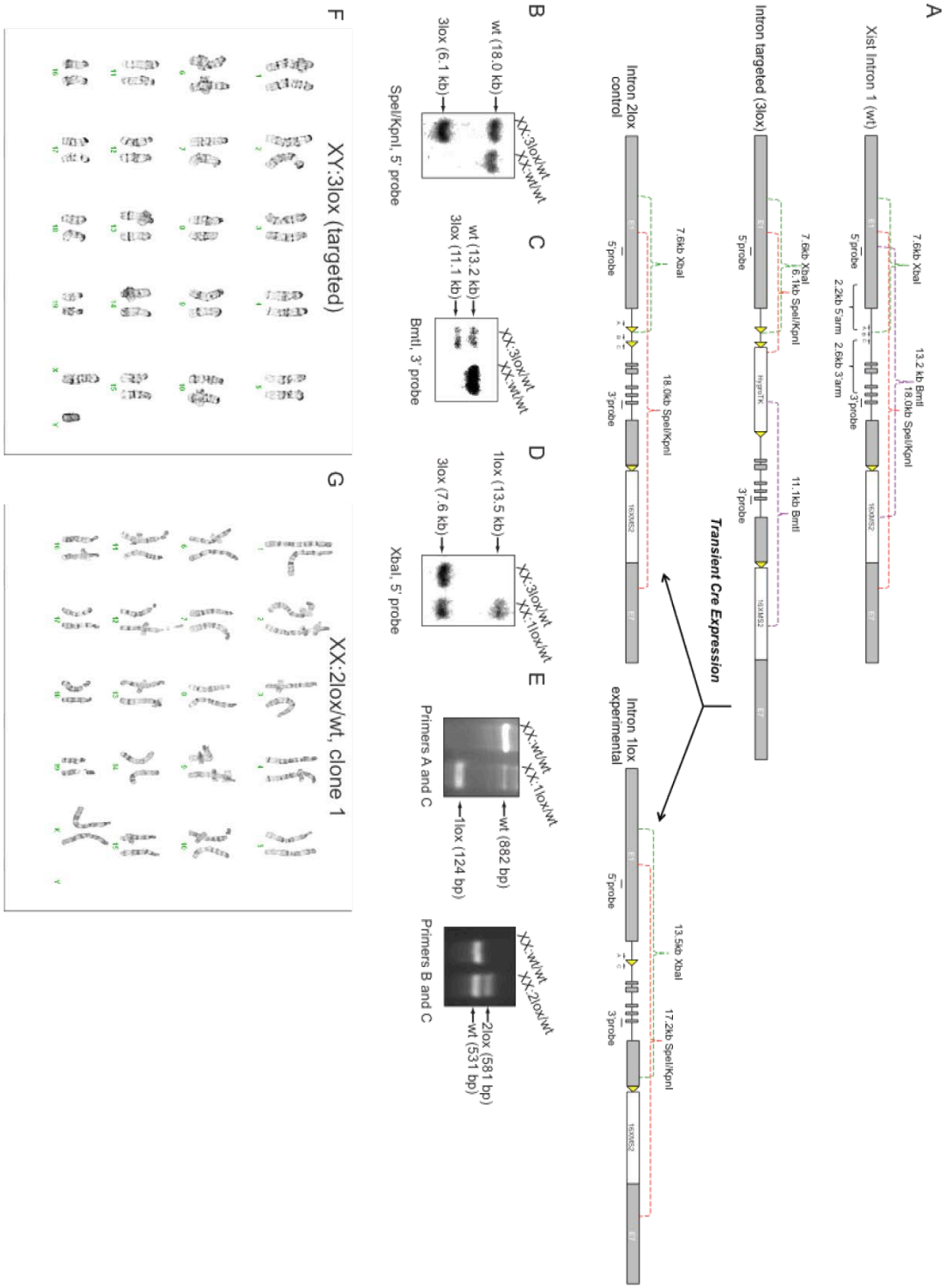

Figure S2.2. Generation of the conditional Xist intron1 allele in female mouse ESCs. (A) Gene targeting and Southern analysis strategy schematic for female mouse ESCs (F1 2-1; derived from a F1 cross of 129SV/Jae with CAST/ei) with an *Xist* RNA tag of 16 MS2 sequence repeats in exon 7 of the Xist gene on the 129 allele (Jonkers et al., 2008). (B,C) Targeting of the MS2-tagged X chromosome was confirmed with X allele-discriminating BmtI digest and Southern blotting with the 3' probe. (D) Transient expression of Cre recombinase in properly targeted clones yielded both 2lox (control)

and 1lox (experimental) ESC clones as identified by Southern blotting. (E) PCR genotyping with primers A and C was used to detect the 1lox allele and with primers B and C to detect the 2lox allele. (F) Cytogenetic analysis of targeted ESC clones indicated a normal karyotype. For male V6.5 ESCs targeted for Xist intron1 (3lox clone) all twenty spreads displayed a normal male karyotype as shown in the representative image. 2lox and 1lox subclones of this line were injected into blastocysts and resulting chimeric mice were bred for germline transmission to establish Xist intron1 mouse colonies. (G) For 2lox/wt female ESCs (clone 1) 19 of 20 analyzed cells displayed a normal female karyotype as shown.

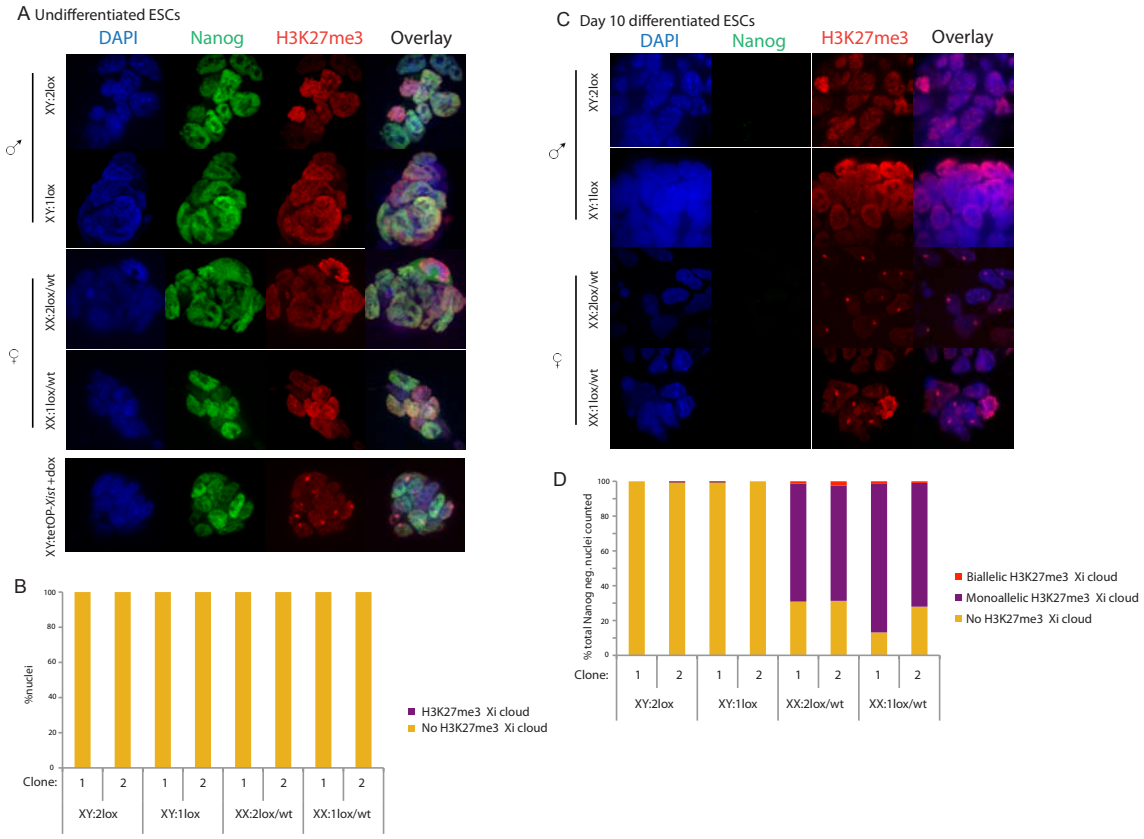

Figure S2.3. Characterization of *Xist* RNA coating in the absence and presence of intron1, by assessing H3K27 trimethylation on the Xi. (A) Immunostaining for Nanog (green) and H3K27me3 (red) in undifferentiated male and female ESC lines of the indicated genotypes. Dapi staining (blue) indicates nuclei. Representative images are shown. A male ESC line carrying a dox-inducible *Xist* allele in the endogenous locus, cultured in the presence of dox for 24 hrs, was used as positive control for detection of *Xist* RNA coating and H3K27me3 enrichment on the Xi. (B) Graph summarizes the proportion of dapi-stained nuclei with the indicated patterns of H3K27me3 for the stainings described in (A). Pairs of independent clones of given genotype were stained and counted. In each case 500 nuclei were counted. (C) As in (A), except that ESCs differentiated for ten days via embryoid bodies were analyzed by immunostaining. (D) Graph summarizing the proportion of dapi-stained, Nanog-negative nuclei with indicated H3K27me3 patterns for differentiated ESC lines as shown in (C).

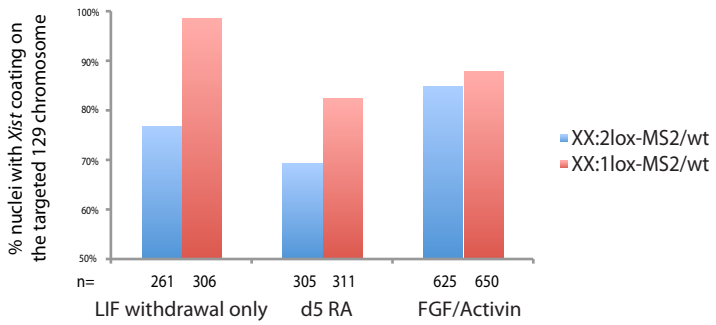

Figure S2.4. Analysis of allele-specific coating of *Xist* in female ESC clones with andwithout intron1, subjected to various in vitro differentiation methods. F1 2-1 ESC lines carrying the MS2 tag and the indicated intron1 mutation within Xist on the 129 allele were differentiated for five days by LIF withdrawal alone, LIF withdrawal and addition of all trans retinoic acid, and by bFGF and Activin A treatment over four passages. As described in Figure 2C in FISH experiments with *Xist* and MS2 probe, *Xist* expression from the 129 chromosome (targeted chromosome), with and without intron1, respectively (2lox or 1lox), is detected by both the *Xist* and MS2 FISH probes (DNA probes), while *Xist* expression from the CAST chromosome is only detected by the *Xist* probe. The graph depicts the percentage of cells where the intron1-targeted 129 chromosome is coated by *Xist* RNA, as identified by co-localization of the *Xist* and MS2 signals. The number of *Xist* clouds analyzed for each sample is given.

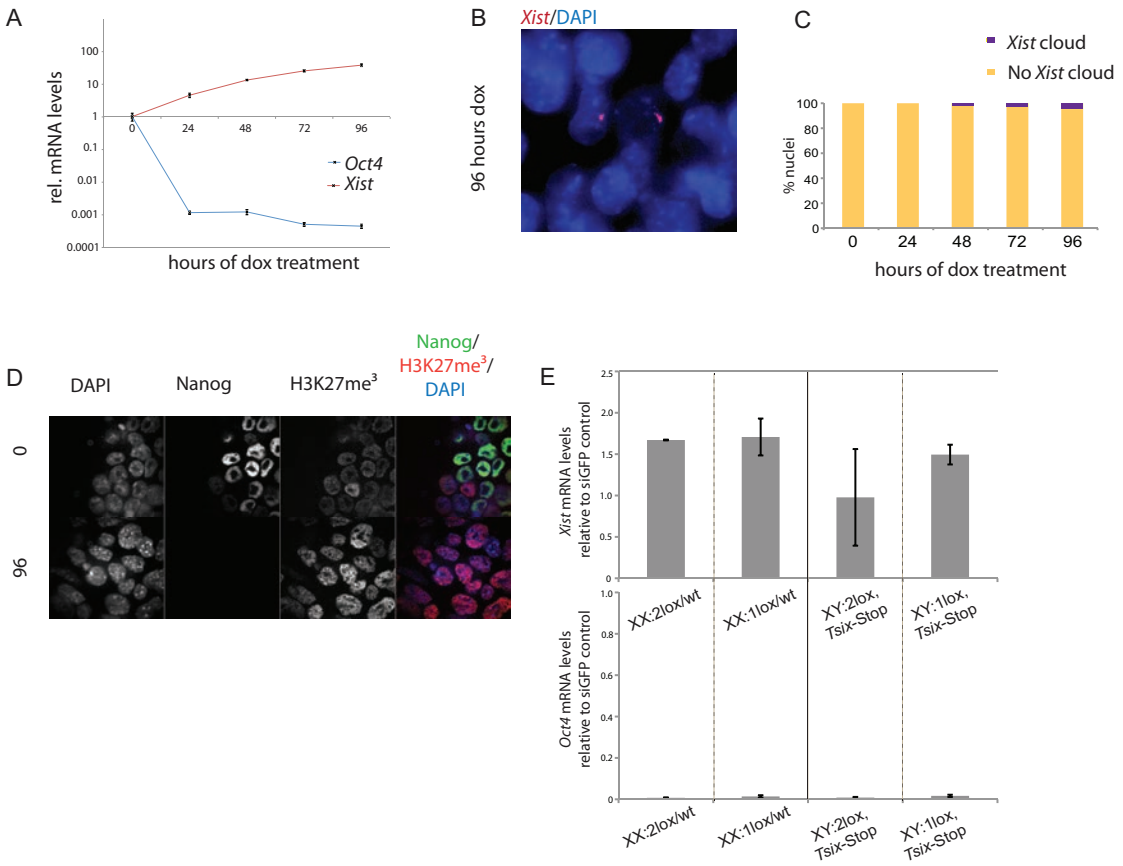

Figure S2.5. *Xist* levels upon acute downregulation of Oct4 in ESCs in the presenceand absence of intron1. (A) The ZHBTc4 doxycycline-repressible Oct4 male ESCs line (Niwa et al., 2000) was treated for the indicated time with doxycycline (dox) and assayed for Oct4 and Xist RNA levels by RT-PCR. Values are normalized to Gapdh mRNA levels and given relative to levels in untreated ZHBTc4 ESCs. Mean values are plotted on a log-10 scale ±SD from triplicate RT-PCR measurements. (B) Representative image of oligo-based, strand-specific RNA FISH (Raj et al., 2008) for *Xist* RNA (red) at 96 hours after dox addition. Dapi-staining indicates nuclei. (C) The graph summarizes the percentage of ZHBTc4 ESCs with a *Xist* RNA cloud signal detected by oligo-based RNA FISH at the indicated time points post dox-addition, as shown in (B). At each timepoint 500 nuclei were assessed. (D) Representative immunostaining images for Nanog (green) and H3K27me3 (red) before and 96 hours after addition of dox, indicating efficient loss of Nanog and therefore induction of differentiation without onset of Xi-like H3K27me3 staining pattern at 96 hrs of dox addition. (E) Heterozygous female ESCs with and without intron1, respectively (2lox/wt versus 1lox/wt), and male ESCs lacking Tsix, with and without intron1, were treated with siRNA targeting Oct4 or GFP as control, and levels of *Xist* RNA (top) and Oct4 transcripts (bottom) were measured by RT-PCR 72 hours later. Values were normalized to Gapdh transcript levels and are shown relative to levels in siGFP treated ESCs and represent mean ±SD from triplicate measurements.

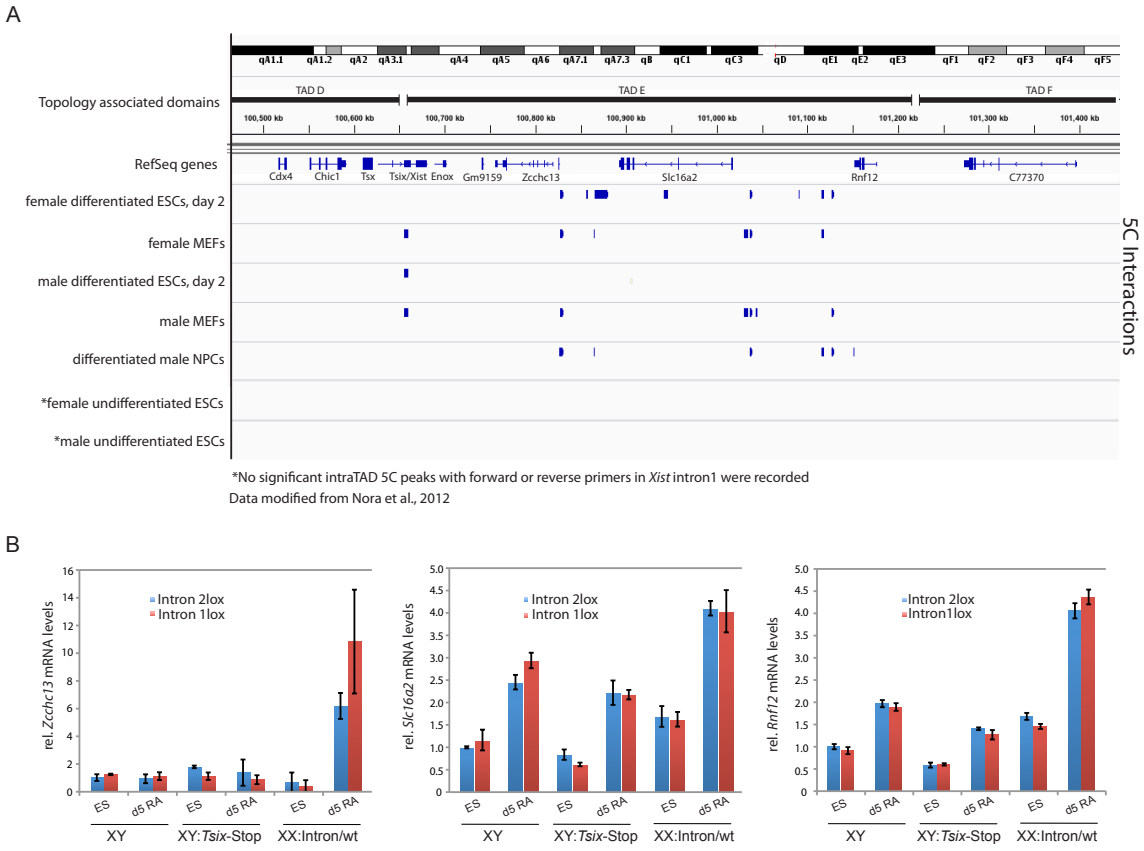

Figure S2.6. Expression analysis of genes in the Xist containing TAD in ESCs with and without intron1. (A) IGV browser view of significant contacts between the Xist intron1 genomic region and other genomic regions within the Xist-containing topological associating domain (TAD) (intra-TAD E events) in indicated cells types. These data are taken from (Nora et al., 2012). Blue ticks indicate the genomic regions that come in close contact to the intron1 region of Xist. (B) Graphs summarizing RT-PCR for *Zcchc13, Slc16a2,* and *Rnf12* mRNA levels normalized to Gapdh transcript levels, in ESCs of the indicated genotypes in the undifferentiated state and at day 5 of retinoic-acid differentiation (n=3, ± 1 SD). These genes are in contact with the intron1 genomic region as indicated in (A).

CHAPTER 2 METHODS

Generation of mutant mouse ESCs and mice

Xist intron1 transgenic mice analyzed in Figures 5B-5E were generated from polymorphic $X^{Xist:2lox\ intron\ (129/Sv)}\ X^{Xist:\ wt\ (CAST/Ei)}$ ESC line 29, in which a 1.8 kb region of *Xist* intron1 was replaced by a floxed neomycin cassette (Barakat et al., 2011). Germline transmission was verified by genotyping for the presence of the neomycin cassette integrated in the intron1 region of *Xist* and XX:2lox/wt females were bred to males expressing pCAGGS-Cre, to loop out the selection cassette. Loopout of the selection cassette was verified by PCR on genomic tail-tip derived DNA. All other intron1- mutant ESC lines and mice carrying the Plath/Minkovsky allele were derived from a targeting construct generated by cloning the respective genomic fragments representing the 5' and 3' homology regions into the pCRII plasmid vector upon PCR amplification (see Supp Table 1 for list of primers used). The 800 bp of intron sequence with a 5' loxP site were ligated between a 2.2 kb 5' homology arm and 3' 2.6 kb homology arm by *Age*I/*Not*I subcloning. A positive-negative CMV-HygroTK cassette flanked by loxP sites was inserted into the unique *Not*I site. A diphtheria toxin gene (PGK-DTA) was inserted into a unique backbone *EcoR*I site. 40 µg of plasmid were linearized by MluI digestion and electroporated into male ESCs (V6.5 line; F1 between C57BL/6 and 129SV/Jae) and into female F1 2-1 ESCs carrying the MS2 tag in the final large exon of *Xist* (F1 between C57BL/6 and CAST/Ei) cells co-cultured with drug-resistant DR4 MEFs (Jonkers et al., 2008; Tucker et al., 1997). Hygromycin selection (140 µg/ml) was started one day after and clones were screened by *Spe*I/*Kpn*I digest and both 5' and 3' external probes. *Bmt*I digest and 3' external probe were used to assess allelism of targeting in F1 2-1 clones. Targeting efficiency was 30% in V6.5 and 1% in F12-1 cells. Two independent V6.5 and one F1 2-1 clones were expanded, electroporated with pPAC-Cre plasmid, and selected with G418 (300 µg/mL) for 8 days. Southern blot screening was

performed with a 5' probe and *Xba*I digest for 1lox and *SpeI*/*Kpn*I for 2lox clones. All subsequent intron1 genotyping was performed by PCR. For intron1/*Tsix*-Stop double transgenic ESC clones, XY:2lox and XY:1lox V6.5 clones were targeted with pAA2Δ1.7 and screened by Southern blot as previously described (Sado et al., 2001). XY:1lox V6.5 ES cells were microinjected into C57BL/6 blastocysts to produce chimeric mice following standard procedures. High agouti coat color-contributing chimeras were bred with C57BL/6 females for germline transmission. All animal experiments were in accordance with the legislation of the Erasmus MC Animal Experimental Commission and the UCLA Animal Research Committee.

Cell culture, differentiation, and reprogramming methods

ESCs were grown on irradiated DR4 mouse embryonic fibroblasts (MEFs) in standard media (DMEM supplemented with 15% FBS, nonessential amino acids, L-glutamine, penicillin-streptomycin, β-mercaptoethanol, and 1000 U/mL LIF). Prior to induction of RA-differentiation, cells were feeder-depleted for 45 minutes on gelatinized plates and plated at a density of 5.0×10^4 cells/ 6-well in MEF media (same as ESC media except 10% FBS and excluding LIF). One day later, MEF media was supplemented with 1μM all trans retinoic acid (Sigma) or with DMSO only (LIF withdrawl) and refreshed every two days. For embryoid body differentiation, ESCs were pre-plated on gelatin overnight to feeder deplete, briefly trypsinized, and put in MEF media for suspension culture on bacterial culture plates for four days, then plated on gelatinized coverslips for another 2 or 6 days. For FGF/Activin differentiation, ESCs were feeder-depleted and 2.0×10^4 cells plated on 6 wells pretreated with fibronectin in DMEMF12/B-27/N-2 (Invitrogen) supplemented with FGF-2 (R&D Systems 40ng/mL) and Activin A (PeproTech, 20 ng/mL). Media was changed daily and colonies were manually passaged onto fibronectin several times then at passage 4 returned to feeder cells.

ZHBTc4 ES cells were induced to differentiate with 1μg/mL doxycycline (resulting in acute repression of Oct4) in standard ESC media (Niwa et al., 2000). For reprogramming, primary MEFs were derived at embryonic day 14.5 and 3-factor retroviral reprogramming was performed following previously published methods (Maherali et al., 2007).

Chromatin immunoprecipitation

ChIP was performed according to previously published methods (Maherali et al., 2007). In summary, formaldehyde-crosslinked chromatin fragments were generated by sonication and 150ug of material were pre-cleared with Protein A sepharose beads. Immunoprecipitation was performed overnight with 5ug antibodies targeting Oct4 (R&D Systems, AF1759) or Sox2 (R&D Systems, AF2018), or with normal goat IgG (Santa Cruz, sc-2028) and subsequent incubation with protein A sepharose beads for 3 hours. Beads were washed and eluted in TE/0.67% SDS. Both IP and input samples were reverse cross-linked overnight at 65 degrees and treated with RNAse A and Proteinase K before DNA phenol-chloroform purification. The proportion of input material immunoprecipitated was calculated using standard curves constructed from input serial dilutions and comparing fractional measurements in IP and input relative to a known region positive for Oct4 and Sox2 binding (Rest, (Berg et al., 2008) ChIP with goat IgG antibody did not find any enrichment (data not shown).

Immunofluorescence and FISH analysis

Cells were plated on glass coverslips (and in the case of embryoid body differentiation permeabilized with 5 minute washes of ice-cold CSK buffer, followed by CSK buffer with 0.5%Triton, and another wash in CSK buffer, washed once with PBS, and fixed for 10 minutes in 4% paraformaldehyde (Plath et al., 2003). Immunonostaining

with antibodies against Nanog (BD Pharmingen 560259) and H3K27me3 (Active Motif 39155) and combined immunostaining/FISH with double-strand *Xist* DNA probe labeled with FITC were performed as previously reported and mounted with Prolong Gold reagent with DAPI (Tchieu et al., 2010). *Xist* and *Tsix* strand-specific RNA probes were made by *in vitro* transcription of T3-ligated PCR products of cDNA templates using Riboprobe system T3 (Promega) with Cy3-CTP (VWR) or FITC-UTP (Perklin Elmer) (Maherali et al., 2007).

qRT-PCR Analysis and allele-specific qRT-PCR

Cells were harvested from a 6 well format in Trizol (Invitrogen) and RNA purification was performed with the RNeasy kit (Qiagen) according to manufacturer's instructions with on-column DNAse treatment (Qiagen). cDNA was prepared using SuperScript III (Invitrogen) with random hexamers and qRT-PCR was performed using a Stratagene Mx3000 thermocycler with primers listed in Supp Table 1. Results were normalized to Gapdh by the ΔCt method. To assess XCI skewing in adult mice, parts of organs were collected, snap-frozen and triturated using micropestles in 1 ml of Trizol reagent (Invitrogen). After an additional centrifugation to clear debris, 700 µl was added to 300 µl fresh Trizol, and RNA was purified following manufacturer's instructions. RNA was reverse-transcribed with SuperScript II (Invitrogen) using random hexamers. Allele-specific *Xist* expression was analyzed by RT-PCR amplifying a length polymorphism using primers *Xist* LP 1445 and *Xist* LP 1446. To determine allele-specific X-linked gene expression of *Mecp2* and *G6pdx* primers MeCP2-*Dde*I-F and R and G6PD-*ScrF*I-F and R were used to amplify respective RFLPs. PCR products were gel-purified and digested with the indicated restriction enzymes and analyzed on a 2% agarose gel stained with ethidium bromide. Allele-specific expression was determined by measuring relative band intensities using a Typhoon image scanner and ImageQuant software.

Luciferase enhancer assay

XY:2lox ESCs were transfected by electroporation, as in intron1 targeting, with 40 µg of one of three *BamH*I-linearized pgl4.27-cloned constructs (Promega, Supp. Table 1) and transferred to hygromycin selection (140µg/mL) one day later. After serial passaging and outgrowth of stable transfectants 1.0×10^5 or 2.0×10^4 ESCs were seeded for differentiation with and without (no LIF) retinoic acid for 3 and 5 days and harvested along with 2.0×10^5 ES cells and measured for luciferase activity with the luciferase assay system (Promega).

REFERENCES

Barakat, T.S., Gunhanlar, N., Pardo, C.G., Achame, E.M., Ghazvini, M., Boers, R., Kenter, A., Rentmeester, E., Grootegoed, J.A., and Gribnau, J. (2011). RNF12 activates Xist and is essential for X chromosome inactivation. PLoS Genet *7*, e1002001.

Berg, D.L.C. van den, Zhang, W., Yates, A., Engelen, E., Takacs, K., Bezstarosti, K., Demmers, J., Chambers, I., and Poot, R.A. (2008). Estrogen-Related Receptor Beta Interacts with Oct4 To Positively Regulate Nanog Gene Expression. Mol. Cell. Biol. *28*, 5986–5995.

Brockdorff, N., Ashworth, A., Kay, G.F., Cooper, P., Smith, S., McCabe, V.M., Norris, D.P., Penny, G.D., Patel, D., and Rastan, S. (1991). Conservation of position and exclusive expression of mouse Xist from the inactive X chromosome. Nature *351*, 329–331.

Brown, C.J., Ballabio, A., Rupert, J.L., Lafreniere, R.G., Grompe, M., Tonlorenzi, R., and Willard, H.F. (1991). A gene from the region of the human X inactivation centre is expressed exclusively from the inactive X chromosome. Nature *349*, 38–44.

Cattanach, B.M., and Isaacson, J.H. (1967). Controlling elements in the mouse X chromosome. Genetics *57*, 331–346.

Chaumeil, J., Le Baccon, P., Wutz, A., and Heard, E. (2006). A novel role for Xist RNA in the formation of a repressive nuclear compartment into which genes are recruited when silenced. Genes Dev. *20*, 2223–2237.

Chen, X., Xu, H., Yuan, P., Fang, F., Huss, M., Vega, V.B., Wong, E., Orlov, Y.L., Zhang, W., Jiang, J., et al. (2008). Integration of external signaling pathways with the core transcriptional network in embryonic stem cells. Cell *133*, 1106–1117.

Chenoweth, J.G., and Tesar, P.J. (2010). Isolation and maintenance of mouse epiblast stem cells. Methods Mol. Biol. *636*, 25–44.

Chow, J., and Heard, E. (2009). X inactivation and the complexities of silencing a sex chromosome. Curr. Opin. Cell Biol. *21*, 359–366.

Chureau, C., Prissette, M., Bourdet, A., Barbe, V., Cattolico, L., Jones, L., Eggen, A., Avner, P., and Duret, L. (2002). Comparative sequence analysis of the X-inactivation center region in mouse, human, and bovine. Genome Res. *12*, 894–908.

Chuva de Sousa Lopes, S.M., Hayashi, K., Shovlin, T.C., Mifsud, W., Surani, M.A., and McLaren, A. (2008). X Chromosome Activity in Mouse XX Primordial Germ Cells. PLoS Genet *4*, e30.

Creyghton, M.P., Cheng, A.W., Welstead, G.G., Kooistra, T., Carey, B.W., Steine, E.J., Hanna, J., Lodato, M.A., Frampton, G.M., Sharp, P.A., et al. (2010). Histone H3K27ac separates active from poised enhancers and predicts developmental state. Proc. Natl. Acad. Sci. U.S.A. *107*, 21931–21936.

Dixon, J.R., Selvaraj, S., Yue, F., Kim, A., Li, Y., Shen, Y., Hu, M., Liu, J.S., and Ren, B. (2012). Topological domains in mammalian genomes identified by analysis of chromatin interactions. Nature *485*, 376–380.

Donohoe, M.E., Silva, S.S., Pinter, S.F., Xu, N., and Lee, J.T. (2009). The pluripotency factor Oct4 interacts with Ctcf and also controls X-chromosome pairing and counting. Nature *460*, 128–132.

Eggan, K., Akutsu, H., Hochedlinger, K., Rideout, W., 3rd, Yanagimachi, R., and Jaenisch, R. (2000). X-Chromosome inactivation in cloned mouse embryos. Science *290*, 1578–1581.

Erwin, J.A., Del Rosario, B., Payer, B., and Lee, J.T. (2012). An ex vivo model for imprinting: mutually exclusive binding of Cdx2 and Oct4 as a switch for imprinted and random X-inactivation. Genetics *192*, 857–868.

Gontan, C., Achame, E.M., Demmers, J., Barakat, T.S., Rentmeester, E., Van IJcken, W., Grootegoed, J.A., and Gribnau, J. (2012). RNF12 initiates X-chromosome inactivation by targeting REX1 for degradation. Nature *485*, 386–390.

Huynh, K.D., and Lee, J.T. (2003). Inheritance of a pre-inactivated paternal X chromosome in early mouse embryos. Nature *426*, 857–862.

Jonkers, I., Monkhorst, K., Rentmeester, E., Grootegoed, J.A., Grosveld, F., and Gribnau, J. (2008). Xist RNA is confined to the nuclear territory of the silenced X chromosome throughout the cell cycle. Mol. Cell. Biol. *28*, 5583–5594.

Jonkers, I., Barakat, T.S., Achame, E.M., Monkhorst, K., Kenter, A., Rentmeester, E., Grosveld, F., Grootegoed, J.A., and Gribnau, J. (2009). RNF12 is an X-Encoded dose-dependent activator of X chromosome inactivation. Cell *139*, 999–1011.

Kalantry, S., Purushothaman, S., Bowen, R.B., Starmer, J., and Magnuson, T. (2009). Evidence of Xist RNA-independent initiation of mouse imprinted X-chromosome inactivation. Nature *460*, 647–651.

Kay, G.F., Penny, G.D., Patel, D., Ashworth, A., Brockdorff, N., and Rastan, S. (1993). Expression of Xist during mouse development suggests a role in the initiation of X chromosome inactivation. Cell *72*, 171–182.

Lee, J.T., Davidow, L.S., and Warshawsky, D. (1999). Tsix, a gene antisense to Xist at the X-inactivation centre. Nat. Genet *21*, 400–404.

Loh, Y.-H., Wu, Q., Chew, J.-L., Vega, V.B., Zhang, W., Chen, X., Bourque, G., George, J., Leong, B., Liu, J., et al. (2006). The Oct4 and Nanog transcription network regulates pluripotency in mouse embryonic stem cells. Nature Genetics *38*, 431–440.

Luikenhuis, S., Wutz, A., and Jaenisch, R. (2001). Antisense transcription through the Xist locus mediates Tsix function in embryonic stem cells. Mol. Cell. Biol. *21*, 8512–8520.

Ma, Z., Swigut, T., Valouev, A., Rada-Iglesias, A., and Wysocka, J. (2011). Sequence-specific regulator Prdm14 safeguards mouse ESCs from entering extraembryonic endoderm fates. Nature Structural & Molecular Biology *18*, 120–127.

Maherali, N., Sridharan, R., Xie, W., Utikal, J., Eminli, S., Arnold, K., Stadtfeld, M., Yachechko, R., Tchieu, J., Jaenisch, R., et al. (2007). Directly reprogrammed fibroblasts show global epigenetic remodeling and widespread tissue contribution. Cell Stem Cell *1*, 55–70.

Mak, W., Nesterova, T.B., De Napoles, M., Appanah, R., Yamanaka, S., Otte, A.P., and Brockdorff, N. (2004). Reactivation of the paternal X chromosome in early mouse embryos. Science *303*, 666–669.

Marahrens, Y., Panning, B., Dausman, J., Strauss, W., and Jaenisch, R. (1997). Xist-deficient mice are defective in dosage compensation but not spermatogenesis. Genes Dev. *11*, 156–166.

Marahrens, Y., Loring, J., and Jaenisch, R. (1998). Role of the Xist Gene in X Chromosome Choosing. Cell *92*, 657–664.

Marson, A., Levine, S.S., Cole, M.F., Frampton, G.M., Brambrink, T., Johnstone, S., Guenther, M.G., Johnston, W.K., Wernig, M., Newman, J., et al. (2008). Connecting microRNA genes to the core transcriptional regulatory circuitry of embryonic stem cells. Cell *134*, 521–533.

Mason, M.J., Plath, K., and Zhou, Q. (2010). Identification of context-dependent motifs by contrasting ChIP binding data. Bioinformatics *26*, 2826–2832.

Minkovsky, A., Patel, S., and Plath, K. (2012). Concise review: Pluripotency and the transcriptional inactivation of the female Mammalian X chromosome. Stem Cells *30*, 48–54.

Namekawa, S.H., Payer, B., Huynh, K.D., Jaenisch, R., and Lee, J.T. (2010). Two-step imprinted X inactivation: repeat versus genic silencing in the mouse. Mol. Cell. Biol. *30*, 3187–3205.

De Napoles, M., Nesterova, T., and Brockdorff, N. (2007). Early Loss of Xist RNA Expression and Inactive X Chromosome Associated Chromatin Modification in Developing Primordial Germ Cells. PLoS ONE *2*, e860.

Navarro, P., Chambers, I., Karwacki-Neisius, V., Chureau, C., Morey, C., Rougeulle, C., and Avner, P. (2008). Molecular coupling of Xist regulation and pluripotency. Science *321*, 1693–1695.

Navarro, P., Oldfield, A., Legoupi, J., Festuccia, N., Dubois, A., Attia, M., Schoorlemmer, J., Rougeulle, C., Chambers, I., and Avner, P. (2010). Molecular coupling of Tsix regulation and pluripotency. Nature *468*, 457–460.

Navarro, P., Moffat, M., Mullin, N.P., and Chambers, I. (2011). The X-inactivation trans-activator Rnf12 is negatively regulated by pluripotency factors in embryonic stem cells. Hum. Genet. *130*, 255–264.

Nesterova, T.B., Senner, C.E., Schneider, J., Alcayna-Stevens, T., Tattermusch, A., Hemberger, M., and Brockdorff, N. (2011). Pluripotency factor binding and Tsix expression act synergistically to repress Xist in undifferentiated embryonic stem cells. Epigenetics Chromatin *4*, 17.

Niwa, H., Miyazaki, J., and Smith, A.G. (2000). Quantitative expression of Oct-3/4 defines differentiation, dedifferentiation or self-renewal of ES cells. Nat. Genet. *24*, 372–376.

Nora, E.P., Lajoie, B.R., Schulz, E.G., Giorgetti, L., Okamoto, I., Servant, N., Piolot, T., Van Berkum, N.L., Meisig, J., Sedat, J., et al. (2012). Spatial partitioning of the regulatory landscape of the X-inactivation centre. Nature *485*, 381–385.

Okamoto, I., Otte, A.P., Allis, C.D., Reinberg, D., and Heard, E. (2004). Epigenetic dynamics of imprinted X inactivation during early mouse development. Science *303*, 644–649.

Patrat, C., Okamoto, I., Diabangouaya, P., Vialon, V., Le Baccon, P., Chow, J., and Heard, E. (2009). Dynamic changes in paternal X-chromosome activity during imprinted X-chromosome inactivation in mice. Proc. Natl. Acad. Sci. U.S.A. *106*, 5198–5203.

Penny, G.D., Kay, G.F., Sheardown, S.A., Rastan, S., and Brockdorff, N. (1996). Requirement for Xist in X chromosome inactivation. Nature *379*, 131–137.

Plath, K., Fang, J., Mlynarczyk-Evans, S.K., Cao, R., Worringer, K.A., Wang, H., De la Cruz, C.C., Otte, A.P., Panning, B., and Zhang, Y. (2003). Role of histone H3 lysine 27 methylation in X inactivation. Science *300*, 131–135.

Rastan, S., and Robertson, E.J. (1985). X-chromosome deletions in embryo-derived (EK) cell lines associated with lack of X-chromosome inactivation. J Embryol Exp Morphol *90*, 379–388.

Reményi, A., Lins, K., Nissen, L.J., Reinbold, R., Schöler, H.R., and Wilmanns, M. (2003). Crystal structure of a POU/HMG/DNA ternary complex suggests differential assembly of Oct4 and Sox2 on two enhancers. Genes Dev. *17*, 2048–2059.

Sado, T., Wang, Z., Sasaki, H., and Li, E. (2001a). Regulation of imprinted X-chromosome inactivation in mice by Tsix. Development *128*, 1275–1286.

Sado, T., Li, E., and Sasaki, H. (2002). Effect of TSIX disruption on XIST expression in male ES cells. Cytogenet. Genome Res. *99*, 115–118.

Silva, J., Mak, W., Zvetkova, I., Appanah, R., Nesterova, T.B., Webster, Z., Peters, A.H.F.M., Jenuwein, T., Otte, A.P., and Brockdorff, N. (2003). Establishment of histone h3 methylation on the inactive X chromosome requires transient recruitment of Eed-Enx1 polycomb group complexes. Dev. Cell *4*, 481–495.

Silva, J., Nichols, J., Theunissen, T.W., Guo, G., Van Oosten, A.L., Barrandon, O., Wray, J., Yamanaka, S., Chambers, I., and Smith, A. (2009). Nanog is the gateway to the pluripotent ground state. Cell *138*, 722–737.

Stadtfeld, M., Maherali, N., Breault, D.T., and Hochedlinger, K. (2008). Defining molecular cornerstones during fibroblast to iPS cell reprogramming in mouse. Cell Stem Cell *2*, 230–240.

Sugimoto, M., and Abe, K. (2007). X Chromosome Reactivation Initiates in Nascent Primordial Germ Cells in Mice. PLoS Genet *3*.

Tada, M., Takahama, Y., Abe, K., Nakatsuji, N., and Tada, T. (2001). Nuclear reprogramming of somatic cells by in vitro hybridization with ES cells. Curr. Biol. *11*, 1553–1558.

Tsai, C.-L., Rowntree, R.K., Cohen, D.E., and Lee, J.T. (2008). Higher order chromatin structure at the X-inactivation center via looping DNA. Dev. Biol. *319*, 416–425.

Tucker, K.L., Wang, Y., Dausman, J., and Jaenisch, R. (1997). A transgenic mouse strain expressing four drug-selectable marker genes. Nucleic Acids Res *25*, 3745–3746.

Williams, L.H., Kalantry, S., Starmer, J., and Magnuson, T. (2011). Transcription precedes loss of Xist coating and depletion of H3K27me3 during X-chromosome reprogramming in the mouse inner cell mass. Development *138*, 2049–2057.

Wutz, A., and Jaenisch, R. (2000). A shift from reversible to irreversible X inactivation is triggered during ES cell differentiation. Mol. Cell *5*, 695–705.

High Throughput Screening for XCI Maintenance Factors

CHAPTER 3

INTRODUCTION AND BACKGROUND

Summary

X chromosome inactivation (XCI) is a developmental program of heterochromatin formation that initiates during early female mammalian embryonic development and is maintained through a lifetime of mitotic cell divisions in somatic cells. Despite the characterization of the long noncoding RNA *Xist* and protein factors in the establishment of inactive X chromosome (Xi) heterochromatin, only interference with DNA methylation can reactivate the Xi to a significant extent once XCI has been established. Since the contribution of known factors to silencing is partial, more factors required for faithful maintenance of the Xi are yet to be identified. We took an unbiased screening approach using a genome-wide siRNA library, a collection of chemicals, and novel Xi-linked reporter gene cell lines. X chromosome reactivation was sensitized by inhibition of the maintenance DNA methyltransferase 1 (Dnmt1). We report that Atf7ip functions as a heterochromatin protein that synergizes with DNA methylation to stably maintain Xi silencing. Additionally, we characterize the ability of ribonucleotide reductase inhibitors to potentiate the effect of the Dnmt1-inhibiting drug 5-aza-2'-dC on X Chromosome reactivation (XCR) by boosting analog DNA incorporation. Our findings attribute new functional importance to a chromatin-associated protein and describe the cooperative actions of two drugs in the interference of gene silencing.

Introduction

XCI that is initiated in early embryonic development in epiblast cells is maintained for the lifetime of somatic cells. Once established, this random XCI, which occurs on either the maternally or paternally-inherited X chromosome becomes remarkably stable and is only reversed in the cells that give rise to the female germline (Chuva de Sousa Lopes et al., 2008; Heard and Disteche, 2006; de Napoles et al., 2007; Sugimoto and Abe, 2007). Experimental Xi reactivation is achieved by reversion of the somatic cell to a

pluripotent state by either induced pluripotent cell reprogramming, cell fusion to ES cells, or somatic cell nuclear transfer (Eggan et al., 2000; Maherali et al., 2007; Tada et al., 2001). The correlation of pluripotency with lack of XCI may mean that factors that aid in XCR may also facilitate reprogramming to the pluripotent state. Thus identification of factors that can help to reactivate a stably maintained Xi are of great interest to improve chromatin state manipulation (Ohhata and Wutz, 2012).

Initiation of XCI involves stepwise epigenetic changes that begin with upregulation and spread of the long noncoding RNA *Xist* on the future Xi (Brockdorff et al., 1991; Kay et al., 1993; Sun et al., 2006). *Xist* is required for the initiation of XCI and its upregulation initiates a cascade of silencing events beginning with the exclusion of RNA polymerase II (pol II) from the *Xist*-coated domain (Chaumeil et al., 2006; Marahrens et al., 1997; Penny et al., 1996). Kinetic studies illustrate that, following pol II depletion, XCI proceeds with gain of H3K9me2, loss of H3K4me3 and histone acetylation marks, recruitment of Polycomb complexes (PRC) 1 and 2 (and deposition of their respective marks H2AK119ub1 and H3K27me3), and gain of H4K20me1 (reviewed by Heard, 2004). Xi-linked gene silencing occurs as early as pol II depletion is observed (Chaumeil et al., 2006). After this initiation phase of XCI is a transition to a maintenance phase in which the repressed state of the X is stabilized. The maintenance phase is marked by Xi incorporation of macroH2A and accumulation of promoter CpG DNA methylation (Heard, 2004).

In the course of the initiation of XCI, this cascade of changes is dependent upon continued *Xist* expression and is reversible (Wutz and Jaenisch, 2000). It has been shown that PRC1 and PRC2 complex members are directly recruited by *Xist* (Plath et al., 2003; Schoeftner et al., 2006). The transition to maintenance phase is marked by the appearance of an Xi that is synchronously replicated in the mid-S phase and is also characterized by the Xi's resistance to reactivation by *Xist* deletion (Casas-Delucchi et

al., 2011; Wutz and Jaenisch, 2000). Still, in maintenance phase *Xist* RNA remains associated with the Xi, recruits MacroH2A, and dissociates in mitosis and re-coats the inactive X in early G1 of cell cycle (Clemson et al., 1996; Csankovszki et al., 1999).

Many of the factors implicated in XCI were identified based on their nuclear enrichment on the Xi by immunofluorescence (Heard, 2004) Yet, Eed (histone methyltransferase of PRC2), Ring1b (E3 ligase of PRC1), or other enzymatic complexes implicated in XCI such as G9a (methylase of H3K9me1 and H3K9me2), and Dnmt3a/b (the de novo DNA methyltransferase) were found to be dispensable for both initiation and maintenance of XCI in transgenic mice (Kalantry and Magnuson, 2006; Leeb and Wutz, 2007; Ohhata et al., 2004; Sado et al., 2004).

Studies of X chromosome reactivation from the maintenance phase have described synergism between *Xist* RNA, DNA methylation, histone variants, and histone hypoacetylation for maintaining XCI (Csankovszki et al., 2001; Hernández-Muñoz et al., 2005; Nusinow et al., 2007; Pasque et al., 2011). Assay of primary mouse embryonic fibroblasts (MEFs) harboring an Xi-linked GFP reporter showed a maximum reactivation in ~11% of cells 13 days after simultaneous Adenovirus-Cre mediated deletion of double-conditional *Xist* and *Dnmt1* alleles (bred onto the Xi-GFP reporter genetic background) (Csankovszki et al., 2001). The contribution of *Xist* to silencing is considerably smaller than that of Dnmt1; *Xist* deletion alone only doubled the a low "spontaneous" background rate of reactivation to 0.05% while *Dnmt1* deletion alone led to 5% reactivation. Treatment with 0.3 uM 5-aza-2'-dC, a deoxycytidine analog that when incorporated into DNA inhibits Dnmt1, led to GFP reactivation in 0.2% of cells (Csankovszki et al., 2001; Ghoshal et al., 2005). These effects were similar when XCR was scored monitoring reactivation of the X-linked *Hprt* gene by biochemical assay (Csankovszki et al., 2001). However, the extent of gene reactivation across the chromosome in these studies was likely partial: the Xi remained late-replicating by BrdU

stain on metaphase chromosome spreads and the GFP-positive Xi reporter cells had only a small increase in reactivation of the *Hprt* reporter in *cis* (Csankovszki et al., 2001). Thus multiple epigenetic layers act together to maintain the silenced state of the Xi and *Xist* retains some role in gene silencing in the maintenance phase that is appreciated only when other repressive modifications are inhibited.

In summary, these studies demonstrate that the Xi is relatively resistant to reactivation by interference with known factors and that seemingly distinct silencing mechanisms act in a combinatorial fashion to "lock-in" the heterochromatin state. This layered regulation is further illustrated by other studies where the contribution of the factor to silencing is monitored on a sensitized XCR background where DNA methylation and/or histone deacetylation are inhibited. For instance, knockdown of *MacroH2A* or *Cullin3* and *SPOP* (members of an E3 ligase complex that can ubiquitinate MacroH2A) does not reactivate Xi-GFP but rates of reactivation increase approximately 2-fold when sensitized by 5-aza-2'-dC and TSA treatment (Hernández-Muñoz et al., 2005; Nusinow et al., 2007)

Many of the factors known to play a functional role in XCI are not specific to Xi heterochromatin maintenance. For instance, macroH2A has well-described autosomal silencing roles yet was initially characterized on the inactive X chromosome (Agelopoulos and Thanos, 2006; Costanzi and Pehrson, 1998; Pasque et al., 2012). We set out to identify novel factors with gene silencing functions by screening for factors than contribute to faithful maintenance of XCI.

CHAPTER 4

DESIGN AND OPTIMIZATION OF THE ASSAY

Design and optimization of a high throughput screen for X chromosome reactivation

To monitor X chromosome reactivation, we adapted a luciferase reporter because of the sensitivity and simplicity of the assay, which we then scaled to a semi-automated screening platform. In order to approximate *in vivo* Xi chromatin dynamics as closely as possible, we incorporated the reporter into mouse ES cells, generated transgenic mice, and derived primary mouse embryonic fibroblasts (MEFs) in which the reporter was developmentally silenced by XCI. The CAGGS (a fusion of Chicken ß-actin and CMV early enhancer element) promoter-driven firefly luciferase sequence was introduced by site-specific FLP-mediated integration into an frt-primed homing site engineered into the *Hprt* locus in male ES cells where the X chromosome is active (Beard et al., 2006). Properly targeted ES cells were identified by Southern blot and demonstrated high levels of luciferase expression (Supp Fig 4.1). Targeted ES cells were injected into C57BL/6 blastocysts and efficiently contributed to chimeras. Chimeric mice were bred with C57BL/6 females to obtain germline transmission. Absolute skewing of XCI to the luciferase-bearing X chromosome was accomplished by breeding male reporter mice with females heterozygous for an *Xist* knockout allele (Marahrens et al., 1997). MEFs with a nuclear fluorescent reporter, a fusion of H2B and Citrine (a yellow fluorescent protein) in the place of luciferase were similarly generated in order to monitor XCR on the single-cell level. CAGGS-promoter driven reporters were subject to developmental XCI as MEFs derived from female XX:HPRT-luciferase/*ΔXist* or XX:HPRT-H2B:Citrine/*ΔXist* d14 embryos had no detectable reporter expression (Fig 4.1A/C, Fig 7.1B).

To assess whether the Xi HPRT-luciferase reporter could be used to monitor XCR, we showed that the inhibition of DNA methylation by knockdown of *Dnmt1* or treatment with the Dnmt1 inhibiting drug, 5-aza-2'-dC could reactivate the luciferase

reporter (Figure 4.1B). We adapted a siRNA-mediated XCR assay to 384-well format. Since mutation of *Dnmt1* has been described to give the highest levels of Xi reporter activation, we aimed to optimize a high throughput screen with the knockdown of *Dnmt1* (Fig 4.1B, Csankovszki et al., 2001). Though in larger format *Dnmt1* knockdown led to robust but small reporter reactivation in ~0.5% of cells, we did not see significant differences on the 384-well screening scale (Fig 4.1C, 5.1D) . We hypothesized that addition of the *Dnmt1* inhibitor chemical 5-aza-2'-dC would critically further reduce *Dnmt1* levels below the threshold needed to detect the ~0.5% of Xi reactivated cells in this smaller starting population in the screening format (Fig 4.1C). We found that at a concentration range of 0.10 to 0.20 uM, 5-aza-2'-dC had a sensitizing effect on eliciting XCR; alone there was no significant difference in luciferase signal compared to untreated wells however, when combined with *Dnmt1* knockdown, we observed consistent increase in luciferase signal (Fig 4.1C). At the concentration of 1.0 uM the magnitude of luciferase signal change attributable to siDnmt1 decreased (the ratio of luciferase signal in the siDnmt1 condition over no knockdown at the given 5-aza-2'-dC concentration) (Fig 4.1C). Therefore, we chose to treat with 0.2 uM 5-aza-2'-dC for the genome-wide siRNA screen to sensitize for reactivation (Fig 4.1E). A scatter plot of plate well values from positive and negative control samples and the Z factor measure of separation between positive and negative control populations of 0.11 predicted potential false negatives and/or false positives, but also indicated that our siRNA-based assay could measure XCR in a high throughput assay (Fig 4.1D, Zhang et al., 1999).

The screen was performed by reverse-transfecting two thousand reporter MEF cells on 384-well plates with siDnmt1 (positive control), with no siRNA (negative control), or with a siRNA from the Ambion silencer mouse genome-wide library (Fig 4.1E). Cells were incubated for 72 hours in the presence of 5-aza-2'-dC and luciferase measurements were collected. Raw ALU values were normalized to individual plate

median values by robust Z score to eliminate batch effects (Supp Fig 4.2, Birmingham et al., 2009). To compensate for the low Z factor of the screen, the library was screened in duplicate and duplicate screen values pooled so that each gene was represented with a total of 4 to 6 luciferase readings from 2 to 3 different siRNAs. siRNA screening data was analyzed using the redundant siRNA activity analysis (RSA) to prioritize gene hits with multiple active siRNAs (Fig 4.1F, König et al., 2007). Internal validation of the methods was provided by the number one hit with this workflow, *Dnmt1* from the genome-wide library (siDnmt1 was also on every plate as a quality control measure). To validate novel hits, we selected the top 54 genes in the RSA analysis with at least two unique active siRNAs, omitting hits we deemed irrelevant such as olfactory receptor genes and reordered the active siRNAs against these genes (Fig 4.1G, Figure S4.3). Luciferase assay in 24-well format, again in the presence of 0.2 uM 5-aza-dC, demonstrated striking increases in luciferase signal from siRNAs against the *Atf7ip* (activating transcription factor 7 interacting protein, also named Mbd1-Containing Chromatin-Associated Factor) and *Rrm2* (ribonucleotide reductase M2) genes.

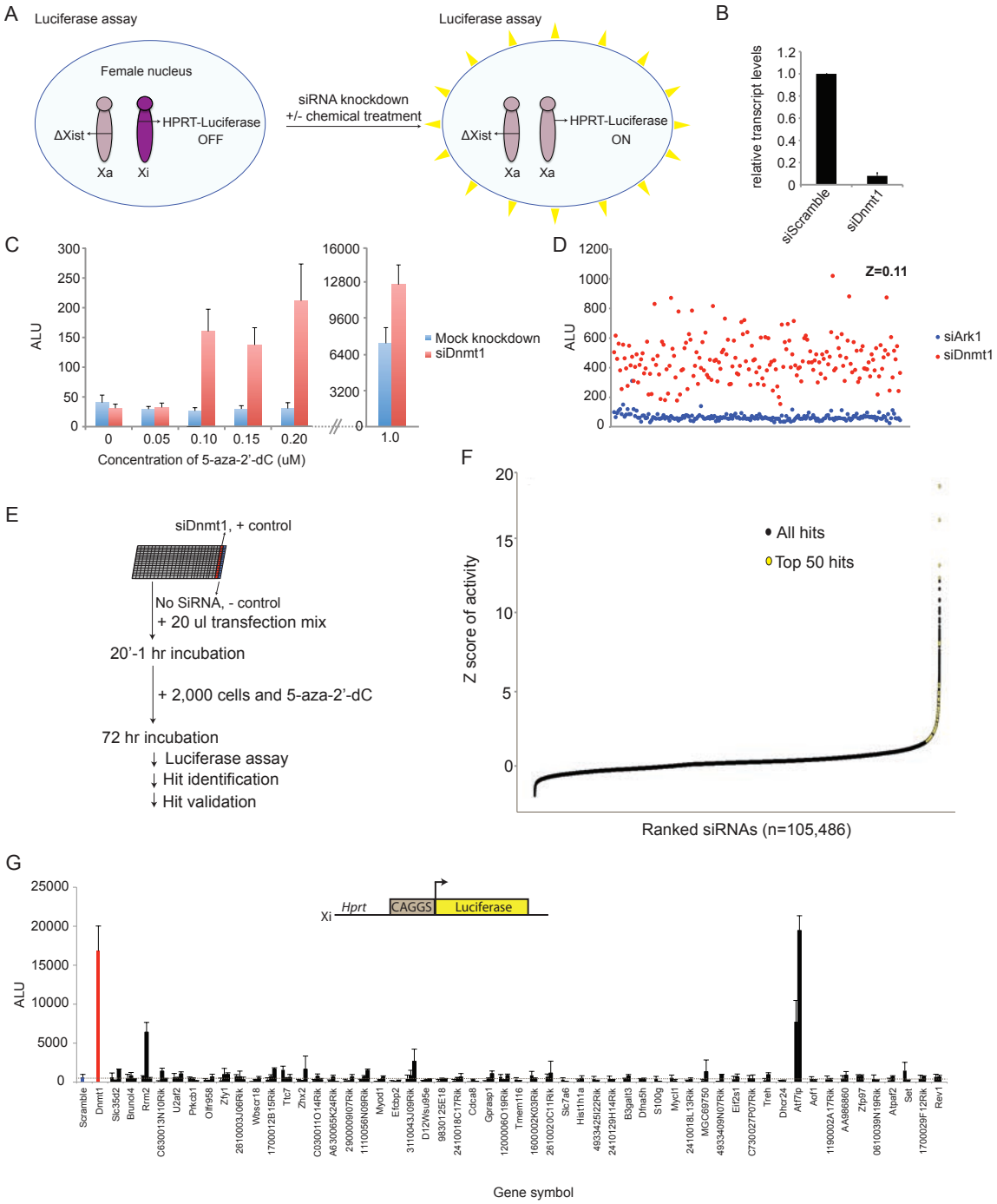

Figure 4.1. Design and optimization of a high throughput assay of X chromosome reactivation. A. Diagram of a primary mouse embryonic fibroblast (MEF) cell with an inactive X chromosome bearing a CAGGS promoter-driven luciferase transgene in the HPRT locus. Reactivation upon *Dnmt1* knockdown is quantified by luciferase assay. B. RT-qPCR for *Dnmt1* RNA levels normalized to siScramble control and GAPDH expression. Error bar indicates standard deviation from two independent experiments measured in triplicate. C. Bar chart illustrating luciferase activity (arbitrary luminescence units, ALU) from reporter MEFs upon knockdown of *Dnmt1* and treatment with varying concentration of 5-aza-2'-dC in 384 well format (error bars denote one standard deviation from the mean, n=8). (D) Scatter plot of individual data points from optimized assay in 384 well format, knockdown of Aurora Kinase 1 (siArk1) is a negative control knockdown. The Z factor, a measure of separation between positive and negative control populations used in the assessment of high throughput assays, is shown. (E) Diagram of screening workflow. Briefly, 1 picomole of

siRNA from the Ambion mouse genome-wide Silencer ® library was plated on 384 well plates and the library screened in duplicate. Each plate contained a row of positive (siDnmt1) and negative (no siRNA) controls for quality control. Two thousand cells were reverse-transfected bringing the final 5-aza-2'-dC concentration to 0.2 uM and cells were incubated for 72 hours prior to luciferase assay. (F) Ranked Z-score distribution for pooled replicates, top 50 hits defined by redundant siRNA activity analysis are in yellow (G). Validation of resynthesized hit siRNAs in 24-well luciferase assay with 2 or 3 active siRNAs for each gene plotted (error bars indicate one standard deviation from duplicate wells).

CHAPTER 4 SUPPLEMENTARY FIGURES

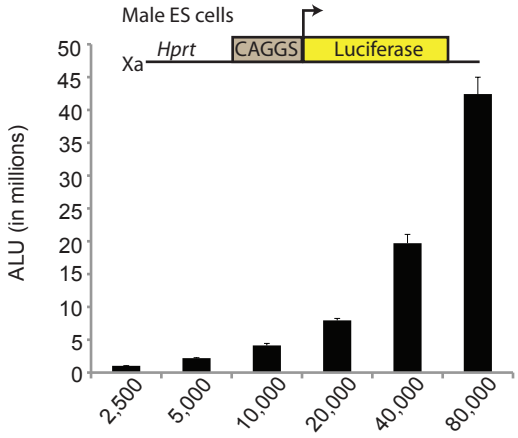

Supp Figure 4.1. Luciferase activity of targeted male HPRT ES cells. Luciferase assay of male ES cells carrying the CAGGS luciferase transgene in the *Hprt* locus on the single male X chromosome, which is active under these conditions due to the absence of XCI in male cells. Cell number titration of constitutively luciferase-expressing male ESC cells demonstrating proportional increase in luminescence units.

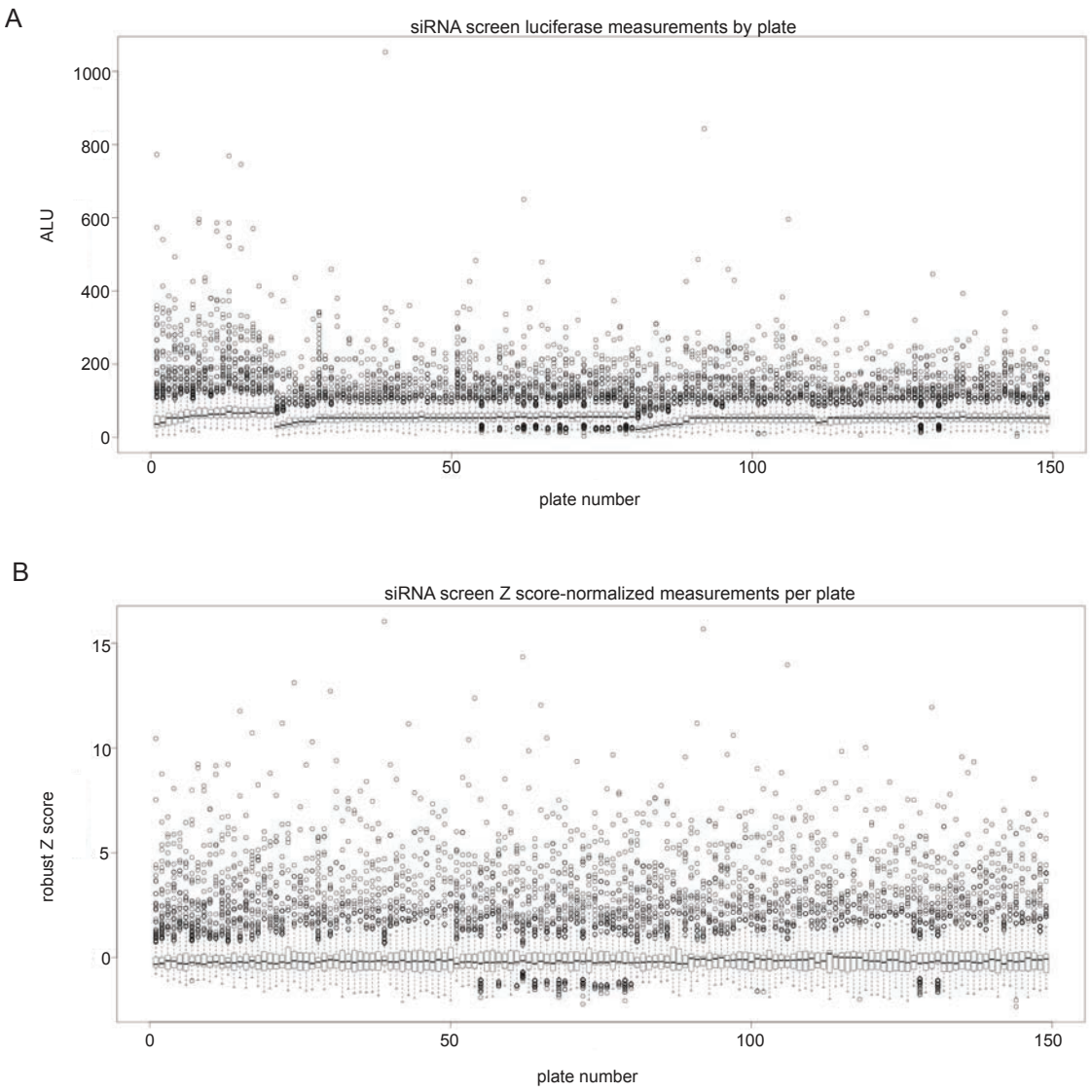

Supp Figure 4.2. siRNA screen batch effects and Z score normalization. (A) Box and whisker plot of all raw luciferase measurements from one duplicate of the screen by individual 384-well plate. (B) Same as in A except each measurement is normalized by robust Z score (the number of median absolute deviations the individual measurement is from the plate median).

Supp Figure 4.3. Table of top RSA hits from siRNA screen, page 1 of 3

Internal control		46	AA98686(	95	Brunol4	144	Enpp2	193	Ankrd32	242	C030018G13
siRNA reordered		47	AA98686(	96	Brunol4	145	Enpp2	194	02N15Rik	243	C030018G13
Further validated		48	AA98686(	97	Brunol4	146	1200009K	195	4631402N15	244	4930470P17
Rank	siRNA Gene	49	Efcbp2	98	Brunol4	147	Olfr676	196	9530080O11	245	Asf1a
1	Dnmt1	50	Efcbp2	99	9030603L14	148	Olfr676	197	9530080O11	246	4930518C23
2	Dnmt1	51	Efcbp2	100	9030603L14	149	Olfr676	198	2610020C11	247	Apxl
3	Dnmt1	52	Efcbp2	101	Hectd2	150	Olfr676	199	2610020C11	248	Apxl
4	Dnmt1	53	Dfna5h	102	43J09Rik	151	Kcnk2	200	2610020C11	249	Apxl
5	Cdkl3	54	Dfna5h	103	3110043J09	152	Kcnk2	201	3.01E+22	250	Apxl
6	Cdkl3	55	Olfr1462	104	43J09Rik	153	Bin3	202	9.83E+24	251	A230083G16
7	1200006O19	56	Olfr1462	105	3110043J09	154	Bin3	203	9.83E+24	252	A230083G16
8	1200006O19	57	Rps19	106	1700012B15	155	Adcy5	204	9.83E+24	253	4632412N22
9	06O19Rik	58	Eif2s1	107	1700012B15	156	Adcy5	205	OR135-11	254	4632412N22
10	1200006O19	59	Eif2s1	108	12B15Rik	157	Adcy5	206	MOR135-11	255	Prkcb1
11	C030011O14	60	Eif2s1	109	Axin2	158	Creb5	207	MOR135-11	256	Prkcb1
12	C030011O14	61	Eif2s1	110	Magee1	159	Creb5	208	MOR135-11	257	Prkcb1
13	C030011O14	62	Lmyc1	111	Magee1	160	Ms4a4d	209	Mrpl49	258	Prkcb1
14	11O14Rik	63	Lmyc1	112	Magee1	161	Ms4a4d	210	Mrpl49	259	Vps29
15	1600002K03	64	Lmyc1	113	Wbscr18	162	Try10l	211	Mrpl49	260	Vps29
16	1600002K03	65	Panx3	114	Wbscr18	163	Try10l	212	Mrpl49	261	2210408I21R
17	1600002K03	66	1110056N	115	Wbscr18	164	Try10l	213	Nanos1	262	2210408I21R
18	1600002K03	67	1110056N	116	Wbscr18	165	Zfp97	214	Nanos1	263	08I21Rik
19	1700029F12	68	1110056N	117	C030022K2	166	Zfp97	215	Nanos1	264	2210408I21R
20	1700029F12	69	8430437C	118	C030022K2	167	Zfp97	216	Nanos1	265	H2-Ke6
21	1700029F12	70	Slc35d2	119	22K24Rik	168	31G14Rik	217	3110052N05	266	Mafg
22	0610039N19	71	Slc35d2	120	Cdca8	169	Osbpl10	218	3110052N05	267	Mafg
23	39N19Rik	72	Slc35d2	121	Cdca8	170	Osbpl10	219	52N05Rik	268	Mafg
24	0610039N19	73	Zhx2	122	Cdca8	171	Osbpl10	220	Bcdo2	269	Myst2
25	Atf7ip	74	Zhx2	123	Echs1	172	Steap	221	Bcdo2	270	9430007A20
26	Atf7ip	75	Zhx2	124	29H14Rik	173	Steap	222	Bcdo2	271	07A20Rik
27	Atf7ip	76	Zhx2	125	29H14Rik	174	Steap	223	4632423N09	272	Olfr6
28	Gpr18	77	Calb3	126	2410129H14	175	Steap	224	4632423N09	273	Olfr6
29	Ttc7	78	Calb3	127	2410129H14	176	09I07Rik	225	03J06Rik	274	Olfr6
30	Ttc7	79	Stk19	128	Dhcr24	177	2900009I0	226	2610003J06	275	Olfr6
31	Ttc7	80	MGC6975	129	Dhcr24	178	2900009I0	227	2610003J06	276	Ube4b
32	Ttc7	81	MGC6975	130	Dhcr24	179	Rps6ka4	228	03J06Rik	277	Ube4b
33	Ttc7	82	MGC6975	131	Syngr4	180	Rps6ka4	229	1110036O03	278	Ube4b
34	2210415K24	83	Treh	132	Syngr4	181	Trim8	230	1110036O03	279	Crry
35	15K24Rik	84	Treh	133	Atpaf2	182	Trim8	231	1110036O03	280	Crry
36	2210415K24	85	Ogt	134	Atpaf2	183	Trim8	232	45E13Rik	281	Crry
37	Slc7a6	86	Rev1l	135	Atpaf2	184	Trim8	233	04H02Rik	282	Myod1
38	Slc7a6	87	Rev1l	136	Atpaf2	185	Il2rb	234	B430104H02	283	Myod1
39	Slc7a6	88	Mrpl53	137	Caskin2	186	Il2rb	235	04H02Rik	284	Myod1
40	B3galt3	89	Mrpl53	138	B430306N03	187	Il2rb	236	AI316787	285	Slc9a3r2
41	B3galt3	90	Mrpl53	139	09N07Rik	188	Il2rb	237	AI316787	286	Olfr202
42	B3galt3	91	Olfr958	140	4933409N07	189	Sf3b2	238	AI316787	287	Olfr202
43	2410018L13	92	Olfr958	141	4933409N07	190	Tktl1	239	Slamf6	288	Arid5a
44	2410018L13	93	Olfr958	142	Enpp2	191	Tktl1	240	Slamf6	289	Arid5a
45	AA986860	94	Olfr958	143	Enpp2	192	Tktl1	241	18G13Rik	290	Arid5a

Supp Figure 4.3. contd. Table of top RSA hits from siRNA screen, page 2 of 3

291	Arid5a	**340**	BC02189	**389**	BC011209	**438**	Dfy	**487**	Catnal1	**536**	Olfr518
292	Dusp6	**341**	A930026L	**390**	BC011209	**439**	C230086A	**488**	Cd36	**537**	Olfr518
293	15B01Rik	**342**	Prss3	**391**	Olfr627	**440**	C230086A	**489**	Tpk1	**538**	Olfr518
294	Zfy1	**343**	4933400F	**392**	Olfr463	**441**	86A09Rik	**490**	Kcnn3	**539**	Olfr918
295	Zfy1	**344**	4933400F	**393**	Olfr463	**442**	Zfp451	**491**	1190002A17	**540**	Olfr918
296	Zfy1	**345**	Scamp1	**394**	Il1rl1l	**443**	D330014H	**492**	02A17Rik	**541**	Olfr577
297	Cnnm1	**346**	Scamp1	**395**	A230098A12	**444**	D330014H	**493**	02A17Rik	**542**	Rassf1
298	Cnnm1	**347**	Scamp1	**396**	A230098A12	**445**	14H01Rik	**494**	Klhl8	**543**	Rassf1
299	C630013N10	**348**	Rspondin	**397**	U2af2	**446**	Usp8	**495**	Klhl8	**544**	Rassf1
300	C630013N10	**349**	Rspondin	**398**	U2af2	**447**	1110036H2	**496**	1110034A24	**545**	Defb11
301	13N10Rik	**350**	Rspondin	**399**	U2af2	**448**	1110036H2	**497**	1110034A24	**546**	Defb11
302	Semcap2	**351**	Cyp11a1	**400**	4933425I22F	**449**	4933434I2	**498**	1110034A24	**547**	Defb11
303	Olfr1271	**352**	Cyp11a1	**401**	4933425I22F	**450**	34I20Rik	**499**	1700021K02	**548**	Myoz3
304	Olfr1271	**353**	Insl5	**402**	4933425I22F	**451**	34I20Rik	**500**	1700021K02	**549**	Myoz3
305	Olfr1271	**354**	Insl5	**403**	Abcc5	**452**	15D10Rik	**501**	21K02Rik	**550**	Gpr40
306	Dcl1	**355**	Insl5	**404**	Tmod3	**453**	4932415D	**502**	12M14Rik	**551**	Gpr40
307	Wdr8	**356**	Olfr178	**405**	Tmod3	**454**	4921511H(	**503**	Set	**552**	P2ry1
308	Wdr8	**357**	Olfr178	**406**	Hist1h1a	**455**	4921511H(	**504**	Set	**553**	Whrn
309	Wdr8	**358**	Olfr178	**407**	Hist1h1a	**456**	AI449441	**505**	Set	**554**	Whrn
310	Ankrd6	**359**	Tcfcp2l1	**408**	2610304F09	**457**	AI449441	**506**	Ly6e	**555**	Whrn
311	Sc4mol	**360**	Rad51c	**409**	Ndufs4	**458**	Slc22a13	**507**	Ly6e	**556**	BC051227
312	Sc4mol	**361**	Rad51c	**410**	Ndufs4	**459**	Pde7b	**508**	Olfr908	**557**	Acad9
313	Ripk3	**362**	Slitrk6	**411**	Mare	**460**	Pde7b	**509**	Olfr908	**558**	Acad9
314	Ripk3	**363**	Rce1	**412**	Apg4a	**461**	Pde7b	**510**	Olfr908	**559**	Acad9
315	Ripk3	**364**	Rce1	**413**	Apg4a	**462**	Pax1	**511**	MGC5739	**560**	B930007L02F
316	2810453L12F	**365**	1700129L	**414**	Apg4a	**463**	Pax1	**512**	MGC5739	**561**	Cd209e
317	Il12rb2	**366**	29L13Rik	**415**	Esx1	**464**	Pax1	**513**	9130423L19	**562**	Cd209e
318	Il12rb2	**367**	1700129L	**416**	Esx1	**465**	Mtx1	**514**	9130423L19	**563**	Flrt3
319	Il12rb2	**368**	2810468K	**417**	LOC433332	**466**	Mtx1	**515**	23L19Rik	**564**	Flrt3
320	Cp	**369**	F7	**418**	LOC433332	**467**	49K14Rik	**516**	Syngr3	**565**	4.93E+26
321	Cp	**370**	F7	**419**	LOC433332	**468**	1700049K	**517**	Nck1	**566**	4.93E+26
322	Cp	**371**	F7	**420**	Rrm2	**469**	Adam4	**518**	Nck1	**567**	Rgn
323	Dhrs4	**372**	Tbx21	**421**	Rrm2	**470**	Adam4	**519**	Nck1	**568**	A630065K24F
324	Dhrs4	**373**	Tbx21	**422**	AI894139	**471**	Olfr1135	**520**	Ndor1	**569**	65K24Rik
325	Nfx1	**374**	9130014C	**423**	AI894139	**472**	Olfr1135	**521**	F10	**570**	A630065K24F
326	Olfr661	**375**	9130014C	**424**	AI894139	**473**	Sn	**522**	F10	**571**	Ormdl2
327	Olfr661	**376**	Olfr699	**425**	6720430O15	**474**	Sn	**523**	F10	**572**	Olfr32
328	Th	**377**	Olfr699	**426**	Scamp4	**475**	Sn	**524**	Lrrn1	**573**	Olfr32
329	Th	**378**	Olfr73	**427**	Scamp4	**476**	37I24Rik	**525**	61M12Rik	**574**	Olfr32
330	BC008103	**379**	Olfr73	**428**	Scamp4	**477**	37I24Rik	**526**	1810061M12	**575**	2310015I08R
331	BC008103	**380**	V1rc21	**429**	2810406C15	**478**	C130032J	**527**	Tnni3k	**576**	15I08Rik
332	BC008103	**381**	V1rc21	**430**	06C15Rik	**479**	32J12Rik	**528**	Tnni3k	**577**	Acsl6
333	Inhba	**382**	V1rc21	**431**	2810406C15	**480**	Kif20a	**529**	Ddefl1	**578**	Acsl6
334	Inhba	**383**	2410018C	**432**	Osmr	**481**	Abcb9	**530**	Myh14	**579**	Pcdhb17
335	Reg1	**384**	2410018C	**433**	Osmr	**482**	Nck2	**531**	Myh14	**580**	Pcdhb17
336	Reg1	**385**	18C17Rik	**434**	Lim2	**483**	Nck2	**532**	Myh14	**581**	Pcdhb17
337	BC021891	**386**	Ascc2	**435**	Lim2	**484**	Nck2	**533**	AB041803	**582**	Syt14
338	BC021891	**387**	Opn1sw	**436**	Lim2	**485**	Zfp13	**534**	AB041803	**583**	Syt14
339	BC021891	**388**	Opn1sw	**437**	Dfy	**486**	Catnal1	**535**	Psma1	**584**	Syt14

Supp Figure 4.3. contd. Table of top RSA hits from siRNA screen, page 3 of 3

585	Psx2	**634**	F730014I05Rik	**683**	Sec22l3
586	Tbx4	**635**	F730014I05Rik	**684**	Sec22l3
587	Tbx4	**636**	AI413414	**685**	Sec22l3
588	1700012B18I	**637**	Olfr1511	**686**	Acvr1
589	1700012B18I	**638**	Olfr1511	**687**	Acvr1
590	Sfrs14	**639**	Adamts13	**688**	Acvr1
591	Dlat	**640**	Adamts13	**689**	H3f3a
592	Dlat	**641**	Phldb2	**690**	BC020025
593	Dlat	**642**	Pcdhb13	**691**	4432409M07Rik
594	48H24Rik	**643**	Pcdhb13	**692**	4432409M07Rik
595	4930548H24	**644**	Robo1	**693**	Bfar
596	Enpp1	**645**	Robo1	**694**	Bfar
597	Enpp1	**646**	Exosc6	**695**	Bfar
598	Enpp1	**647**	Exosc6	**696**	12Wsu95e
599	Myadm	**648**	5930416I19Rik	**697**	D12Wsu95e
600	Myadm	**649**	5930416I19Rik	**698**	D12Wsu95e
601	D6Ertd32e	**650**	A430041E03		
602	3830417A13I	**651**	30000000		
603	3830417A13I	**652**	A430041E03		
604	3830417A13I	**653**	B230312A22Rik		
605	Tcl1b1	**654**	12A22Rik		
606	Tcl1b1	**655**	B230312A22Rik		
607	Tcl1b1	**656**	Trim26		
608	Tas2r109	**657**	Ankrd16		
609	Tas2r109	**658**	Ankrd16		
610	C730027P07	**659**	Ankrd16		
611	C730027P07	**660**	12E08Rik		
612	27P07Rik	**661**	9230112E08Rik		
613	30019M04	**662**	Nupl1		
614	0610006O14	**663**	Nupl1		
615	0610006O14	**664**	Myo7b		
616	Aof1	**665**	Myo7b		
617	Aof1	**666**	Myo7b		
618	80H04Rik	**667**	Pdlim7		
619	4930529M08	**668**	Pdlim7		
620	4930529M08	**669**	Pdlim7		
621	29M08Rik	**670**	Fv1		
622	Scd3	**671**	6030457N17Rik		
623	Scd3	**672**	01I01Rik		
624	BC060631	**673**	3230401I01Rik		
625	BC060631	**674**	3230401I01Rik		
626	Smox	**675**	4930563M21Rik		
627	Agtpbp1	**676**	4930563M21Rik		
628	Agtpbp1	**677**	79K19Rik		
629	2410014A08I	**678**	4930579K19Rik		
630	2410014A08I	**679**	Dffb		
631	14A08Rik	**680**	Dffb		
632	BC034834	**681**	Fads1		
633	BC034834	**682**	Cts3		

CHAPTER 5

CHARACTERIZATION OF THE ROLE OF ATF7IP IN XCI

Atf7ip contributes to maintenance of XCI

Both top RSA hits from the library against *Atf7ip* reduced *Atf7ip* transcript levels by half after 72 hours of knockdown (Fig 5.1A, Supp Fig 5.1). These intermediate levels of *Atf7ip* RNA knockdown prompted us to further investigate whether these siRNAs were targeting *Atf7ip* expression by assaying whether they could knock down overexpressed *Atf7ip* (Fig 5.1B/2C). Female MEFs transduced with a retroviral vector containing a FLAG-tagged *Atf7ip* cDNA showed a similar nuclear distribution of FLAG-tagged to endogenous protein (Fig 5.1B). This overexpression was 6-fold greater than endogenous levels by RT-qPCR and the *Atf7ip*-targeting siRNA was also able to target the exogenous product and reduce transcript levels by half (Fig 5.1C). Unlike other known factors with a functional in maintenance of XCI that have nuclear enrichment on the Xi, *Atf7ip* enrichment was not seen in the *Xist* RNA domain (Fig 2B, Supp Fig 5.2).

Atf7ip knockdown alone produced a weak though reproducible effect on luciferase reporter reactivation (Fig 5.1D). When combined with low levels of 5-aza-2'-dC, as it was in the screen, reporter reactivation due to *Atf7ip* knockdown was greatly enhanced (Fig 5.1D). We further investigated the role of 5-aza-2'-dC in sensitizing XCR due to *Atf7ip* knockdown. To see if the action of 5-aza-2'-dC was due to inhibition of Dnmt1, we performed knockdown of Dnmt1 in the place of 5-aza-2'-dC treatment and again observed synergy in reporter reactivation (Fig 5.1D). Therefore we believe some loss of DNA methylation is necessary to observe reversal of *Atf7ip*-mediated gene silencing. The similar effect of low concentration 5-aza-2'-dC and siDnmt1 is probably due to a critical level of DNA demethylation they cause since the extent of XCR as quantified by luciferase measurement is comparable between low 5-aza-2'-dC alone and siDnmt1 alone. These effects were recapitulated (though to slightly different extent) in two independent XCR fluorescent primary MEF reporter cell lines that permitted single-cell quantitation of reactivation rates (Fig 5.1E, Hadjantonakis et al., 1998). The activity

of siAtf7ip against two other reporters rules out that knockdown effect is luciferase-specific. Our results suggest that *Atf7ip* plays a role in the maintenance of XCI.

We then addressed whether *Atf7ip* knockdown leads to reactivation of endogenous Xi-linked genes by assaying their allelic expression using DNA FISH probes directing against *Atrx, Gpc4, Rnf12,* and *Mecp2* RNA (Fig 5.1F). These genes should go from being monoallelicly expressed on the active X chromosome to biallelicly expressed upon XCR. The number of FISH pinpoint signals (representing transcription foci) in nuclei of untreated cells or cells subjected to siAtf7ip and low 5-aza-2'dC-mediated reactivation were counted (Fig 5.1G). The increases in rates of biallelic Xi-linked gene expression with XCR treatment ranged from 5-16% in the genes assayed (Fig 5.1G). We noted a wide distribution in the number of pinpoint FISH signals per nucleus from 0 to 4 pinpoints and attribute this to factors including abnormal ploidy that quickly occurs upon expansion of fibroblasts *in vitro* and to heterogeneous allelic gene expression in the cell population (Baker, 2012; Dodge et al., 2005). To rule out the possibility that siAtf7ip and low 5-aza-2'-dC affect ploidy, we counted the number of X chromosomes using X chromosome painting but did not see the same trends as noted in the RNA FISH counts (Fig 5.1H/5.1I). Thus reactivation treatments increased rates of biallelic X-linked gene expression rather than increasing X chromosome numbers. We conclude that Atf7ip knockdown together with 5-aza-2'dC treatment leads to Xi-linked gene reactivation, thereby validating our reporter approach.

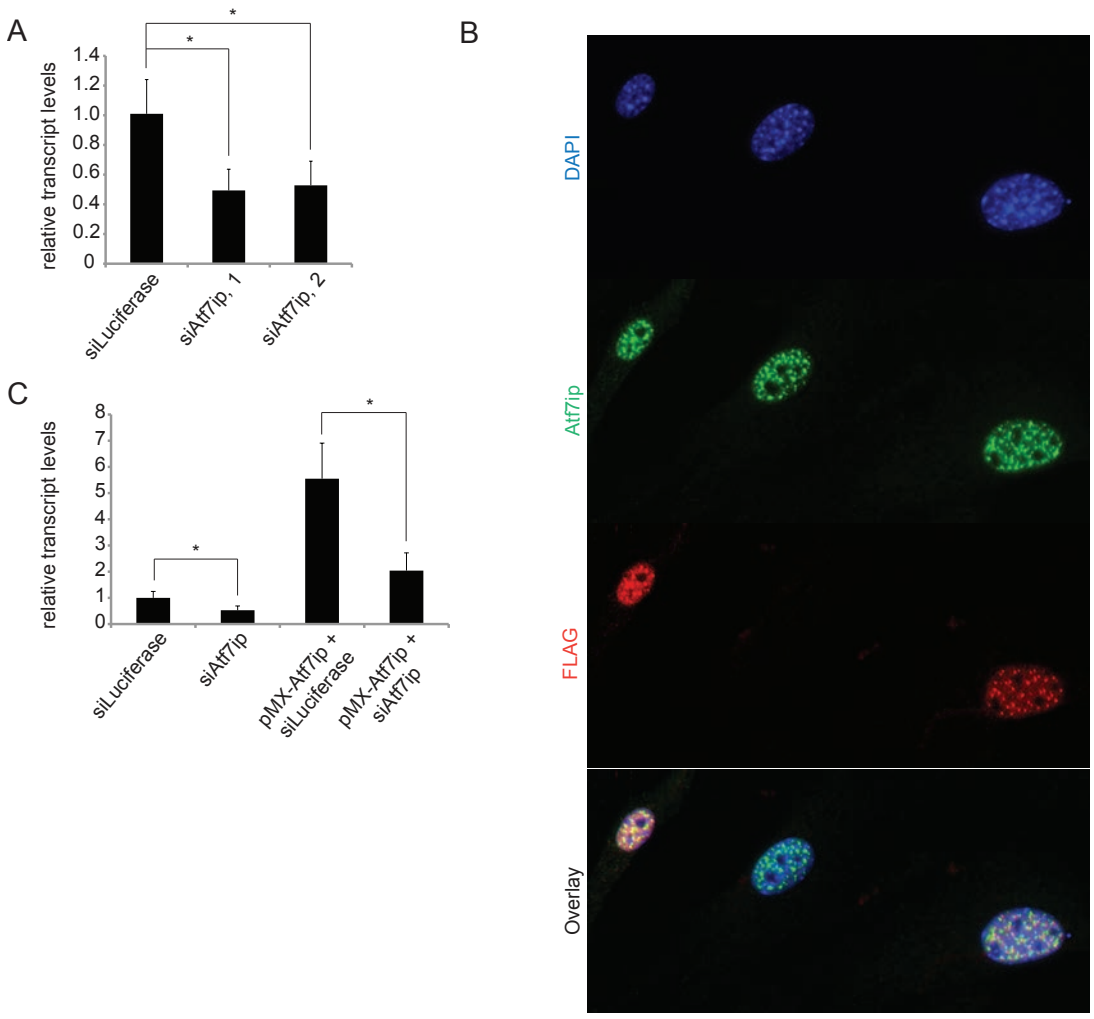

Figure 5.1. Validation of Atf7ip knockdown in X chromosome reactivation (part 1 of 2). A. RT-qPCR for *Atf7ip* RNA levels normalized to siLuciferase control and *Gapdh* expression for two independent siRNAs targeting *Atf7ip*. Error bars indicate one standard deviation from triplicate RT-qPCR measurements in one experiment. B. Immunofluoresence in pMX-Atf7ip infected female MEFs for endogenous Atf7ip and FLAG-tagged Atf7ip. C. RT-qPCR for *Atf7ip* RNA levels normalized to siLuciferase control and *Gapdh* expression in cells infected (mock or pMX-Atf7ip) for 72 hours and then treated with siRNA for another 72 hours. Error bars indicate one standard deviation from triplicate RT-qPCR measurements in one experiment, * indicates $p<0.01$ by Student's T-test.

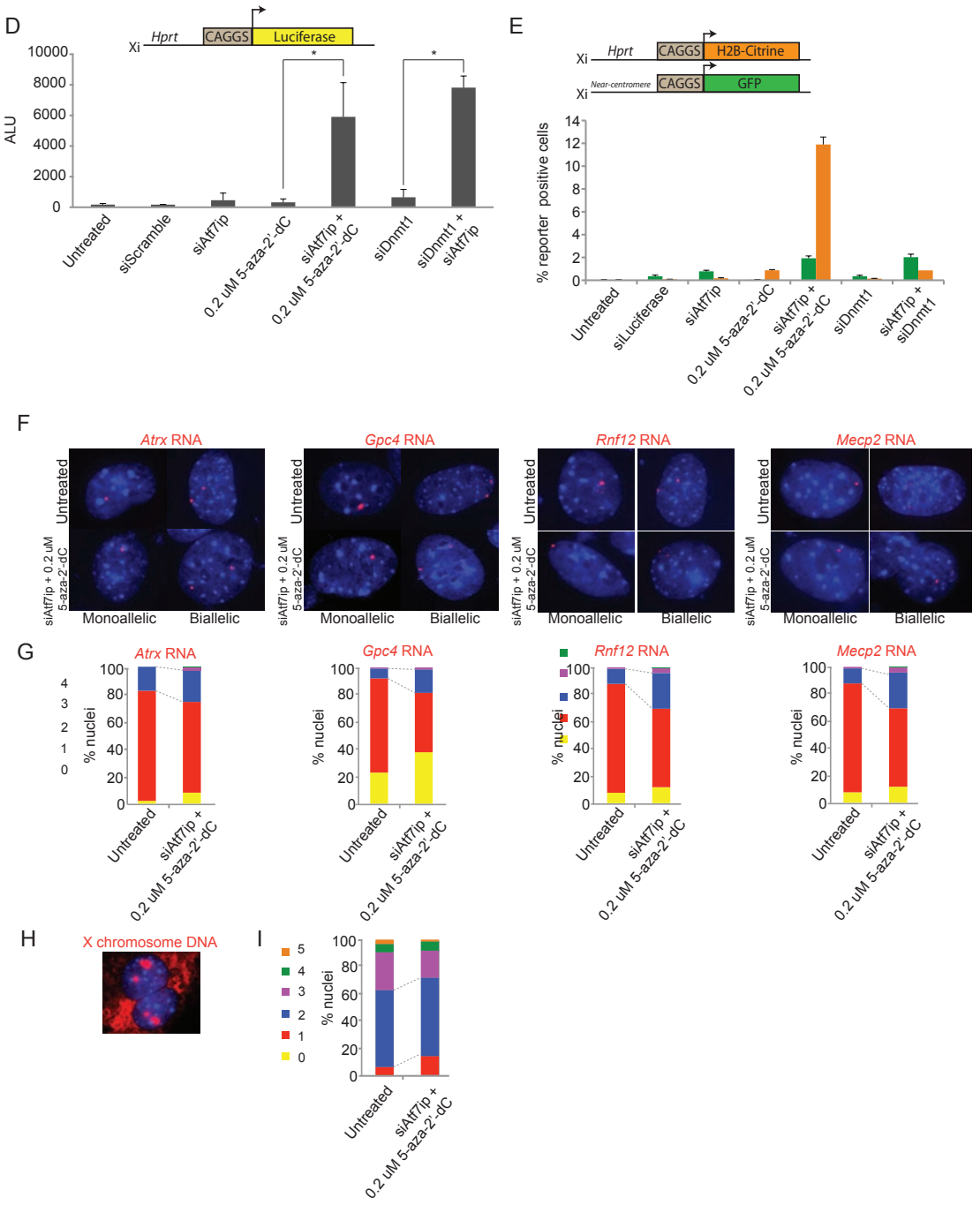

Figure 5.1. Validation of Atf7ip knockdown in X chromosome reactivation (part 2 of 2). D. Graph summarizing luciferase assay in 12 well format. Error bars indicate standard deviation of raw ALU values from 3 individual wells with a given treatment in one experiment, * indicates p<0.01 by Student's T-test. E. Graph summarizing flow cytometry data upon treatment as in 5.1D. scoring % FITC positive MEFs for two independent fluorescent reporters of X reactivation, a citrine allele in the place of the luciferase reporter under the HPRT locus and a centromeric GFP allele (Csankovszki et al., 2001b; Hadjantonakis et al., 1998). F. FISH with DNA probes targeting RNA of four different X-linked gene transcripts without treatment or with siAtf7ip-mediated reactivation treatment as in 5.1D and 5.1E. G. Graphs summarizes count of cells shown in 5.1F as the proportion of DAPI-stained nuclei (200 counted per sample) with indicated numbers of transcription foci for the respective X-linked gene. H. Chromosome paint of untreated MEFs displaying normal X ploidy. I. Graph summarizes the proportion of DAPI-stained nuclei with indicated numbers of X chromosome domains before and after reactivation treatment.

Atf7ip's canonical binding partners Mbd1 and Eset also play a role in XCI

Atf7ip has been described to mediate either transcriptional gene activation or repression (Chang et al., 2005; Ichimura et al., 2005; Liu et al., 2009). In its silencing context, *Atf7ip* acts as a bridging factor by recruiting H3K9me2 methylase *Setdb1* to Methyl-CpG DNA Binding Domain Protein 1 (*Mbd1*) on DNA, thereby coupling DNA methylation to H3K9 trimethylation (De Graeve et al., 2000; Ichimura et al., 2005; Wang et al., 2003). We next addressed whether other factors in *Atf7ip*'s autosomal gene silencing pathway play a role in XCI by testing to see if knockdown of these repressive *Atf7ip* interactors phenocopies the XCR effect. Indeed, like siAtf7ip, knockdown of *Mbd1* and *Setdb1* activated the luciferase reporter when knocked down alone and acted synergistically with low concentration of 5-aza-2'-dC (Fig 5.2A). Thus the *Mbd1-Atf7ip-Setdb1* pathway has a role in maintenance of XCI. The additive enhancement of reactivation by combinatorial knockdown is likely due to hypomorphic effect of individual siRNA knockdowns that when superimposed, reduce overall silencing contribution of the *Mbd1-Atf7ip-Setdb1* arm in the XCI pathway (Fig 5.2A/5.2B/5.2C). siRNAs against *Mbd1* and *Setdb1* were included in the genome-wide library and discarded as false negatives. To further assess whether the *Mbd1-Atf7ip-Setdb1* pathway is a specific autosomal gene silencing mechanism that is involved in maintenance of XCI and rule out other related autosomal mechanisms also have a role in XCI, we re-screened a panel of siRNAs validated to target other mediators of transcriptional silencing including heterochromatin proteins (*Cbx3* and *Cbx5*) and H3K9 methylases (*Ehmt2* and *Suv39h1*) (Fig 5.2D, Völkel and Angrand, 2007). No significant activity was observed with knockdown alone or with 5-aza-2'-dC or siDnmt1 sensitization compared to siGFP control (Fig 5.2D/5.2E). We conclude interfering with a specific pathway described to couple DNA methylation and histone 3 lysine 9 trimethylation causes XCR.

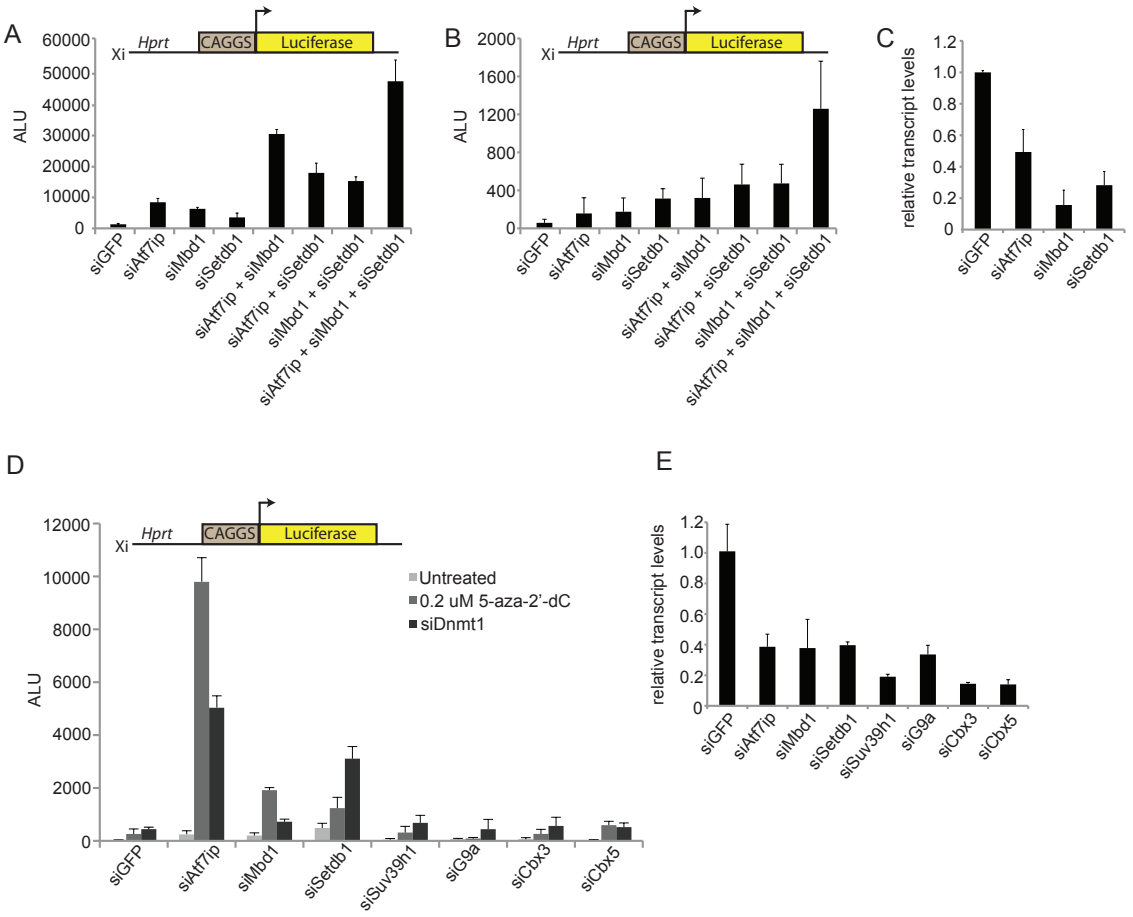

Figure 5.2. Knockdown of factors in the *Atf7ip* pathway linking DNA and histone methylation also reactivate the inactive X reporter. (A) Graph summarizing luciferase assay as in Fig 5.1D., knockdowns were performed in the presence of 0.2 uM 5-aza-2'-dC. Error bars indicate standard deviation of raw ALU values from 3 individual wells with a given treatment in one experiment. (B) Luciferase assay as in Fig 5.1D except that 5-aza-2'-dC was omitted. (C) RT-qPCR for RNA levels of respective transcript normalized to siGFP control and *Gapdh* expression, RNA was harvested in parallel to luciferase assays 3 days after knockdown as shown in Fig5.2A-B. Error bars indicate one standard deviation from triplicate RT-qPCR measurements in one experiment. (D) Luciferase assay as in Fig 5.2A. Knockdown of other important known mediators of heterochromatin formation (with or without sensitization by inhibition of DNA methylation by siDnmt1 or 0.2 uM 5-aza-2'-dC) was performed to determine specificity of *siAtf7ip* mechanism for X chromosome reactivation. (E) RT-qPCR as in Fig 5.2C to determine knockdown efficiencies in the experiment shown in Fig 5.2D.

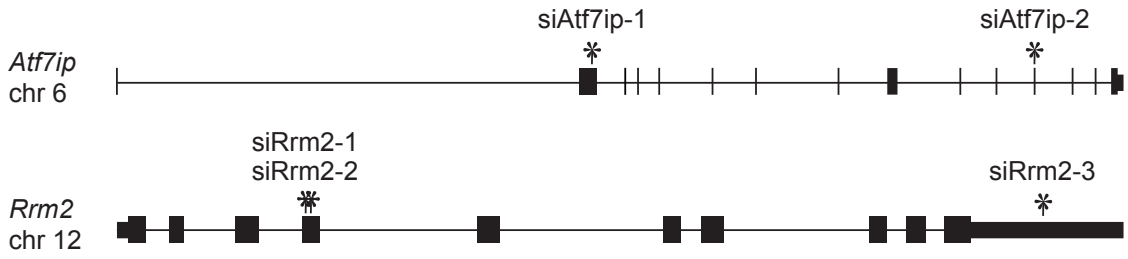

Supp Figure 5.1. Summary of *Atf7ip* and *Rrm2* siRNA sequence alignments. *Aft7ip* and *Rrm2* gene structures are shown with siRNA seed sequences designated.

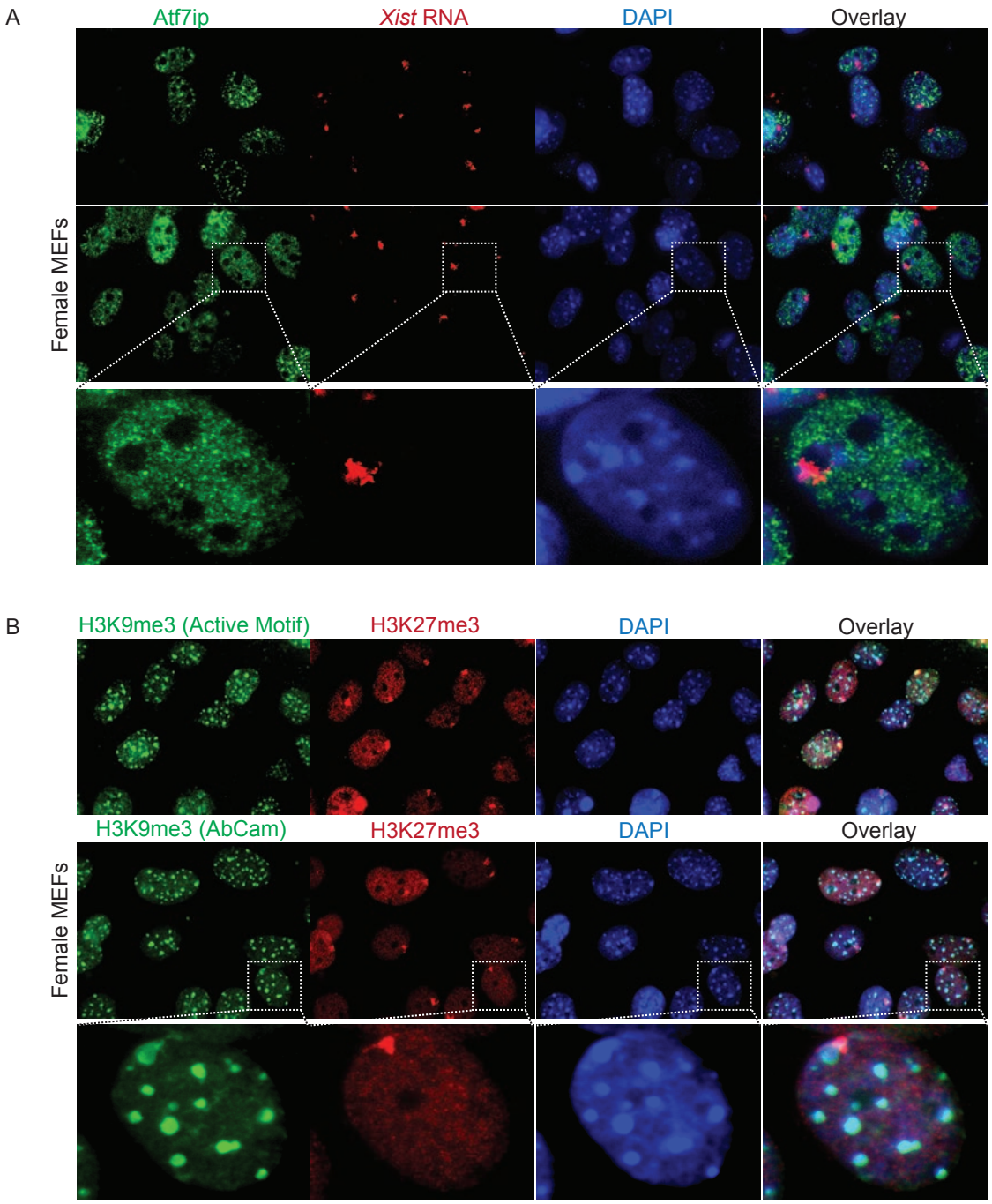

Supp Figure 5.2. Atf7ip does not enrich in the *Xist* Xi domain. (A) Immunostaining /FISH images show the nuclear distribution of Atf7ip (green) relative to *Xist* RNA coating (red) in female MEFs treated with 0.2 uM 5-aza-2'-dC for three days. Two different fields are shown and the third panel is a zoomed-in view of one nucleus from the second field. (B) Co-immunostaining for H3K9me3 (green, with Active Motif or AbCam antibodies) and H3K27me3 (red). The third panel is a zoomed-in view of one nucleus from the second field.

CHAPTER 6

CHARACTERIZATION OF RIBONUCLEOTIDE REDUCTASE INHIBITION

Inhibition of Rrm2 potentiates the effect of 5-aza-2'-dC to elicit X chromosome reactivation

We turned our attention to the other robustly validated hit, the gene *Rrm2* coding for an essential subunit of ribonucleotide reductase (RNR) (Fig 4.1G). As with *Atf7ip*, knockdown was confirmed for the active siRNAs from the library by measuring RNA levels using RT-qPCR (Fig 6B, Supp Fig 5.1). Unlike siAtf7ip, siRrm2 demonstrated complete dependence on combination with low concentration of 5-aza-2'-dC for any luciferase signal above background (Fig 6A/4B). Further support for the role of *Rrm2* as a XCR hit came from a companion chemical screen dataset generated for a collection of 4,094 annotated chemicals assayed at 10 uM concentration of drug (Supp Fig 6.1). From this screen, Resveratrol, a chemical agent known for mimicking cellular effects of caloric restriction demonstrated the potential to activate the luciferase reporter in a dose-dependent fashion (Fig 6C, Hubbard et al., 2013; Wood et al., 2004). Resveratrol is described to mediate its metabolic effects through direct and indirect activation of the histone deacetylase Sirt1 though no role for reversal of gene silencing or role in XCI has been characterized (Hubbard et al., 2013; Park et al., 2012). In search for a mechanistic explanation for the ability of Resveratrol to elicit XCR in the presence of 5-aza-2'-dC we noted a study describing Resveratrol as an inhibitor of RNR's Rrm2 subunit, the same subunit knocked down by our siRNA hit, thus strongly suggesting that Rrm2 was playing a role in XCR (Fontecave et al., 1998). Resveratrol and 0.2 uM 5-aza-2'-dC also activated the H2B-Citrine XCR reporter (Fig 7B).Thus a chemical and siRNA hit support that RNR inhibition contributes to XCR in the presence of 5-aza-2'-dC.

We first sought to address whether hydroxyurea, another chemical inhibitor of RNR (though with a higher IC_{50} than Resveratrol) could cause XCR (Fontecave et al., 1998). All three forms of RNR inhibition-mediated XCR (siRrm2, Resveratrol, and

hydroxurea) demonstrated a complete dependence on low levels of 5-aza-2'-dC to elicit XCR (Fig 6A/6C/6F). In contrast to siAtf7ip, knockdown of *Dnmt1* could not replace the requirement for 5-aza-2'-dC (Fig 6D/6E). This observation suggests that the drug combination synergism is not dependent on low levels of DNA methylation inhibition, as suspected for *Atf7ip.*

Next, we sought to understand how RNR inhibition interacts with low concentration 5-aza-2'-dC to cause XCR. RNR catalyzes the conversion of ribonucleoside 5'-disphosphates to their 2'-deoxyribonucleoside form in the rate-limiting step of dNTP biosynthesis and the Rrm2 subunit, which is specifically upregulated at S phase of cell cycle, is necessary for the activity of the complex (Engström et al., 1985). The pool of dNTPs in the nucleus is tightly regulated and studies have speculated that RNR inhibition can increase the likelihood of nucleoside analog DNA incorporation by reducing the pools of endogenous nucleotide concentrations (Clouser et al., 2012). RNR inhibition could, therefore, increase 5-aza-2'-dCTP concentration in the nucleus relative to endogenous dCTP, increase DNA incorporation, and further decrease DNA methylation levels (Fig 6J). To begin to examine this model, we tested whether Resveratrol and knockdown of *Rrm2* could increase the amount of tritiated (3H) 5-aza-2'-dC incorporated into DNA under conditions which lead to XCR (Fig 6G). Indeed, double the amount of 3H-5-aza-2'-dC was incorporated into genomic DNA with either siRrm2 or Resveratrol treatment (Fig 6G). We then performed a rescue experiment to address whether the effect of 5-aza-2'-dC on XCR in the presence of RNR inhibition could be blunted by increasing levels of dCTP. As expected, XCR was reversed when exogenous deoxycytosine (dC) was supplied in the media in the presence of 0.2 uM 5-aza-dC and Resveratrol or siRrm2 (Fig 6H/6I). Such rescue suggests that the relative nuclear concentrations of dCTP:5-aza-2'-dCTP could be shifted by addition of exogenous nucleotide substrates to reduce the effective concentration of analog thereby

preventing XCR secondary to DNA methylation loss (Fig 6J). Uridine was used as a negative control in the rescue experiment because it is a nontoxic precursor of pyrimidine synthesis that, like deoxycytidine, can be taken up by cells and used as a substrate by the nucleoside salvage synthetic pathways (Fig 6H/6I/6J, Reichard and Estborn, 1951). However, unlike dC, uridine is readily converted to CTP and UTP for RNA biosynthesis but RNR inhibition precludes the ability of uridine to contribute to dNTP pools (Larsson et al., 2004). Protein concentrations in lysates were unaffected by treatment, ruling out cell death as the cause of luciferase signal loss (Supp Fig 6.2). In summary, the requirement for XCR sensitization in the screen by low levels of DNA methylation-inhibiting drug led to the identification of hits that potentiated the gene reactivation effect of low concentration 5-aza-2'-dC.

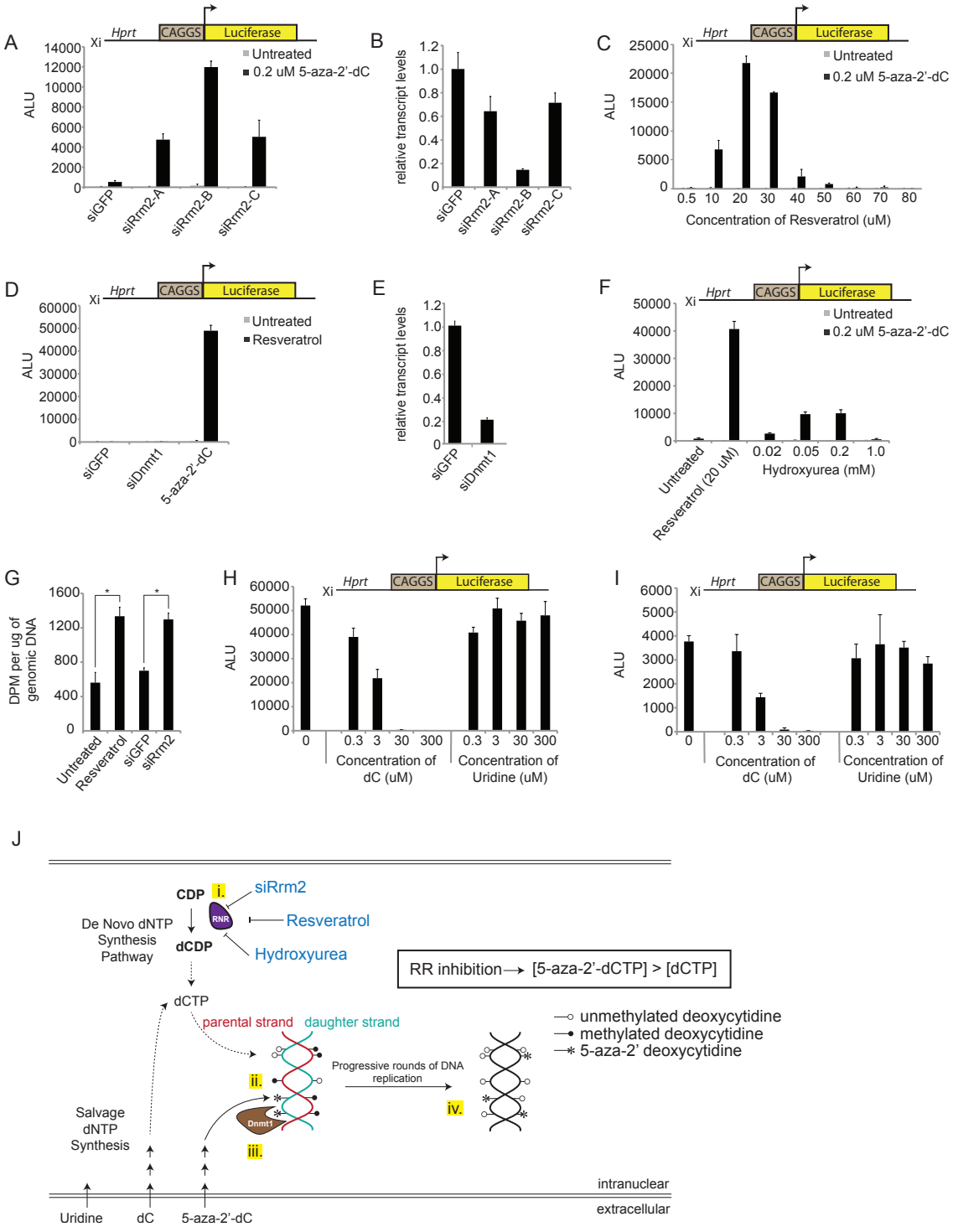

Figure 6. Inhibition of Rrm2 enhances the effect of 5-aza-2'-dC to elicit X chromosome reactivation. A) Graph summarizing luciferase assay as in Fig 5.1D., knockdowns with three independent siRNAs (A, B, or C) against Rrm2 were performed with or without 0.2 uM 5-aza-2'-dC. Error bars indicate standard deviation of raw ALU values from 3 individual wells with a given treatment in one experiment. (B) RT-qPCR for *Rrm2* RNA levels after knockdown normalized to siGFP control and *Gapdh* expression from the experiment shown in Fig 6A. (C) Luciferase assay titrating Resveratrol concentration with or without 0.2 uM

5-aza-2'-dC. (D) Luciferase assay comparing 5-aza-2'-dC and siDnmt1 to elicit reporter reactivation by Resveratrol. (E) RT-qPCR for *Dnmt1* RNA levels normalized to siGFP control and *Gapdh* expression from the experiment shown in Fig 6D. (F) Luciferase assay in the presence or absence of 0.2 uM 5-aza-2'-dC. (G) Quantification of 3H-5-aza-2'-dC incorporation into genomic DNA with and without knockdown of *Rrm2* or Resveratrol treatment for 48 hrs. Genomic DNA was isolated and an equal volume was measured by Beta counter for 3H-5-aza-2'-dC incorporation (disintegrations per minute, DPM) then normalized to amount of DNA loaded (ug), error bars represent one standard deviation from mean value for samples from three independent 6-well wells, asterisk (*) denotes $p<0.01$ by Student's T-test . (H) Luciferase assay demonstrating rescue of reporter silencing in the presence of 5-aza-2'-dC and Resveratrol by exogenous deoxycytidine (dC) and lack of rescue by exogenous uridine addition. (I) As in 6H but with siRrm2-B in the place of Resveratrol, see Fig 6B for knockdown efficiency (J). Illustration of model in which (i) inhibition of ribonucleotide reductase leads to (ii) skewing of dCTP utilization for DNA synthesis from salvage pathways which are supplemented with exogenous 5-aza-2'-dC and (iii) Dnmt*1* inhibition by binding to incorporated 5-aza-2'-dC leading to (iv) increased loss of DNA methylation with successive cell divisions (resulting in X chromosome gene reactivation).

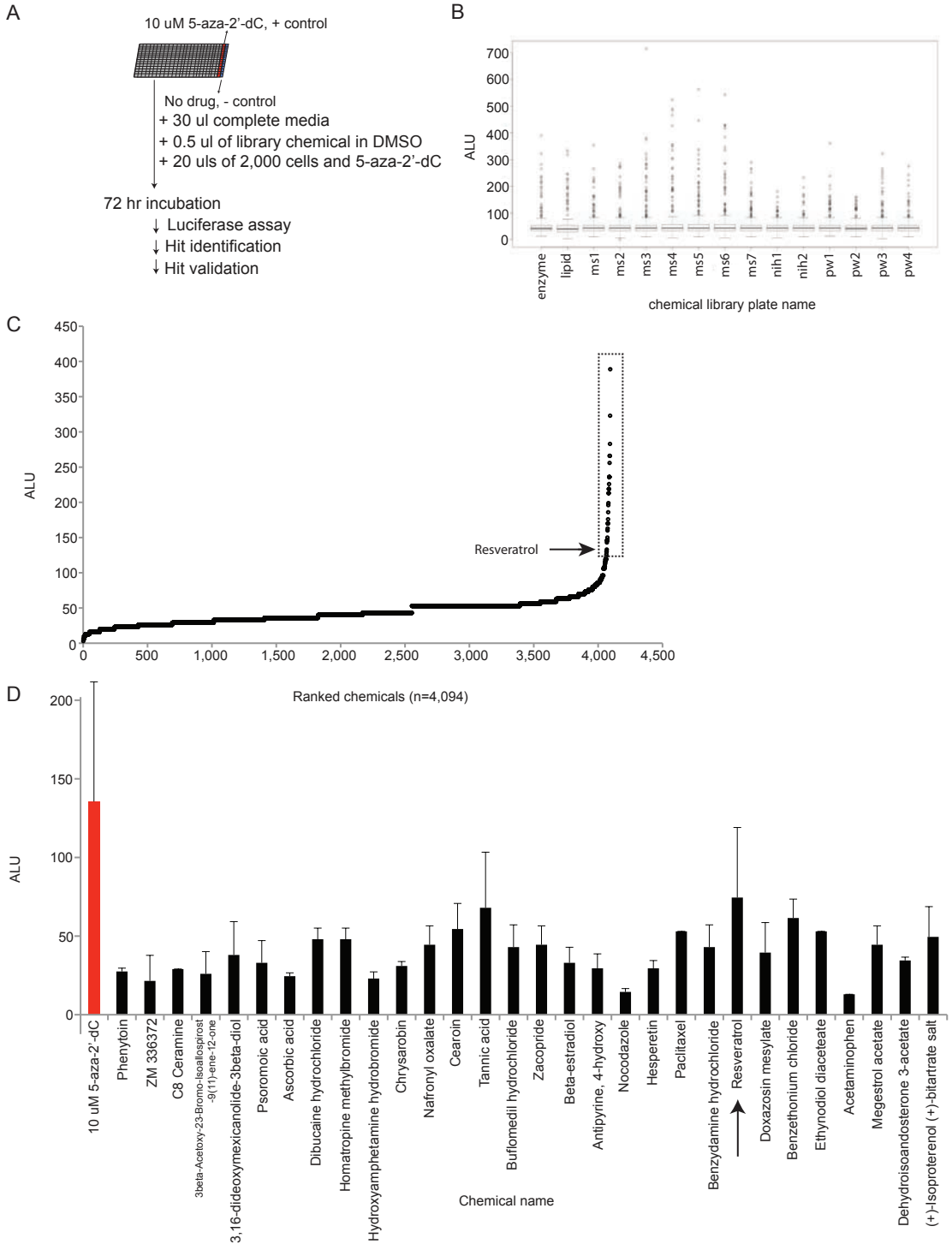

Supp Figure 6.1. Chemical screen for X chromosome reactivation. (A) Diagram of screening workflow. Briefly, media was added to 384 well plates, the library chemical was added, then the cell suspension and 5-aza-2'-dC mixture was delivered. Each plate contained a row of positive (10 uM 5-aza-2'-dC) and negative (no chemical) controls for quality control. Two thousand cells were added in complete media bringing the

final 5-aza-2'-dC concentration to 0.2 uM and the library chemical concentration to 10 uM in each well and cells were incubated for 72 hours prior to luciferase assay. (B) Box and whisker plot of all raw luciferase measurements from the chemical screen by individual 384-well plate. (C) Raw ALU score distribution is shown across all the chemicals, with the well value corresponding to Resveratrol designated, and the chemicals chosen for validation boxed. (D). Validation of selected chemicals in 24-well luciferase assay with mean values of duplicate measurements plotted, error bars indicate one standard deviation from duplicate wells.

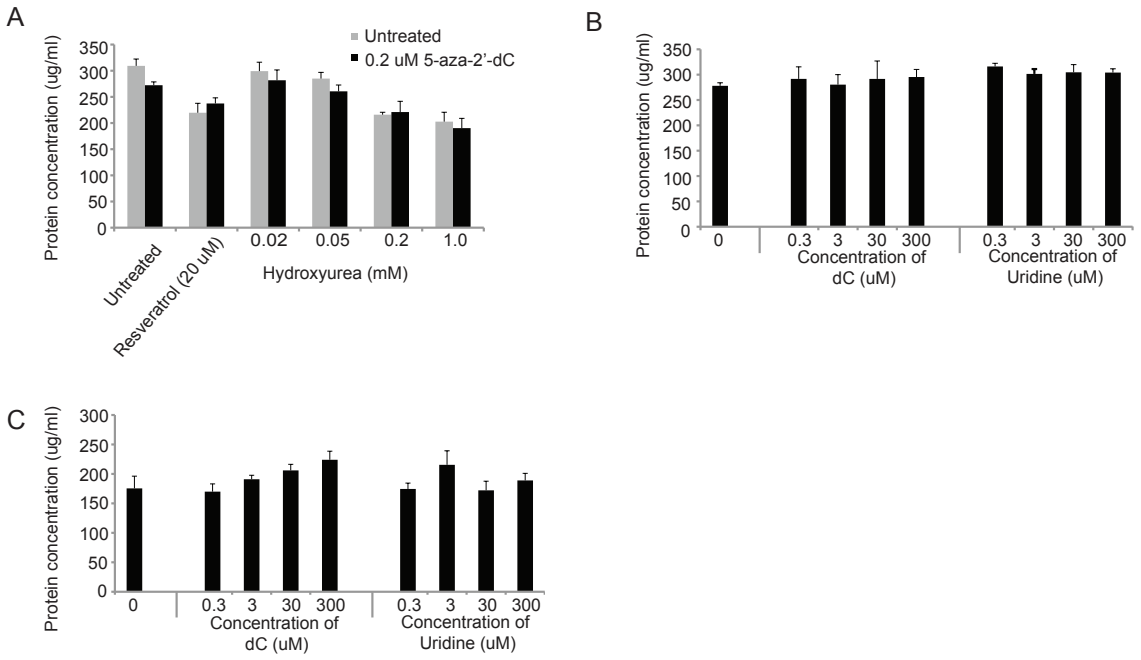

Supp Figure 6.2. Protein concentration measurements from selected luciferase reporter experiments. (A) Protein concentrations of cell lysates corresponding to luciferase measurements in Figure 6F. Error bars indicate standard deviation of values from 3 individual wells with a given treatment in one experiment. (B) As in (A) but for Figure 4H. (C) As in (A) but for Figure 4I.

CHAPTER 7

COMBINATORIAL ACTION OF NOVEL PATHWAYS

Combinatorial effect of Af7ip, Resveratrol, DNA methylation, and *Xist* on maintenance of XCI

In order to compare the combined effects of *Atf7ip* inhibition or *Rrm2* inhibition by Resveratrol treatment together with the known mediators of XCI maintenance, DNA methylation and *Xist* RNA expression; various combinations of treatments were performed (Fig 7). The relative contributions to XCR were assayed by flow cytometry in a primary MEF line analogous the to the luciferase screening MEFs but with the H2B-Citrine reporter in *cis* with a conditional allele of the *Xist* gene on the Xi, obtained through germline recombination in heterozygous females (Fig 6A, Csankovszki et al., 1999). MEFs infected with Adenovirus (Ad)-Cre recombinase or Ad-Null (Empty) control overnight were subjected to combinatorial treatments for 72 hours as before (Fig 6C/7B). Ad-Cre treatment led to loss of *Xist* coating in 98% of cells compared to Ad-Null cells at the time of analysis and Ad-Cre samples were compared to Ad-Null to assess the relative contribution of *Xist* to silencing (Fig 7B/7C). As previously reported, *Xist* deletion in MEFs also inhibited for DNA methylation exhibited close to 2-fold more XCR than MEFs with *Xist* treated with Ad-Null (Fig 7B, Csankovszki et al., 2001). Maximal reactivation of approximately 14%, the highest reported in primary cells, was achieved by 10 uM 5-aza-2'-dC and siAtf7ip or Resveratrol, and was not increased much more by combining all three (Fig 7B). Reactivation conditions which including Resveratrol did not show significant differences between presence and absence of *Xist* RNA (comparing Ad-Null and Ad-Cre treatment). Thus, Resveratrol addition blunted the differences in XCR attributable to *Xist* deletion (Fig 7B). This effect may be due to RNR-independent effects of Resveratrol; we previously observed that knockdown of *Sirt1*, the histone deacetylase that Resveratrol is able to activate, boosts the amount of XCR (Supp Fig 7.1, Hubbard et al., 2013). This could be do to increased histone acetylation as a result of reduced Sirt1 levels. Resveratrol is also described to function as a phosphodiesterase inhibitor and

some of its metabolic effects can be recapitulated with a related phosphodiesterase inhibitor, the compound Rolipram (Park et al., 2012). In our system, Rolipram boosted Resveratrol-mediated XCR (Figure S7.2). We do not know whether these Rrm2-independent effects of Sirt1 and Rolipram directly relate to XCI or indirectly alter luciferase levels. Thus Resveratol has other effects to those described to enhance the action of low dose 5-aza-2'-dC. All together, these results demonstrate that DNA methylation, a *Mbd1-Atf7ip-Setdb1* pathway and, to a lesser extent, *Xist* RNA cooperate in maintaining XCI.

We investigated whether association with the nuclear lamina is another possible mechanism of Xi maintenance. Studies suggest epigenetic dysregulation including changes in histone chromatin marks is an underlying pathology in the autosomal dominant advanced aging syndrome, Hutchinson Gilford Progeria (HGPS)(Goldman et al., 2004; Scaffidi and Misteli, 2006). The HGPS point mutation in the lamin A gene introduces a splice site which deletes 50 amino acids from the C terminus and produces a mutant protein that is resistant to enzymatic cleavage, leading to accumulation of farnesylated intermediate prelamin A and disruption of the nuclear lamina (Shumaker et al., 2006). Wild type cells process prelamin A with the protease Zmpste24 and homozygous loss of *Zmpste24* also leads to accumulation of prelamin A and is associated with other progeroid syndromes (Bergo et al., 2002; Pendás et al., 2002; Schreiber and Kennedy, 2013). There is evidence that the mechanism of disease in advanced aging also takes place in healthy old adults as fibroblasts from individuals aged 70+ years old also display accumulation of prelamin A caused by sporadic use of the splice site mutated in HGPS (Scaffidi and Misteli, 2006).

The nuclear defects associated with prelamin A accumulation increase with serial passage in tissue culture (Goldman et al., 2004). They include nuclear shape abnormalities, DNA damage (assessed by foci of phosphorylated H2AX), and reductions

in H3K9me3 and heterochromatin protein 1 (Goldman et al., 2004; Scaffidi and Misteli, 2006; Shumaker et al., 2006). One study reported that fibroblasts from female HGPS patients lost H3K27me3 on the *Xist*-demarcated Xi and that this change in the Xi chromatin preceded the general nuclear shape changes that occurred in subsequent tissue culture passages (Shumaker et al., 2006). HEK-293 cells overexpressing the mutant HPGS lamin A gene also lost Xi-like foci of H3K27me3 (Shumaker et al., 2006). In summary, studies of advanced aging pathologies have suggested the nuclear lamina has a role in the maintenance of chromatin state and lamin dysfunction leads to epigenetic dysregulation that impacts the normal aging process.

We sought to address whether accumulation of prelamin A leads to loss in the stability of X chromosome inactivation. We took an analogous approach to looking at the contribution of *Xist* to our novel mechanisms from the screen: namely, monitoring reactivation rates of the Xi by luciferase reporter from MEFs derived by crosses with *Zmpste24* knockout mice (Supp Figure 7.2A, Bergo et al., 2002; Leung et al., 2001). Xi reporter *Zmpste24*-/- MEFs displayed accumulation of prelamin A and a prolonged passage-dependent increase in abnormally shaped nuclei as previously described (Supp Figure 7.2B/7.2C, Pendás et al., 2002). However, when comparing luciferase reactivation levels between *ZmpSte24* +/+ and -/-, MEFs in the various combinatorial reactivation conditions, we did not see any significant differences in their sensitivities to reactivation treatments (Supp Figure 7.2D). On further examination of the primary MEFs, we did not see changes in the rates of H3K27me3 coating on the Xi from early passage to a less proliferative later passage 6 (data not shown). Furthermore, tail-tip fibroblasts (TTFs) derived from 4 month-old *Zmpste24*-/- mice that displayed the overt pathology of the *Zmpste24* progeroid syndrome showed as much H3K27me3 Xi foci as cells from age-matched *Zmpste24*+/+ TTFs (data not shown). Noting that in the HPGS study, the H3K27me3 Xi loss occurred after 10 passages, we looked at spontaneously

immortalized passage 50+ female *Zmpste24*+/+ and *Zmpste 24* -/- MEFs. Here, only the *Zmpste24*-/- MEFs demonstrated loss of *Xist* coating and H3K27me3 accumulation. We conclude from this study that secondary effects of extended passage and/or immortalization modify the *Zmpste24* genotype to induce the cellular phenotypic effect of Xi dysregulation but that there are no immediate consequences of prelamin A accumulation to dysregulation of X silencing or *Xist* RNA coating of the Xi.

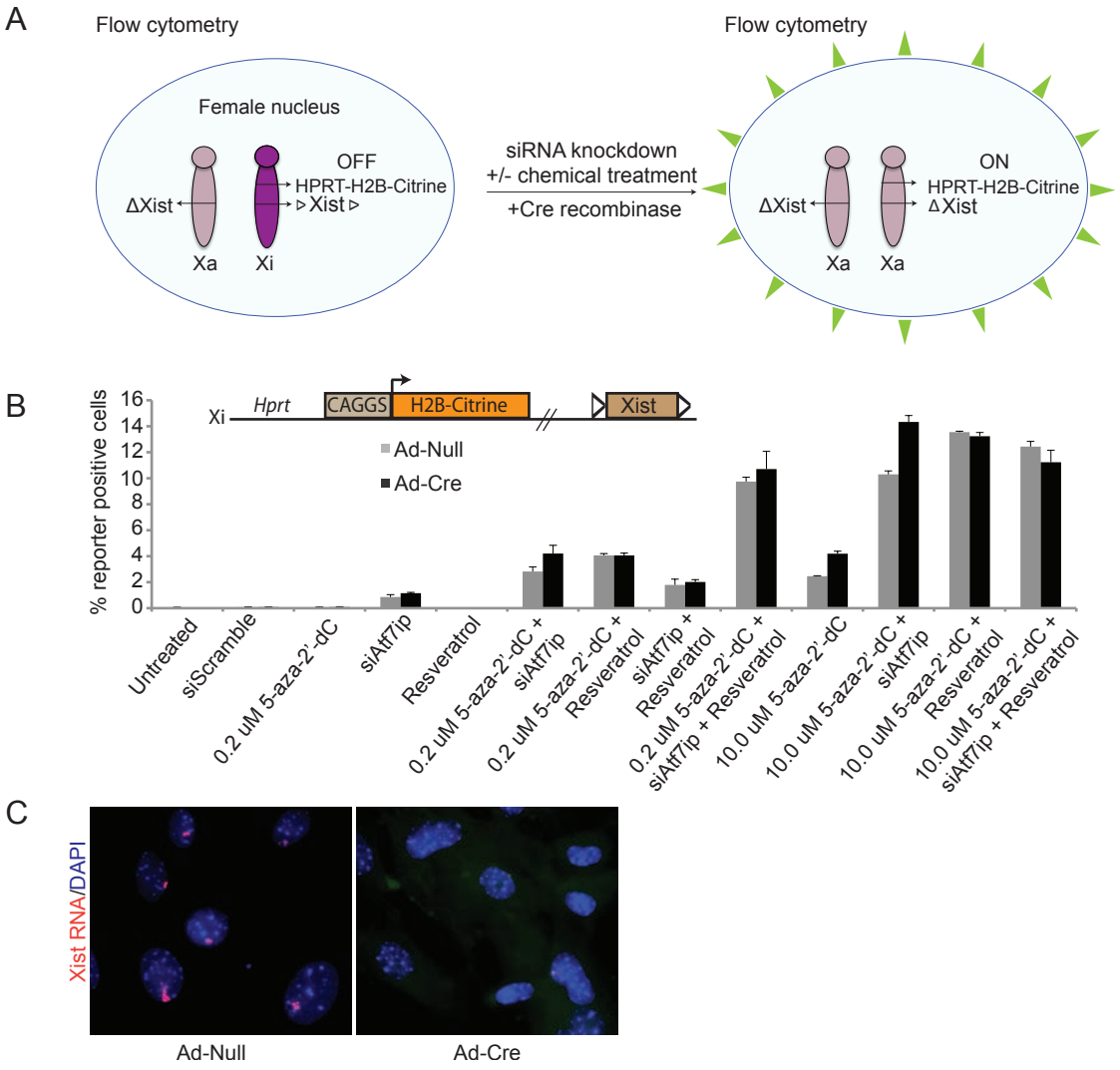

Figure 7. Combinatorial effects of siAf7ip, Resveratrol, loss of DNA methylation, and *Xist* deletion on inactive X reporter activity. (A) Diagram of a primary MEF with an inactive X chromosome bearing a conditional loxP-flanked allele of *Xist* and a CAGGS-driven H2B-Citrine transgene in the HPRT locus. (B) FACS analysis of MEFs shown in Fig 7A treated with either Adenovirus(Ad)-Cre or Ad-Null (empty vector) for 24 hours, then subjected to knockdown and/or chemical treatments for an additional 72 hours, and analyzed by flow cytometry. (C) Representative image of *Xist* RNA FISH with DNA probe in Ad-Null and Ad-Cre treated MEFs at the time of flow cytometry summarized in Figure 7B. 98% of cells lacked *Xist* signal (n=200 counted).

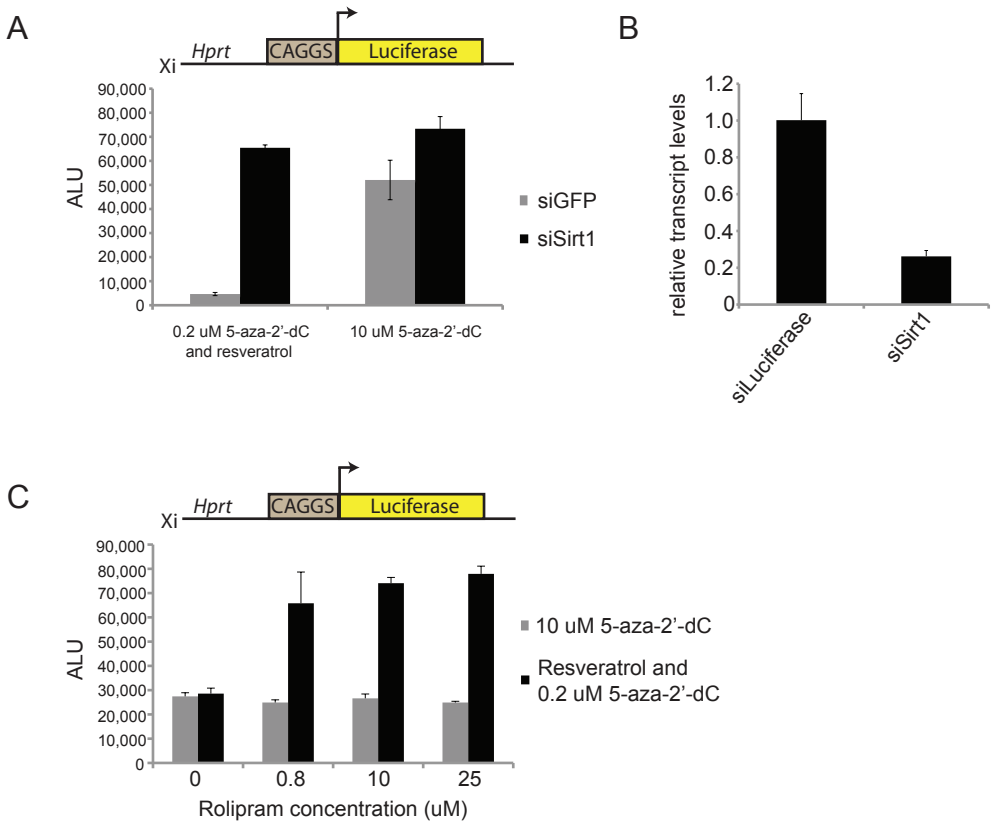

Supp Figure 7.1. Rrm2-independent Resveratrol targets have effects that both enhance and counter XCR. (A) Knockdown of *Sirt1* boosts Resveratrol and 0.2 uM 5-aza-2'-dC-mediated XCR. Graph summarizing luciferase assay in 12 well format. Error bars indicate one standard deviation of raw ALU values from 3 individual wells with a given treatment in one experiment. (B) RT-qPCR for *Sirt1* RNA levels after siSirt1 knockdown normalized to siLuciferase control and *Gapdh* expression from the experiment shown in (A). (C) Rolipram, a cAMP phosphodiesterase inhibitor described to mimic the metabolic effect of Resveratrol, boosts X chromosome reactivation due to Resveratrol and 0.2 uM 5-aza-2'-dC (Park et al., 2012). Graph summarizing luciferase assay in 12 well format. Error bars indicate one standard deviation of raw ALU values from 3 individual wells with a given treatment in one experiment.

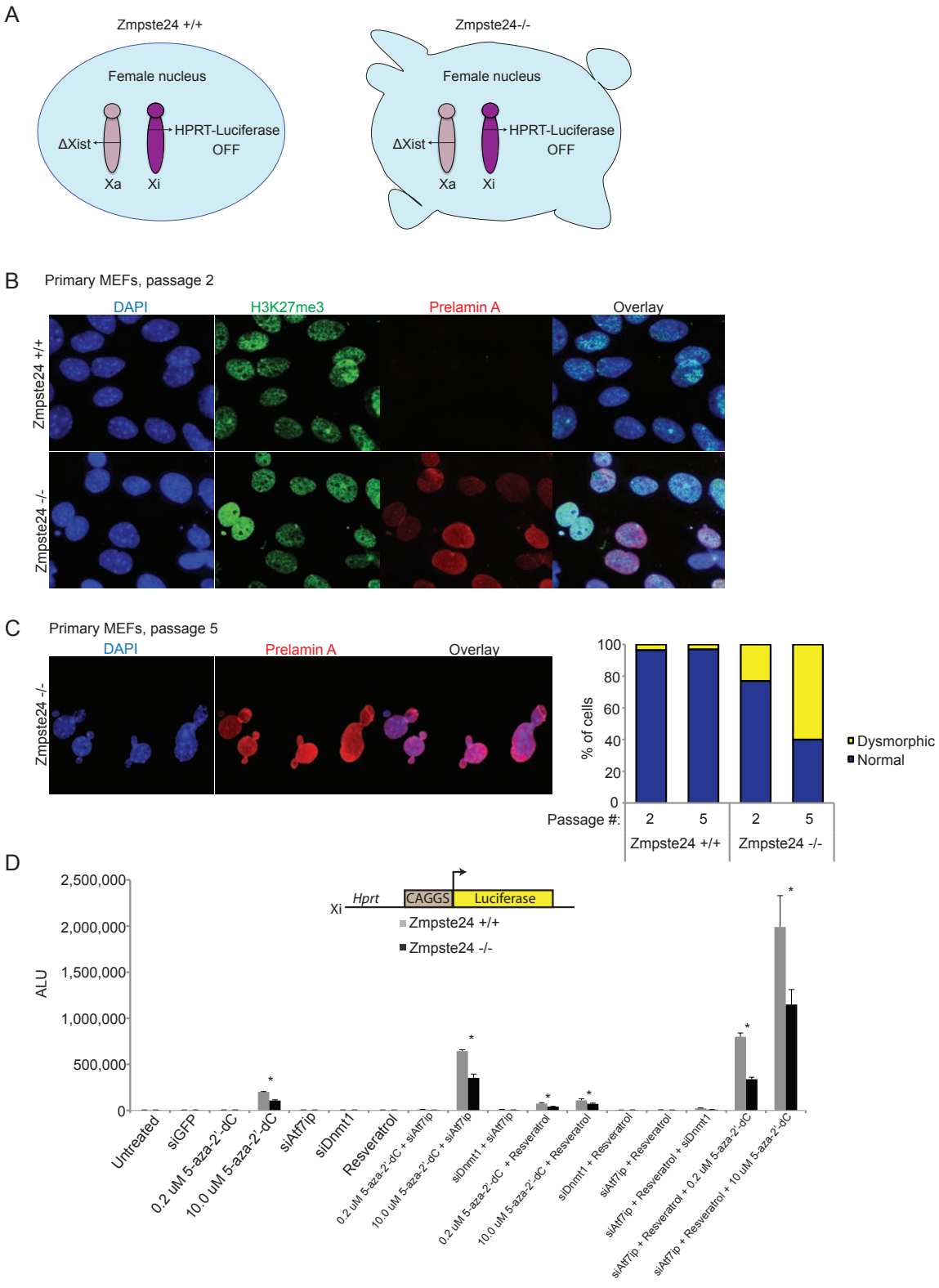

Supplementary Figure 7.2. A mouse model of progeria does not sensitize to X chromosome reactivation. (A) Diagram of a female MEF cell with an inactive X chromosome bearing a CAGGS promoter-driven luciferase transgene in the HPRT locus and either wildtype (+/+) or homozygous deleted (-/-) *Zmpste24* alleles. The shape of the -/- nucleus reflects nuclear shape abnormalities associated with the Zmpste24 phenotype. Reactivation upon chemical and/or siRNA treatment is quantified by luciferase assay.

(B) Immunofluoresence in passage 2 MEFs as diagrammed in (A) for H3K27me3 (green), prelamin A (red), and DAPI (blue). (C) Representative image of nuclear dysmorphia observed in passage 5 Zmpste24 -/- MEFs stained for DAPI (blue) and prelamin A (red). On the right is a quantification of the rate of appearance of dysmorphic nuclei from passage 2 to passage 5 (n=100 cells counted per condition). (D) Summary of luciferase assay of passage 2 MEFs subjected to knockdown and/or chemical treatments for 72 hours * Note the differences in Zmpste24 +/+ and -/- MEFs are likely attributable to cell number and that the relative sensitivities to any of the treatments are not different.

High Throughput Screening for XCI Maintenance Factors

CHAPTER 8

DISCUSSION AND METHODS

DISCUSSION

We performed a genome-wide RNAi screen in mammalian cells for factors that can reactivate an epigenetically silenced gene and validated 2 hits. Challenges in such studies include cell heterogeneity and genetic instability in screening cell lines (Echeverri and Perrimon, 2006). Rather than using immortal cells where transformation can compromise normal gene silencing mechanisms, we used primary MEFs that were rapidly expanded from transgenic embryos without the need for immortalization (Esteller, 2008). We have partially overcome the challenges of off-target effects and the inherent variability in transfection-based siRNA delivery with built-in gene redundancy in our screening libraries (Martin et al., 1996). The transient gene knockdown and early 3-day timepoint was intended to limit appearance of secondary effects. As illustrated by the *Atf7ip*-interactors *Mbd1* and *Setdb1*, where no siRNAs in the screen demonstrated luciferase activity but handpicked siRNAs in a scaled-up assay showed robust effect, we encountered false negatives. This low sensitivity is partially characteristic of siRNA-mediated loss of function where the threshold of knockdown needed to elicit the phenotype is gene-specific. Yet incomplete knockdown was also beneficial in detecting hits that are essential factors where hypomorphic knockdown can show XCR effects without cell-cycle arrest and death associated with more complete loss, as exemplified by *Rrm2* knockdown (Kittler et al., 2004). More maintenance factors in XCI could potentially be found by screening with further sensitization to XCR by genetic deletion (*Xist* or *Atf7ip* deletion) and/or drug addition (Resveratrol and low 5-aza-2'-dC, TSA). Significant hits represent factors that can be knocked down in living cells because even if a lethal knockdown caused low levels of reactivation, the presumable loss of luciferase signal due to cell death prevents our strategy from detecting such a hit. Furthermore, the requirement for DNA methylation inhibition with reported hits, which in our study was carried out by passive demethylation either by 5-aza-2'-dC or knockdown of *Dnmt1*,

suggests that cells treated with siRNA screen hits must not only be alive but also dividing to lose DNA methylation. The mechanistic validation of the two highest scoring hits from the RSA analysis illustrates the high specificity of our screening approach.

Interestingly, both *Atf7ip* and *Rrm2* are described to have cell cycle-dependent function. The *Mbd1-Setdb1* complex has been shown to be S-phase specific and recruited to DNA by Chromatin Assembly Factor 1 (*CAF-1*) (Sarraf and Stancheva, 2004). RNR is controlled during the cell cycle by the protein levels of the Rrm2 subunit that with a 3 hour half-life is maximally transcribed during S phase and associates with the more stable constitutively expressed Rrm1 subunit (Engström et al., 1985). This connection supports a model where heterochromatin is mostly stable at interphase and subject to remodeling upon cell division and DNA replication when maintenance factors actively function. We speculate that the requirement for cell cycling may explain why only a subpopulation of cells reactivate the reporter with any known XCR treatment. Synchronizing MEFs to undergo XCR treatment at S phase entry may increase rates of reactivation. In contrast, the ability of siAtf7ip to effect XCR may be lost in the presence of a cell cycle inhibitor. This experiment is technically complicated by the fact that in our system, robust levels of XCR due to Atf7ip loss required passive DNA demethylation through cell division. Therefore it would be necessary to see if Atf7ip knockdown could be coupled to active DNA demethylation. Full knockout of *Atf7ip* could circumvent this dependence on DNA demethylation as greater loss of function may continue to increase rates of XCR. It is unclear whether *Atf7ip* is necessary for XCI initiation and maintenance *in vivo*, though its patterns of expression would be consistent with such a role as in situ hybridization shows it is ubiquitously expressed in d9.5 embryos with more specific tissue distribution at later timepoints (De Graeve et al., 2000). *Atf7ip* interactors *Mbd1* and *Setdb1* have very different knockout phenotypes, namely mild spatial learning defects in adult mice lacking *Mbd1* and early peri-embryonic lethality at 3.5-5.5 days

post conception (DPC) in embryonic mice with *Setdb1* deletion. Therefore it would be interesting to see the biological significance of *Atf7ip* in tethering the two (Dodge et al., 2004; Zhao et al., 2003).

The identification of *Atf7ip* as a factor involved in maintenance of XCI suggests that the downstream effect of its binding partner *Setdb1*, namely enzymatic conversion of H3K9me2 to H3K9me3, is also required. H3K9me has previously been reported to play a role in XCI on the basis of enrichment of a pan-methyl H3K9 antibody on the Xi in mouse and human cells though it is unclear if the antibody used in these studies has cross-reactivity to H3K27me3 (Boggs et al., 2002; Heard et al., 2001; Mermoud et al., 2002). Another study comparing H3K27me3 and H3K9me2 by ChIP establishes that both increase on the Xi in MEFs relative to the active X (Rougeulle et al., 2004). These studies have contributed to the belief that H3K9me2 is a feature of facultative (developmentally-labile) heterochromatin while H3K9me3 is characteristic of constitutive heterochromatin (Trojer and Reinberg, 2007). Our study is the first demonstration of a functional role for an effector of H3K9me3 in XCI yet it is unclear if knockdown of *Setdb1* undoes transcriptional repression by the loss of H3K9me3: complete knockout of *Setdb1* does not lead to global changes in H3K9me3 levels or DNA methylation though embryos show an early phenotype and arrest at 5.5 DPC (Dodge et al., 2004). Reader heterochromatin proteins *Cbx1, Cbx3* and/or *Cbx5* are thought to mediate H3K9me3 transcriptional repression yet, in this study, knockdown of *Cbx3* or *Cbx5* individually had no XCR effect (Fig 5.2D/5.2E). Furthermore, we do not see specific enrichment of *Atf7ip* or H3K9me3 on the Xi by immunofluoresence suggesting that they bind and mediate heterochromatin on autosomes broadly in both facultative and constitutive contexts (Supp Fig 5.2). ChIP studies of H3K9me3 on Xi genes with and without knockdown of *Atf7ip* will be necessary to refine the pathway for *Atf7ip*. The dependence of siAtf7ip on inhibition of DNA methylation for XCR could be tested by coupling ChIP with bisulfite

sequencing. We hypothesize that low levels of DNA methylation loss are necessary to "unlock" the stably silenced chromatin, but the relationship between H3K9me3 and DNA methylation may be reciprocal and H3K9me3 could also recruit DNA methylation machinery (Lehnertz et al., 2003). Therefore, the balance between H3K9me3 demethylation and loss of DNA methylation as well as the distribution of that loss (i.e. promoter, intragenic) are likely critical to achieve synergy in targeting both pathways. Finally, our study suggests a heterogeneous nature to gene silencing on the Xi where loci have differential dependence on various combinations of silencing mechanisms. This is demonstrated by comparing the different rates of reactivation between transgenes and endogenous genes in response to the various treatments though these may have different thresholds for being called reactivated because of the different cytomery versus FISH-based readouts (Fig 5.1E/5.1G). Despite the fact that our screening approach was biased in favor of conditions in which the positive control, knockdown of *Dnmt1* gave robust signal, we did not detect a hit that significantly improved the rates of XCR; targeting of Atf7ip in addition to DNA methylation and *Xist* as in previous studies mildly improved the rates of XCR in primary MEFs (Csankovszki et al., 2001). It would be interesting to see if conditions with the highest rates of XCR have the most chromosome-wide XCR as well by performing FISH with combinations of probes to X-linked genes.

The demonstration that Xi gene reactivation by 5-aza-2'-dC could be augmented by inhibiting RNR shows XCR screening is a useful tool for understanding and drugging the general mechanisms of gene silencing. The FDA-approved clinical use of 5-aza-2'-dC is limited to hematologic malignancies where it is thought to function by reactivating the expression of tumor suppressor genes silenced by DNA methylation and perhaps also by changing a cancerous epigenetic profile of the cell (Yang et al., 2010). The use of 5-aza-2'-dC is limited by its toxicity where a high concentration causes DNA damage

and cytotoxicity (Qin et al., 2009). In vitro resistance mechanisms have been shown to limit 5-aza-2'-dC incorporation into DNA (Qin et al., 2009). Coupling to *Rrm2* inhibition, which we show here increases 5-aza-2'-dC incorporation into DNA and boosts the efficacy of 5-aza-2'-dC-mediated gene reactivation at lower concentrations, may therefore enhance 5-aza-2'-dC action while reducing toxicity and limiting resistance. *Rrm2* inhibition has long had application in clinical oncology with the use of hydroxyurea as a chemotherapy since it is recognized to slow proliferation of cells depending on high rates of de novo dNTP synthesis (Donehower, 1992). More specific siRNA and chemical inhibitors of *Rrm2* have performed well in preclinical testing, therefore further studies to assess the efficacy of combination of 5-aza-2'-dC and *Rrm2* inhibition on growth inhibition in malignancy are merited (Finch et al., 2000; Heidel et al., 2007). Basic research studies of gene silencing such as this one may therefore serve to provide advances in cancer therapy.

METHODS

Cell culture and treatment methods

ESCs were grown on irradiated DR4 mouse embryonic fibroblasts (MEFs) in standard media (DMEM supplemented with 15% FBS, nonessential amino acids, L-glutamine, penicillin-streptomycin, β-mercaptoethanol, and 1000 U/mL LIF). MEFs were derived at embryonic day 14.5 and cultured in MEF media (same as ESC media except 10% FBS and excluding LIF). For reactivation assays, MEFs at passage 1 or 2 post-derivation were seeded at a density of 60,000 cells per 12-well well and chemicals in MEF media (and/or knockdowns in Opti-MEM) were added and incubated for 72 hours. For chemicals in DMSO, final DMSO concentration was below 0.1% and total volumes of MEF and/or Opti-MEM media were normalized across samples.

Generation of reporter MEFs

HPRT-Luciferase and HPRT-H2B-Citrine MEFs were harvested from transgenic female C57Bl/6 mouse embryos derived from male V6.5 ES cells. These ES cells were modified by two-step targeting: first, a homologous targeting to place a Frt site under the HPRT locus then using FLP-e mediated recombination to introduce the luciferase or H2B-Citrine transgene into the primed site (Beard et al., 2006). In order to place a frt-hygro-pA “homing” cassette downstream of Hprt, the ColA1 arms of the pgkATGfrt plasmid were replaced with Hprt arms. The targeting vector was linearized and introduced into V6.5 ES cells by electroporation followed by selection with 350 ug/ml G418. DNA from picked clones was analyzed for proper targeting Southern blot using Hprt external probe. Site-directed insertion of transgene was accomplished by cotransfection of FLPe transient expression vector with pBS32 vector bearing luciferase or H2B-Citrine. The pBS32 vector was made by exchanging the tetracycline-responsive

operating binding sequence in the pBS31 plasmid with a constitutive CAGS promoter (Beard et al., 2006). Luciferase or H2B Citrine were introduced into pBS32 by Gateway ® cloning (Life Technologies). To make pBS32 destination vector-compatible (pBS32-GW), a Gateway cassette with attR sites and a ccdB gene was flanked by SgrAI restriction sites and ligated into a unique EcoRI site on pBS32. One-step BP and LR cloning was performed with pDonr221 entry vector, attB-primer amplified luciferase from pGL3 vector (Promega) or H2B Citrine (gift of Elowitz lab) and pBS32-GW. Targeting was performed as previously reported (Beard et al., 2006). DNA from selected clones was digested with BglII and screened by Southern blot using 3' external probe. ES cells were microinjected into C57BL/6 blastocysts to produce chimeric mice following standard procedures. High agouti coat color-contributing chimeras were bred with C57BL/6 females for germline transmission. All animal experiments were in accordance with the legislation of the UCLA Animal Research Committee.

Luciferase assay

Treatments were performed in triplicate 12-well wells for 72 hours and lysed with 200 ul passive lysis buffer (PLB, Promega) for 20 mins at room temperature on an orbital shaker. Lysate was cleared by 30 seconds of centrifugation and 20 ul was assayed for luciferase activity with 50 ul of LARI reagent (Promega) on a GloMax microplate luminometer (Promega). Protein concentration measurements were performed on corresponding PLB lysates by Quick Start™ Bradford Protein Assay Kit (Bio-Rad) and analyzed by interpolating to standard curve according to Manufacturer's Instruction.

RT-qPCR analysis

Cells were harvested from a 6-well format in Trizol (Invitrogen) and RNA purification was performed with the RNeasy kit (Qiagen) according to manufacturer's

instructions with on-column DNAse treatment (Qiagen). cDNA was prepared using SuperScript III (Invitrogen) with random hexamers and RT-qPCR was performed using a Stratagene Mx3000 thermocycler with primers listed in Supp Table 1. Results were normalized to Gapdh by the ΔCt method.

Knockdown and overexpression

Knockdown of MEFs with siRNA was performed by reverse transfection at 25 nM final concentration of siRNA. Briefly, a cell suspension was added to a preincubated mixture of Lipofectamine RNAimax, 100 ul of reduced serum Opti-MEM media, and siRNA. For experiments involving multiple knockdowns, control siRNA was added to equalize the final siRNA concentration across all wells. For overexpression of pMX-Atf7ip, virus was raised in transfected platE cells and MEFs were transduced as previously described (Maherali et al., 2007). Atf7ip was introduced into the pMX retroviral vector by In-Fusion ® cloning (Clonetech) of the Atf7ip cDNA.

Immunofluorescence, FISH, and chromosome paint analysis

Cells were plated on glass coverslips, washed once with PBS, and fixed for 10 minutes in 4% paraformaldehyde (Plath et al., 2003). Immunostaining with antibodies against Atf7ip (Abcam 84497), H3K27me3 (Active Motif 39155), H3K9me3 (Active Motif 39161, AbCam ab8898), FLAG M2 (Sigma F3165) and FISH with double-strand *Xist, Rlim (Rnf12), Atrx, Gpc4,* and *MeCp2* DNA probes, and IF/FISH combinations thereof were performed as previously reported and mounted with Prolong Gold reagent with DAPI (Tchieu et al., 2010). For X Chromosome paint (Applied Spectral Imaging), cells were fixed in 3:1 methanol:acetic acid and staining was performed according to manufacturer's instruction.

Flow cytometry

Cells were trypsinized, washed in PBS, loaded through cell strainer caps (BD Biosciences) and analyzed on a FACSDiva machine (BD Biosciences) with FlowJo software (Tree Star, Inc.).

3H Decitabine Incorporation

This assay was analogous to reactivation treatment assays with several modifications; assays were scaled 2.5-fold to 6-well format, 1 ul (1 uCi) of tritiated 5-aza-2'-dC (3H-Decitabine, Moravek Biochemicals Inc.) was added instead of cold 5-aza-2'-dC, and samples were harvested at 48 hours. Cells were trypsinized and genomic DNA was isolated by Quick-gDNA MinPrep kit (Zymo Research) and measured by QuBit ® fluorometer (Life technologies). Tritium content of 25 ul of genomic DNA was measured by scintillation counter and normalized to measured DNA concentration.

Genome-wide siRNA library plate preparation

Silencer ® Mouse Druggable siRNA Library V3 and Extension set V3 (Ambion) were provided as 250 pmol of lyophilized powder in a total of 153 384-well source plates. Plates were centrifuged at 1700x g, 50ul of nuclease-free water was added to each well, and plates were sealed and briefly vortexed to resuspend siRNA. RNA concentrations were confirmed by measuring 1 ul of sample from 14 randomly chosen wells by NanoDrop spectrophotometer (Thermo Scientific). 2 ul of siRNA diluted to 0.5 pMol/uL from each source plate was stamped in duplicate onto Matrix white opaque 384-well tissue culture treated plates (Thermo Scientific) by BenchCel 4X system with a PlateLoc plate sealer, Vcode Barcode Printer, and Vprep pipettor fitted with a 96 LT head (all from Agilent Technologies) and stored in -80.

High throughput screening assay

Primary MEFs from four embryos were pooled and expanded to passage 4 then frozen as stocks for screening. For each batch of 30 plates in the genome-wide library, cells were thawed from this stock in MEF media. After one day in culture, adherent cells were trypsinized, live cells excluding Trypan blue were counted by hemocytometer and brought up in suspension with MEF media agitated by stir bar. Meanwhile, positive control was stamped by BenchCel 4X system with an 8 channel LT head (Agilent Technologies) into 32 wells of column 1 of library plates by adding 4 ul of nuclease-free water containing 1 picomole of siDnmt1 to each well (Ambion, 161526). The 32 wells of the column 12 were reserved as negative control and contained no siRNA. Transfection was initiated by adding 20 ul of Opti-MEM (Life Technologies) and 0.05 ul RNAimax (Life Technologies) per well by Multidrop384 and incubating for 20 minutes to 1 hour. 20 ul of cell suspension containing 2,000 cells with 5-aza-2'-dC (Sigma) was added to a final concentration of 0.2 uM. Cells were incubated for 3 days in a humidified 37-degree incubator at 5% CO_2. 20 ul of media was then aspirated off using an ELx 405 plate washer (Bio-Tek Instruments) and 20 ul of One-Glo™ luciferase assay reagent (Promega) was added with Multidrop 384 and incubated for 20 minutes. As luminescence data was collected on an Acquest (Molecular Devices) machine, quality control for each plate was performed by visual inspection of positive and negative controls on heatmap during data collection. Chemical screening was performed analogously with several exceptions: 384-well plates were not pre-treated. Rather, 50 ul of cell suspension with 2,000 cells was plated then screening compounds were added using a Biomek FX (Beckman Coulter) in 0.5 ul DMSO for a final concentration of 10uM. After 72-hour incubation, 30 ul of media was aspirated off and luciferase assay was performed as with the siRNA screen. Libraries screened include 4,094 compounds from

Microsource, Biomol enzyme inhibitor and bioactive lipid libraries, Prestwick chemical library, and NIH clinical collections at the UCLA MSSR.

High throughput siRNA screening analysis

The screen assay was optimized to maximize the Z-factor statistical measure of signal-to-noise (Zhang et al., 1999). Screening data analysis was performed by first normalizing raw ALU values by robust Z-score which is the number of mean absolute deviations for given well ALU from the plate median ALU (Birmingham et al., 2009). Hit identification was performed by Redundant siRNA Activity (RSA) analysis method with input of robust Z-score (König et al., 2007, http://carrier.gnf.org/publications/RSA/). RSA works by ranking hits in order of activity then assigning P values for genes based on whether their siRNAs rank higher than would be expected by chance.

REFERENCES

Agelopoulos, M., and Thanos, D. (2006). Epigenetic determination of a cell-specific gene expression program by ATF-2 and the histone variant macroH2A. EMBO J *25*, 4843–4853.

Baker, M. (2012). RNA imaging in situ. Nat Meth *9*, 787–790.

Beard, C., Hochedlinger, K., Plath, K., Wutz, A., and Jaenisch, R. (2006). Efficient method to generate single-copy transgenic mice by site-specific integration in embryonic stem cells. Genesis *44*, 23–28.

Bergo, M.O., Gavino, B., Ross, J., Schmidt, W.K., Hong, C., Kendall, L.V., Mohr, A., Meta, M., Genant, H., Jiang, Y., et al. (2002). Zmpste24 deficiency in mice causes spontaneous bone fractures, muscle weakness, and a prelamin A processing defect. PNAS *99*, 13049–13054.

Birmingham, A., Selfors, L.M., Forster, T., Wrobel, D., Kennedy, C.J., Shanks, E., Santoyo-Lopez, J., Dunican, D.J., Long, A., Kelleher, D., et al. (2009). Statistical Methods for Analysis of High-Throughput RNA Interference Screens. Nat Methods *6*, 569–575.

Boggs, B.A., Cheung, P., Heard, E., Spector, D.L., Chinault, A.C., and Allis, C.D. (2002). Differentially methylated forms of histone H3 show unique association patterns with inactive human X chromosomes. Nat. Genet. *30*, 73–76.

Brockdorff, N., Ashworth, A., Kay, G.F., Cooper, P., Smith, S., McCabe, V.M., Norris, D.P., Penny, G.D., Patel, D., and Rastan, S. (1991). Conservation of position and exclusive expression of mouse Xist from the inactive X chromosome. Nature *351*, 329–331.

Casas-Delucchi, C.S., Brero, A., Rahn, H.-P., Solovei, I., Wutz, A., Cremer, T., Leonhardt, H., and Cardoso, M.C. (2011). Histone acetylation controls the inactive X chromosome replication dynamics. Nat Commun *2*, 222.

Chang, L.-K., Chung, J.-Y., Hong, Y.-R., Ichimura, T., Nakao, M., and Liu, S.-T. (2005). Activation of Sp1-mediated transcription by Rta of Epstein-Barr virus via an interaction with MCAF1. Nucleic Acids Res. *33*, 6528–6539.

Chaumeil, J., Le Baccon, P., Wutz, A., and Heard, E. (2006). A novel role for Xist RNA in the formation of a repressive nuclear compartment into which genes are recruited when silenced. Genes Dev. *20*, 2223–2237.

Chuva de Sousa Lopes, S.M., Hayashi, K., Shovlin, T.C., Mifsud, W., Surani, M.A., and McLaren, A. (2008). X chromosome activity in mouse XX primordial germ cells. PLoS Genet. *4*, e30.

Clemson, C.M., McNeil, J.A., Willard, H.F., and Lawrence, J.B. (1996). XIST RNA paints the inactive X chromosome at interphase: evidence for a novel RNA involved in nuclear/chromosome structure. J. Cell Biol. *132*, 259–275.

Clouser, C.L., Chauhan, J., Bess, M.A., van Oploo, J.L., Zhou, D., Dimick-Gray, S., Mansky, L.M., and Patterson, S.E. (2012). Anti-HIV-1 activity of resveratrol derivatives and synergistic inhibition of HIV-1 by the combination of resveratrol and decitabine. Bioorg. Med. Chem. Lett. *22*, 6642–6646.

Costanzi, C., and Pehrson, J.R. (1998). Histone macroH2A1 is concentrated in the inactive X chromosome of female mammals. Nature *393*, 599–601.

Csankovszki, G., Panning, B., Bates, B., Pehrson, J.R., and Jaenisch, R. (1999). Conditional deletion of Xist disrupts histone macroH2A localization but not maintenance of X inactivation. Nat. Genet. *22*, 323–324.

Csankovszki, G., Nagy, A., and Jaenisch, R. (2001a). Synergism of Xist RNA, DNA methylation, and histone hypoacetylation in maintaining X chromosome inactivation. J. Cell Biol *153*, 773–784.

Csankovszki, G., Nagy, A., and Jaenisch, R. (2001b). Synergism of Xist RNA, DNA methylation, and histone hypoacetylation in maintaining X chromosome inactivation. J. Cell Biol. *153*, 773–784.

Dodge, J.E., Kang, Y.-K., Beppu, H., Lei, H., and Li, E. (2004). Histone H3-K9 methyltransferase ESET is essential for early development. Mol. Cell. Biol. *24*, 2478–2486.

Dodge, J.E., Okano, M., Dick, F., Tsujimoto, N., Chen, T., Wang, S., Ueda, Y., Dyson, N., and Li, E. (2005). Inactivation of Dnmt3b in mouse embryonic fibroblasts results in DNA hypomethylation, chromosomal instability, and spontaneous immortalization. J. Biol. Chem. *280*, 17986–17991.

Donehower, R.C. (1992). An overview of the clinical experience with hydroxyurea. Semin. Oncol. *19*, 11–19.

Echeverri, C.J., and Perrimon, N. (2006). High-throughput RNAi screening in cultured cells: a user's guide. Nat. Rev. Genet. *7*, 373–384.

Eggan, K., Akutsu, H., Hochedlinger, K., Rideout, W., 3rd, Yanagimachi, R., and Jaenisch, R. (2000). X-Chromosome inactivation in cloned mouse embryos. Science *290*, 1578–1581.

Engström, Y., Eriksson, S., Jildevik, I., Skog, S., Thelander, L., and Tribukait, B. (1985). Cell cycle-dependent expression of mammalian ribonucleotide reductase. Differential regulation of the two subunits. J. Biol. Chem. *260*, 9114–9116.

Esteller, M. (2008). Epigenetics in Cancer. New England Journal of Medicine *358*, 1148–1159.

Finch, R.A., Liu, M.-C., Grill, S.P., Rose, W.C., Loomis, R., Vasquez, K.M., Cheng, Y.-C., and Sartorelli, A.C. (2000). Triapine (3-aminopyridine-2-carboxaldehyde-thiosemicarbazone): A potent inhibitor of ribonucleotide reductase activity with broad spectrum antitumor activity. Biochemical Pharmacology *59*, 983–991.

Fontecave, M., Lepoivre, M., Elleingand, E., Gerez, C., and Guittet, O. (1998). Resveratrol, a remarkable inhibitor of ribonucleotide reductase. FEBS Lett. *421*, 277–279.

Ghoshal, K., Datta, J., Majumder, S., Bai, S., Kutay, H., Motiwala, T., and Jacob, S.T. (2005). 5-Aza-deoxycytidine induces selective degradation of DNA methyltransferase 1 by a proteasomal pathway that requires the KEN box, bromo-adjacent homology domain, and nuclear localization signal. Mol. Cell. Biol. *25*, 4727–4741.

Goldman, R.D., Shumaker, D.K., Erdos, M.R., Eriksson, M., Goldman, A.E., Gordon, L.B., Gruenbaum, Y., Khuon, S., Mendez, M., Varga, R., et al. (2004). Accumulation of mutant lamin A causes progressive changes in nuclear architecture in Hutchinson–Gilford progeria syndrome. PNAS *101*, 8963–8968.

De Graeve, F., Bahr, A., Chatton, B., and Kedinger, C. (2000). A murine ATFa-associated factor with transcriptional repressing activity. Oncogene *19*, 1807–1819.

Hadjantonakis, A.K., Gertsenstein, M., Ikawa, M., Okabe, M., and Nagy, A. (1998). Generating green fluorescent mice by germline transmission of green fluorescent ES cells. Mech. Dev. *76*, 79–90.

Heard, E. (2004). Recent advances in X-chromosome inactivation. Curr. Opin. Cell Biol. *16*, 247–255.

Heard, E., and Disteche, C.M. (2006). Dosage compensation in mammals: fine-tuning the expression of the X chromosome. Genes Dev. *20*, 1848–1867.

Heard, E., Rougeulle, C., Arnaud, D., Avner, P., Allis, C.D., and Spector, D.L. (2001). Methylation of histone H3 at Lys-9 is an early mark on the X chromosome during X inactivation. Cell *107*, 727–738.

Heidel, J.D., Liu, J.Y.-C., Yen, Y., Zhou, B., Heale, B.S.E., Rossi, J.J., Bartlett, D.W., and Davis, M.E. (2007). Potent siRNA Inhibitors of Ribonucleotide Reductase Subunit RRM2 Reduce Cell Proliferation In vitro and In vivo. Clin Cancer Res *13*, 2207–2215.

Hernández-Muñoz, I., Lund, A.H., Stoop, P. van der, Boutsma, E., Muijrers, I., Verhoeven, E., Nusinow, D.A., Panning, B., Marahrens, Y., and Lohuizen, M. van (2005). Stable X chromosome inactivation involves the PRC1 Polycomb complex and requires histone MACROH2A1 and the CULLIN3/SPOP ubiquitin E3 ligase. PNAS *102*, 7635–7640.

Hubbard, B.P., Gomes, A.P., Dai, H., Li, J., Case, A.W., Considine, T., Riera, T.V., Lee, J.E., E, S.Y., Lamming, D.W., et al. (2013). Evidence for a common mechanism of SIRT1 regulation by allosteric activators. Science *339*, 1216–1219.

Ichimura, T., Watanabe, S., Sakamoto, Y., Aoto, T., Fujita, N., and Nakao, M. (2005). Transcriptional repression and heterochromatin formation by MBD1 and MCAF/AM family proteins. J. Biol. Chem. *280*, 13928–13935.

Kalantry, S., and Magnuson, T. (2006). The Polycomb group protein EED is dispensable for the initiation of random X-chromosome inactivation. PLoS Genet. *2*, e66.

Kay, G.F., Penny, G.D., Patel, D., Ashworth, A., Brockdorff, N., and Rastan, S. (1993). Expression of Xist during mouse development suggests a role in the initiation of X chromosome inactivation. Cell *72*, 171–182.

Kittler, R., Putz, G., Pelletier, L., Poser, I., Heninger, A.-K., Drechsel, D., Fischer, S., Konstantinova, I., Habermann, B., Grabner, H., et al. (2004). An endoribonuclease-prepared siRNA screen in human cells identifies genes essential for cell division. Nature *432*, 1036–1040.

König, R., Chiang, C., Tu, B.P., Yan, S.F., DeJesus, P.D., Romero, A., Bergauer, T., Orth, A., Krueger, U., Zhou, Y., et al. (2007). A probability-based approach for the analysis of large-scale RNAi screens. Nat. Methods *4*, 847–849.

Larsson, K.-M., Jordan, A., Eliasson, R., Reichard, P., Logan, D.T., and Nordlund, P. (2004). Structural mechanism of allosteric substrate specificity regulation in a ribonucleotide reductase. Nat. Struct. Mol. Biol. *11*, 1142–1149.

Leeb, M., and Wutz, A. (2007). Ring1B is crucial for the regulation of developmental control genes and PRC1 proteins but not X inactivation in embryonic cells. J. Cell Biol. *178*, 219–229.

Lehnertz, B., Ueda, Y., Derijck, A.A.H.A., Braunschweig, U., Perez-Burgos, L., Kubicek, S., Chen, T., Li, E., Jenuwein, T., and Peters, A.H.F.M. (2003). Suv39h-mediated histone H3 lysine 9 methylation directs DNA methylation to major satellite repeats at pericentric heterochromatin. Curr. Biol. *13*, 1192–1200.

Leung, G.K., Schmidt, W.K., Bergo, M.O., Gavino, B., Wong, D.H., Tam, A., Ashby, M.N., Michaelis, S., and Young, S.G. (2001). Biochemical Studies of Zmpste24-deficient Mice. J. Biol. Chem. *276*, 29051–29058.

Liu, L., Ishihara, K., Ichimura, T., Fujita, N., Hino, S., Tomita, S., Watanabe, S., Saitoh, N., Ito, T., and Nakao, M. (2009). MCAF1/AM is involved in Sp1-mediated maintenance of cancer-associated telomerase activity. J. Biol. Chem. *284*, 5165–5174.

Maherali, N., Sridharan, R., Xie, W., Utikal, J., Eminli, S., Arnold, K., Stadtfeld, M., Yachechko, R., Tchieu, J., Jaenisch, R., et al. (2007). Directly reprogrammed fibroblasts show global epigenetic remodeling and widespread tissue contribution. Cell Stem Cell *1*, 55–70.

Marahrens, Y., Panning, B., Dausman, J., Strauss, W., and Jaenisch, R. (1997a). Xist-deficient mice are defective in dosage compensation but not spermatogenesis. Genes Dev. *11*, 156–166.

Marahrens, Y., Panning, B., Dausman, J., Strauss, W., and Jaenisch, R. (1997b). Xist-deficient mice are defective in dosage compensation but not spermatogenesis. Genes Dev. *11*, 156–166.

Martin, C.S., Wight, P.A., Dobretsova, A., and Bronstein, I. (1996). Dual luminescence-based reporter gene assay for luciferase and beta-galactosidase. BioTechniques *21*, 520–524.

Mermoud, J.E., Popova, B., Peters, A.H.F.M., Jenuwein, T., and Brockdorff, N. (2002). Histone H3 lysine 9 methylation occurs rapidly at the onset of random X chromosome inactivation. Curr. Biol. *12*, 247–251.

De Napoles, M., Nesterova, T., and Brockdorff, N. (2007). Early Loss of Xist RNA Expression and Inactive X Chromosome Associated Chromatin Modification in Developing Primordial Germ Cells. PLoS ONE *2*, e860.

Nusinow, D.A., Hernández-Muñoz, I., Fazzio, T.G., Shah, G.M., Kraus, W.L., and Panning, B. (2007). Poly(ADP-ribose) Polymerase 1 Is Inhibited by a Histone H2A Variant, MacroH2A, and Contributes to Silencing of the Inactive X Chromosome. J. Biol. Chem. *282*, 12851–12859.

Ohhata, T., and Wutz, A. (2012). Reactivation of the inactive X chromosome in development and reprogramming. Cell. Mol. Life Sci.

Ohhata, T., Tachibana, M., Tada, M., Tada, T., Sasaki, H., Shinkai, Y., and Sado, T. (2004). X-inactivation is stably maintained in mouse embryos deficient for histone methyl transferase G9a. Genesis *40*, 151–156.

Park, S.-J., Ahmad, F., Philp, A., Baar, K., Williams, T., Luo, H., Ke, H., Rehmann, H., Taussig, R., Brown, A.L., et al. (2012). Resveratrol ameliorates aging-related metabolic phenotypes by inhibiting cAMP phosphodiesterases. Cell *148*, 421–433.

Pasque, V., Gillich, A., Garrett, N., and Gurdon, J.B. (2011). Histone variant macroH2A confers resistance to nuclear reprogramming. EMBO J *30*, 2373–2387.

Pasque, V., Radzisheuskaya, A., Gillich, A., Halley-Stott, R.P., Panamarova, M., Zernicka-Goetz, M., Surani, M.A., and Silva, J.C.R. (2012). Histone variant macroH2A marks embryonic differentiation in vivo and acts as an epigenetic barrier to induced pluripotency. J Cell Sci *125*, 6094–6104.

Pendás, A.M., Zhou, Z., Cadiñanos, J., Freije, J.M.P., Wang, J., Hultenby, K., Astudillo, A., Wernerson, A., Rodríguez, F., Tryggvason, K., et al. (2002). Defective prelamin A processing and muscular and adipocyte alterations in Zmpste24 metalloproteinase–deficient mice. Nat Genet *31*, 94–99.

Penny, G.D., Kay, G.F., Sheardown, S.A., Rastan, S., and Brockdorff, N. (1996). Requirement for Xist in X chromosome inactivation. Nature *379*, 131–137.

Plath, K., Fang, J., Mlynarczyk-Evans, S.K., Cao, R., Worringer, K.A., Wang, H., de la Cruz, C.C., Otte, A.P., Panning, B., and Zhang, Y. (2003). Role of histone H3 lysine 27 methylation in X inactivation. Science *300*, 131–135.

Qin, T., Jelinek, J., Si, J., Shu, J., and Issa, J.-P.J. (2009). Mechanisms of resistance to 5-aza-2′-deoxycytidine in human cancer cell lines. Blood *113*, 659–667.

REICHARD, P., and ESTBORN, B. (1951). Utilization of desoxyribosides in the synthesis of polynucleotides. J. Biol. Chem. *188*, 839–846.

Rougeulle, C., Chaumeil, J., Sarma, K., Allis, C.D., Reinberg, D., Avner, P., and Heard, E. (2004). Differential Histone H3 Lys-9 and Lys-27 Methylation Profiles on the X Chromosome. Mol Cell Biol *24*, 5475–5484.

Sado, T., Okano, M., Li, E., and Sasaki, H. (2004). De novo DNA methylation is dispensable for the initiation and propagation of X chromosome inactivation. Development *131*, 975–982.

Sarraf, S.A., and Stancheva, I. (2004). Methyl-CpG binding protein MBD1 couples histone H3 methylation at lysine 9 by SETDB1 to DNA replication and chromatin assembly. Mol. Cell *15*, 595–605.

Scaffidi, P., and Misteli, T. (2006). Lamin A-dependent nuclear defects in human aging. Science *312*, 1059–1063.

Schoeftner, S., Sengupta, A.K., Kubicek, S., Mechtler, K., Spahn, L., Koseki, H., Jenuwein, T., and Wutz, A. (2006). Recruitment of PRC1 function at the initiation of X inactivation independent of PRC2 and silencing. EMBO J *25*, 3110–3122.

Schreiber, K.H., and Kennedy, B.K. (2013). When lamins go bad: nuclear structure and disease. Cell *152*, 1365–1375.

Shumaker, D.K., Dechat, T., Kohlmaier, A., Adam, S.A., Bozovsky, M.R., Erdos, M.R., Eriksson, M., Goldman, A.E., Khuon, S., Collins, F.S., et al. (2006). Mutant nuclear lamin A leads to progressive alterations of epigenetic control in premature aging. Proc. Natl. Acad. Sci. U.S.A. *103*, 8703–8708.

Sugimoto, M., and Abe, K. (2007). X Chromosome Reactivation Initiates in Nascent Primordial Germ Cells in Mice. PLoS Genet *3*.

Sun, B.K., Deaton, A.M., and Lee, J.T. (2006). A transient heterochromatic state in Xist preempts X inactivation choice without RNA stabilization. Mol. Cell *21*, 617–628.

Tada, M., Takahama, Y., Abe, K., Nakatsuji, N., and Tada, T. (2001). Nuclear reprogramming of somatic cells by in vitro hybridization with ES cells. Curr. Biol. *11*, 1553–1558.

Trojer, P., and Reinberg, D. (2007). Facultative Heterochromatin: Is There a Distinctive Molecular Signature? Molecular Cell *28*, 1–13.

Völkel, P., and Angrand, P.-O. (2007). The control of histone lysine methylation in epigenetic regulation. Biochimie *89*, 1–20.

Wang, H., An, W., Cao, R., Xia, L., Erdjument-Bromage, H., Chatton, B., Tempst, P., Roeder, R.G., and Zhang, Y. (2003). mAM facilitates conversion by ESET of dimethyl to trimethyl lysine 9 of histone H3 to cause transcriptional repression. Mol. Cell *12*, 475–487.

Wood, J.G., Rogina, B., Lavu, S., Howitz, K., Helfand, S.L., Tatar, M., and Sinclair, D. (2004). Sirtuin activators mimic caloric restriction and delay ageing in metazoans. Nature *430*, 686–689.

Wutz, A., and Jaenisch, R. (2000). A shift from reversible to irreversible X inactivation is triggered during ES cell differentiation. Mol. Cell *5*, 695–705.

Yang, X., Lay, F., Han, H., and Jones, P.A. (2010). Targeting DNA methylation for epigenetic therapy. Trends in Pharmacological Sciences *31*, 536–546.

Zhang, Chung, and Oldenburg (1999). A Simple Statistical Parameter for Use in Evaluation and Validation of High Throughput Screening Assays. J Biomol Screen *4*, 67–73.

Zhao, X., Ueba, T., Christie, B.R., Barkho, B., McConnell, M.J., Nakashima, K., Lein, E.S., Eadie, B.D., Willhoite, A.R., Muotri, A.R., et al. (2003). Mice lacking methyl-CpG binding protein 1 have deficits in adult neurogenesis and hippocampal function. Proc. Natl. Acad. Sci. U.S.A. *100*, 6777–6782.